Molecular Interactions in Organic Nanoparticles for Phototheranostic Applications

ARTICLE *in* CHEMICAL REVIEWS · AUGUST 2015

Impact Factor: 46.57 · DOI: 10.1021/acs.chemrev.5b00140 · Source: PubMed

2 AUTHORS:

Kenneth K. Ng

University of Toronto

21 PUBLICATIONS **362** CITATIONS

SEE PROFILE

Gang Zheng

Zhejiang University

171 PUBLICATIONS **3,216** CITATIONS

SEE PROFILE

CHEMICAL REVIEWS

Review

pubs.acs.org/CR

Molecular Interactions in Organic Nanoparticles for Phototheranostic Applications

Kenneth K. Ng[†,∥] and Gang Zheng[*,†,‡,§,∥]

[†]Institute of Biomaterials and Biomedical Engineering, [‡]Department of Medical Biophysics, and [§]Department of Pharmaceutical Sciences, Leslie Dan Faculty of Pharmacy, University of Toronto, Toronto, Ontario M5S, Canada

[∥]Princess Margaret Cancer Centre and Techna Institute, University Health Network, Toronto, Ontario M5G 2C4, Canada

CONTENTS

1. INTRODUCTION

Optical and photonic technologies play an important role in human progress. The bending of light to our will has not only enabled our biological self-discovery, but has also allowed us to probe and investigate the natural life around us. These advancements have also served a critical role in modern medicine through phototheranostics, which is the application of light for diagnosis (photodiagnosis) and treatment (phototherapeutic) of disease. There has been significant progress in the application of photonics in medicine in recent decades due to improvements in light generation, delivery, and sensing technologies. Part of the success of photonic techniques in medicine is attributed to the parallel advancements in optical probes, chemical dyes and photosensitizers, which have improved the contrast of biological tissues and enabled localized phototherapy. The advent of nanotechnology has also expanded the optical probe space to encompass ensembles and assemblies of molecules. While this has increased complexity, it has also presented a wealth of opportunities that can be exploited in the development of novel probes that are multifunctional, possess target selectivity, and can react to environmental stimuli.

Of ongoing interest in medical photonics are organic nanoparticles, which for the purposes of this Review are defined as assemblies of carbon-containing macromolecules. The reason for this interest is multifaceted. The first is diversity. Organic nanoparticles are assemblies of organic molecules, of which there are a virtually endless number of unique structures.

Special Issue: Nanoparticles in Medicine

Received: March 9, 2015

DOI: 10.1021/acs.chemrev.5b00140
Chem. Rev. XXXX, XXX, XXX−XXX

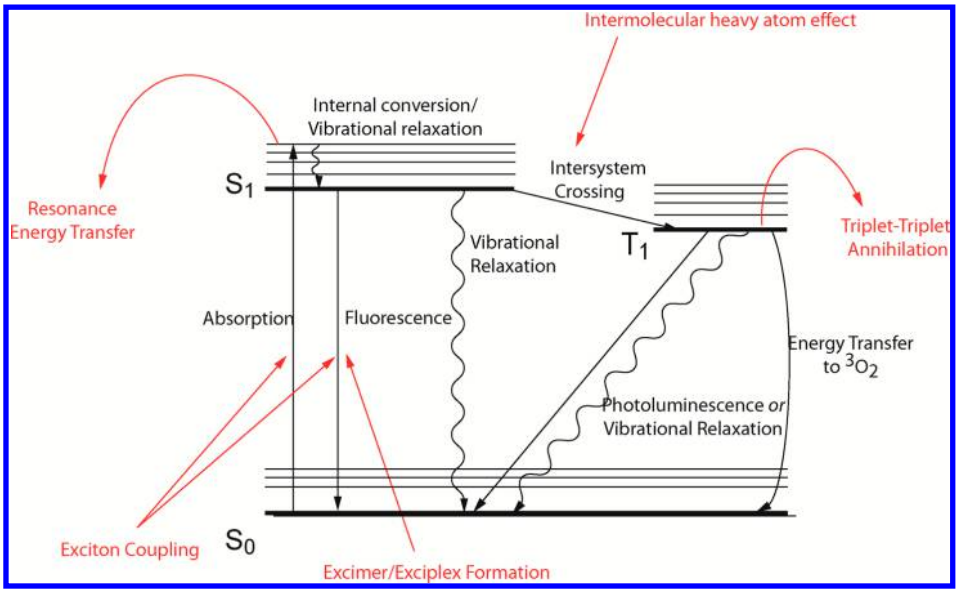

Figure 1. Jablonski diagram illustrating photophysical processes. The red labels indicate where intermolecular interactions between dyes can affect photophysical processes.

It is thus expected that with rational design, it will be possible to create an organic nanoparticle tailored to the requirements of the intended application. Recent innovations using in silico methods can assist in the chemical synthesis process to guide the design of organic molecules with improved optical properties.[1−3] Second, organic nanoparticles are often formed by noncovalent intermolecular interactions. This makes organic nanoparticles more labile in nature, and offers a route for clearance from the body. This flexibility also implies that there may be ways to cause organic nanoparticles to change shape or conformation in response to environmental stimuli. This is important for applications that require detection of physicochemical changes, molecular binding interactions, and stimuli-driven effects. Last, molecular interactions between chromophores within organic nanoparticles can result in optical properties that are not observed in the monomeric species and can be utilized to expand the purview of existing photonic techniques.

2. SCOPE OF REVIEW

This Review is focused on the application of intermolecular dye interactions in organic nanoparticles for phototheranostic applications. It is important to note that while low-dimensional carbon nanostructures (i.e., fullerenes, graphene nanosheets, carbon nanotubes, etc.) fit into our definition of organic nanoparticles, they will not be covered in this Review. Those interested in their photodiagnostic and phototherapeutic applications are referred to other recently published reviews.[4,5]

There have been several excellent reviews published recently that cover the latest advances in nanoparticles for photothermal therapy (PTT),[6] photodynamic therapy (PDT),[7] and theranostics.[8] The goal in this Review is not to "reinvent the wheel", but rather to complement existing works by focusing specifically on photonic organic nanostructures where intermolecular dye interactions are central to their application.

Emphasis will be placed on the progress and development of organic nanostructures that feature assemblies of chromophores that interact via "through-space" mechanisms. We will also discuss the optical imaging and therapy techniques that are dependent on the three main photophysical relaxation pathways for the chromophore: radiative emission, vibrational relaxation, and intersystem crossing/triplet-state relaxation. We will also elaborate on how interacting chromophores within photonic organic nanoparticles can alter their photophysical properties that can be exploited for novel imaging, sensing, and treatment strategies.

3. PRINCIPLES

3.1. Photophysical Processes in Isolated Chromophores

When a photon in the visible/near-infrared spectrum impinges upon a chromophore, it can undergo any one of three processes. These include transmission, scattering, and absorption. Light transmission occurs when the photon passes through the molecule without interaction. Scattering occurs when the photon becomes deflected by matter either with (inelastic scattering) or without (elastic scattering) energy loss. This Review will focus on the photophysical and photochemical processes that follow light absorption. Those interested in the light scattering of nanoparticles and how it can be used for biomedical applications are directed to other published reviews.[9]

In discussing the photophysical and photochemical processes involved upon light absorption, it is useful to describe each process diagrammatically. The Jablonski diagram, named after physicist Aleksander Jablonski,[10] illustrates the electronic and vibrational states for an outer electron of a chromophore (horizontal lines) (Figure 1). States of increasing energy are arranged along a vertical direction, whereas molecular spin multiplicity for the chromophore is given along the horizontal axis. Arrows between states represent photophysical processes. The following discussion will focus on the photophysical processes resulting from light absorption in an isolated chromophore.

Absorption occurs when a photon interacts with a molecule that possesses an electronic transition of equal energy to the photon. The energy from the photon is then transferred to the molecule through the elevation of an electron from its ground

DOI: 10.1021/acs.chemrev.5b00140
Chem. Rev. XXXX, XXX, XXX−XXX

state to a higher excited state. The molecule subsequently relaxes through internal conversion to the lowest excited state.

Once the molecule has relaxed to the lowest vibrational level of the excited state, it can undergo one of three processes. The relaxation of a molecule, which results in the emission of a photon, is known as fluorescence. The difference between the wavelength of the photon emitted and the maximum absorption is known as the Stokes shift.

Vibrational relaxation is a nonradiative mechanism whereby relaxation to the ground state is mediated by collisions between the chromophore and its surrounding environment in a process that leads to the transfer of energy from the chromophore to surrounding molecules. This process is used as a technique to localize a chromophore in the optical-ultrasound hybrid technique known as photoacoustic imaging/spectroscopy.[11,12] Light-based thermal therapies have also used the vibrational relaxation mechanism in individual chromophores to induce the photothermal effect. In this application, a high energy laser source is used to elevate the temperature of the targeted tissue by using the chromophore as a light−heat transducer.[13]

Instead of relaxing through the above-mentioned pathways, it is also possible for an excited chromophore to exit the singlet manifold through intersystem crossing. This forbidden transition involves the conversion of an excited molecule from the singlet to a triplet state, through a change in the spin multiplicity. Once the molecule has entered the triplet state, it will relax through the emission of a photon, known as phosphorescence, or interact with nearby triplet state molecules. In solvents that have a high partial pressure of oxygen, the triplet state will be efficiently quenched by energy transfer to oxygen. This occurs because oxygen has a triplet spin when in the ground state. Intermolecular interaction between the triplet state chromophore with oxygen leads to energy transfer, which causes the formation of toxic reactive oxygen species known as singlet oxygen ($^1O_2$). The generation of this reactive oxygen species causes toxicity in biological organisms and underlies the principles of photodynamic therapy. It is also important to note that while intersystem crossing is an improbable event for most chromophores due to the fact it is a forbidden transition, it is possible to enhance the probability of occurrence by adding paramagnetic metals or heavy atoms (e.g., iodine and bromine) to the structure.[14]

3.2. Influence of Intermolecular Interactions on Photophysical Processes

The previous section described the photophysical processes involved with individually dispersed chromophores. These properties are influenced by proximal chromophores via "through-space" molecular interactions. Specifically, the separation distance between chromophores as well as their relative orientation can have a substantial impact on their radiative and nonradiative relaxation rates. It can also enable energy transfer between molecules. Intermolecular interactions between chromophores can also alter rates of intersystem crossing. Last, it can also induce the formation of coupled states, which can result in shifted absorption and fluorescence spectra.

3.2.1. Resonance Energy Transfer. Resonance energy transfer (RET) can occur between two identical or different fluorophores. It involves the transfer of excitation energy from one fluorophore (donor) to the other (acceptor) through a nonradiative mechanism. While the concept of energy transfer was already known at the time, Förster was the first person to develop a set of equations that could be used to predict the efficiency of the energy transfer by using spectroscopic data.[15,16] The efficiency of Förster RET (FRET) between two molecules is determined by (1) fluorescence quantum yield of the donor, φ_D, (2) overlap between the donor emission spectrum and the acceptor absorption spectrum, J_{DA}, (3) orientation factor between the two molecules, κ, (4) and separation distance, r. In Förster's original formulation, RET has an r^{-6} distance dependence. It is important to note that the Förster theory is only valid if several assumptions are satisfied: (i) the ideal dipole approximation for the donor and acceptor holds,[17] (ii) the orientations of the donor and acceptor are isotropic ($\kappa^2 = 2/3$), and (iii) the electronic structures for the donor and acceptor can be treated independently (weak coupling limit).[18] In the cases where these assumptions do not hold, application-specific modifications of the classical Förster equations are required.[19,20]

Molecules separated in space by up to approximately 10 nm can interact via this mechanism.[21] Of all of the intermolecular energy transfer processes available between fluorophores, FRET has the longest range. As long as the assumptions for the Förster theory are valid for the specific application, this long-range interaction has enabled FRET to be utilized as a "spectroscopic ruler" to estimate distances between nanoscopic objects.[21] While determination of absolute distances with FRET is challenging and requires careful control over all experimental parameters,[22] it has however been used more crudely as a proximity sensor. Some examples of this application include fluorescent molecular beacons[23,24] and structural stability sensors in organic nanoparticles.[25,26]

Another type of RET that can occur is known as Dexter energy transfer (DET). Where FRET is a long-range energy transfer process, DET is a short-range interaction that requires the collision of the donor and acceptor pair. Energy transfer through a Dexter mechanism results in an exponential decrease in energy transfer efficiency between the fluorophore pair.[27] Furthermore, while FRET is a singlet−singlet transfer process, DET is a singlet−singlet and a triplet−triplet transfer process. The collision of triplets can result in interesting phenomena such as photosensitization and upconversion fluorescence, through the photophysical process of triplet−triplet annihilation (vide infra).

3.2.2. Triplet−Triplet Annihilation. Triplet−triplet annihilation (TTA) is an upconversion process in which two triplet excited molecules transfer their energy to two acceptor molecules.[28] As compared to other upconversion processes, such as two-photon absorption, TTA is a low power process and has the possibility of working with noncoherent light. TTA relies on the DET process. Figure 2 illustrates the entire TTA process.[29] In the first step, two molecular sensitizers are excited and quickly convert to the triplet state through intersystem crossing. These two triplet state molecules then undergo heteroenergy transfer to two triplet acceptors. Two excited acceptors diffuse and collide to form an interaction complex. The acceptor can form a number of different complexes with singlet, triplet, or quintet spin multiplicity. There is a 1 in 9 probability that one of the excited acceptors will convert to a singlet state with twice the energy of the triplet state sensitizer.[30] The other excited acceptor will immediately relax back to the ground state. Fluorescence emission from the acceptor results in a photon that is of higher energy than the excitation photon. Assuming that the triplet and quintet states relax only through vibrational relaxation, the maximum upconversion is 11.1%.[30] Unity upconversion in this case is

DOI: 10.1021/acs.chemrev.5b00140
Chem. Rev. XXXX, XXX, XXX−XXX

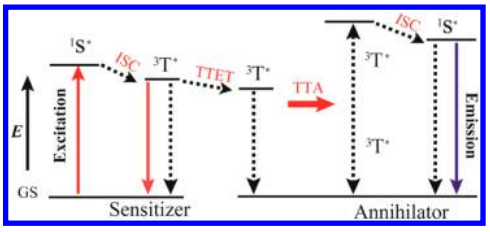

Figure 2. Generalized energy-level diagram of triplet−triplet annihilation (TTA) upconversion processes. Colored solid lines represent radiative processes. ^1S and ^3T are the singlet state and the triplet state of sensitizer or annihilator, respectively. Abbreviations: GS, ground state; ISC, intersystem crossing; TTET, triplet−triplet energy transfer. Reproduced with permission from ref 29. Copyright 2013 Nature Publishing Group.

defined as one upconversion event occurring for every two photons absorbed. This maximal value has been disputed recently, with results showing upward of 25% upconversion efficiency.[30] One possible explanation advanced by the authors was that the triplet and quintet complexes do not relax directly back to the ground state, but instead have further opportunities to contribute to fluorescence.

There are several requirements in selecting the correct molecular sensitizer and triplet state acceptor. Molecular sensitizers need to possess a high quantum yield for intersystem crossing. Another requirement is that the acceptor molecule must possess a very long lifetime in the triplet state. This is because upconversion only occurs upon the formation of the encounter complex, which is a diffusion limited process. Thus, the longer is the lifetime of the triplet acceptor, the greater is the probability for interaction.

3.2.3. Excimers. Excimers (or exciplexes) are complexes of dimers that are formed through the interaction of a fluorophore in the excited state with another fluorophore in its ground state[31] (Figure 3). The distinction between types is achieved by the fact that excimers involve interactions between identical molecules, while exciplexes are complexes formed from dissimilar molecules. Formation of excimers requires close contact between molecules. Studies conducted by Birks and Kazzaz showed that in the case of pyrene excimer crystals, the separation distance between molecules needed to be 3.34 Å for the interaction to occur.[32] Fluorescence from excimers becomes red-shifted and broadened when compared to the monomeric dyes.

3.2.4. Exciton Coupling. The ordered association of molecular dyes and the strength of their interactions can lead to large shifts in absorption spectrum. These changes were first described independently by Jelley[33,34] and Scheibe[35] in the analysis of the absorption spectra for pseudoisocyanine. They each observed that as the concentration of the dye increased, the absorption spectrum would red-shift (bathochromism) and exhibit absorption narrowing. It was postulated that the agent responsible for the unique absorption spectra was the dye itself, forming aggregates within aqueous solutions. These aggregates were named J-aggregates, after Jelley, who was the first one to make the discovery.[36] Since then, J-aggregates have been found to possess photophysical properties such as a minimal Stokes shift and super-radiance at low temperatures.[37] Other arrangements of dyes in aggregates can have an influence on observed optical spectra. This includes aggregates that exhibit a blue-shifted absorption (hypsochromism) spectrum along with a decrease in optical extinction. This macromolecule became known as an H-aggregate.[36] One model that was successfully used to explain the optical absorption shifts of J- and H-aggregates can be found in the work of Kasha et al.[38] He proposed a model that described the excited states of each molecule as Frenkel excitons. Strong coupling between organic dye molecules results in splitting of the absorption transitions, although usually only one band is observed due to the relative orientation of the interacting chromophores. This results in one of the transitions becoming optically forbidden.[38] It was further determined that dyes that interact by stacking in a cofacial manner result in H-aggregates, while arrangement of the dyes in a head-to-tail manner results in J-aggregates[39] (Figure 4).

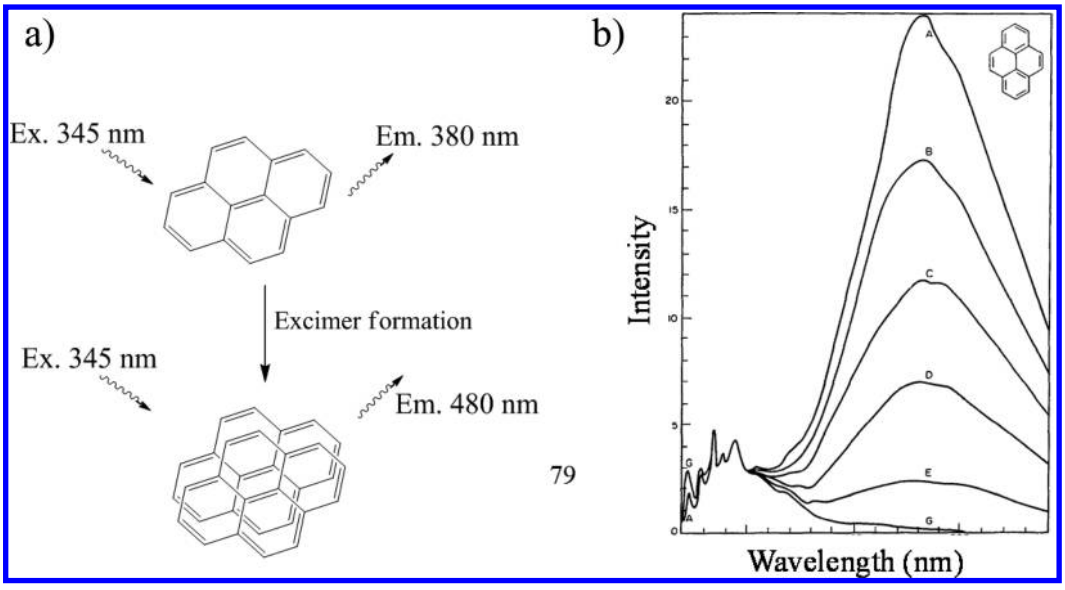

Figure 3. (a) Illustration showing the effect that intermolecular interactions between pyrene-based dyes have on emission spectrum. (b) Fluorescence emission spectra from pyrene as the concentration increases: G = 10^{-4} M, E = 10^{-3} M, D = 3.25 × 10^{-3} M, C = 5.5 × 10^{-3} M, B = 7.75 × 10^{-3} M, A = 10^{-2} M. Emission at 480 nm can be attributed to fluorescence from the pyrene excimer. Reprinted with permission from ref 31. Copyright 1963 Elsevier.

DOI: 10.1021/acs.chemrev.5b00140
Chem. Rev. XXXX, XXX, XXX−XXX

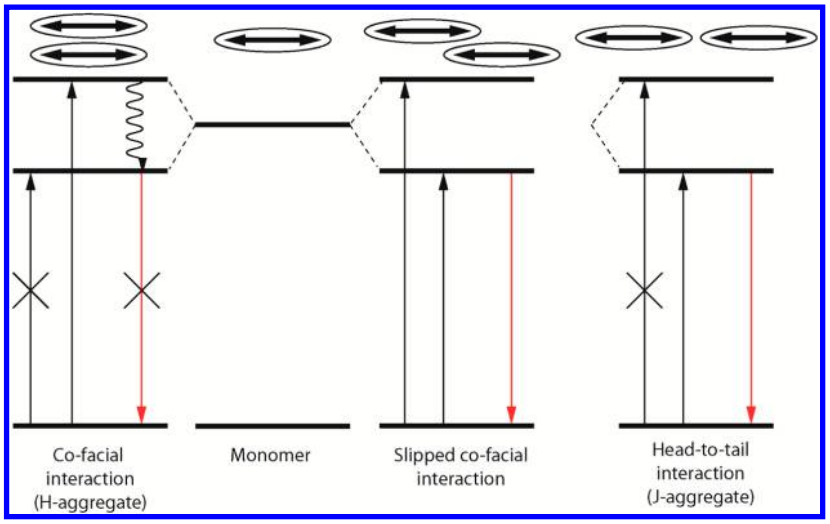

Figure 4. Influence of dye aggregate orientation on energetic transitions through the formation of molecular excitons.

4. PHOTOTHERANOSTIC TECHNIQUES INVOLVING SINGLET STATE RADIATIVE RELAXATION

Fluorescence occurs through the process of radiative relaxation from the singlet excited state. The emission of photons through fluorescence emission has enabled researchers to investigate both microscopic and macroscopic chemical and biological phenomena. In the medical sciences, fluorescence imaging has provided researchers with a detailed understanding of physiological processes and cellular functions. Beyond fluorescence microscopy, some applications of fluorescence in medicine include sentinel lymph node imaging,[40,41] fluorescence bronchoscopy,[42] fluorescence tracking of bacterial load in wound healing,[43] and fluorescence guided surgical resection.[44] These applications are made possible by the expansive number of fluorescent molecules that have been developed for imaging purposes. These include organic dyes, fluorescent proteins, inorganic nanocrystals, and conjugated polymers. The phenomenon of emission is highly influenced by the surrounding environment that the fluorophore is found within. Solvent effects as well as interactions with adjacent dyes or biological environments can change its photophysical properties. While this raises challenges for quantitative fluorescence, the sensitivity of a fluorophore to its environment presents an opportunity to develop nanostructures that can structure fluorophores to tune emission properties for greater imaging contrast and environmental sensing applications.

Various nanoscale systems have recently been developed to induce intermolecular interactions between dye molecules. These dye manipulations were undertaken to modulate their photophysical properties, which result in the enhancement of fluorescence brightness, shifted emission wavelength, and the creation of stimuli-responsive molecular sensors.

4.1. Molecular Interactions To Enhance Fluorescence Imaging

Contrast in molecular fluorescence imaging can be enhanced either by minimizing background signal from autofluorescence and nonselective binding or by increasing the positive signal generated from the labeling fluorophore. The latter can be achieved by increasing the concentration of the fluorophore in the target cell or tissue, or by chemical modification of the fluorophore's structure. However, there is typically a concentration limit beyond which cell toxicity and aggregation-induced quenching can occur.

To improve upon this issue, there have been concerted efforts to synthesize stable organic nanoparticles that are able to encapsulate multiple fluorophores in an emissive state. In some examples, organic dye nanoparticles are synthesized via reprecipitation techniques, which can form stable multimeric species in water, while others are stabilized through the action of amphiphilic surfactants. In other examples, organic dyes are inserted into scaffolds, which act to solubilize and prevent short-range aromatic stacking that can abolish fluorescence.

4.1.1. Fluorescence Enhancing Nanoparticles for Bioimaging Applications. *4.1.1.1. Nanoparticles with Aggregate-Induced Emission.* Contemporary investigations on fluorescent molecular dye aggregates for bioimaging applications were reinitiated by observations in the early 2000s that some organic dyes were fluorescent in the aggregated state despite being nonfluorescent when dissolved in compatible solvents.[45,46] The Tang group discovered that 1-methyl-1,2,3,4,5-pentaphenylsilole showed a 333-fold increase in fluorescence quantum yield when the dye went from a solubilized to an aggregated state.[45] A similar observation was made by An et al. in 1-cyano-*trans*-1,2-bis(4-methylbiphenyl)-ethylene aggregates where a ~700-fold increase in fluorescence quantum yield was observed.[46] In both examples, the aggregates were formed when the dyes were precipitated in water. Several explanations were provided including the formation of J-aggregates as well as interactions that promote planarization of the aromatic molecule.[47] This phenomenon has since been commonly referred to as aggregation-induced emission (AIE).

Similar to the pentaphenylsiloles, aminated tetraphenyl siloles were also found to form fluorescent aggregates in 90% water−THF mixtures.[48] Nanoparticle aggregates were measured to be ~200 nm and exhibited AIE enhancement that was 19-fold greater than the same dye dissolved in pure THF. Fluorescence quantum yield was determined to be 0.36 in the aggregated state and was attributed to planarization of the dye in the packed structure.

Lim and colleagues were interested in functionalizing α-cyanostilbene for in vivo bioimaging. To shift the fluorescence of the dye to the NIR regime, they substituted electron-accepting (3′,4′-dicyano) and electron-donating (4-dialkhylamino) groups into the chromophore. This dye was then

DOI: 10.1021/acs.chemrev.5b00140
Chem. Rev. XXXX, XXX, XXX−XXX

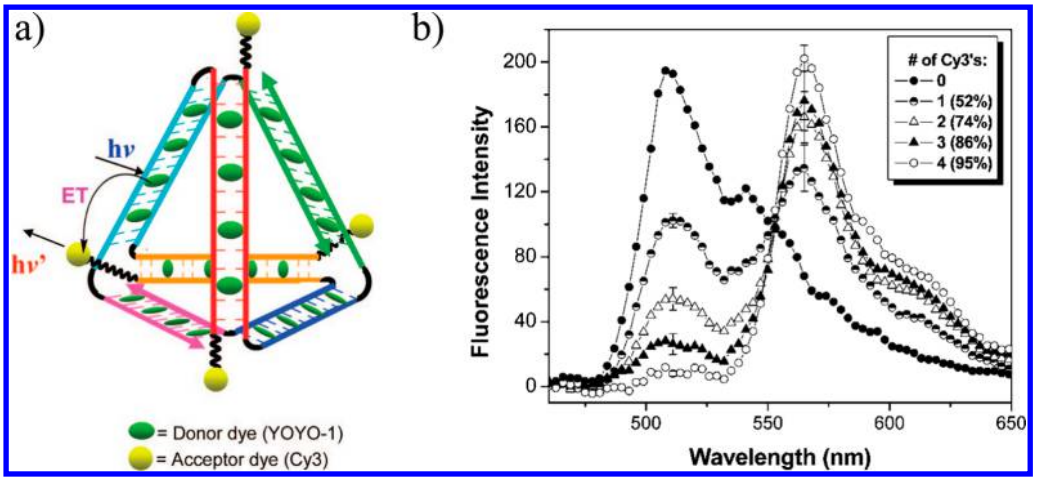

Figure 5. (a) Schematic of energy transfer process in tetrahedron nanotag conjugated with Cy3 and intercalated YOYO-1. (b) The influence of Cy3 loading on YOYO-1 fluorescence. Note the fluorescence quenching from YOYO-1 donor dye as Cy3 concentration increases. Reproduced with permission from ref 57. Copyright 2009 American Chemical Society.

stabilized through conjugation to glycol chitosan polymers.[49] When the ratio of the α-cyanostilbene chain was increased from 5 to 83 (mol %) of the overall polymer, a 9-fold enhancement in fluorescence quantum yield was observed, while a red-shift was observed in the fluorescence emission. Polymeric nanoparticles prepared with this dye were successfully imaged within HeLa cells and subcutaneously in mice. Nanoparticles with 50% labeling were found to be 35 times more fluorescent than the nanoparticle with 20% labeling. Meanwhile, only a 1.4-fold difference was observed in vitro. This difference could be attributed to the NIR shift in the fluorescence emission with α-cyanostilbene loading.

Tetraphenylethene (TPE)-based dyes have also been investigated for their AIE properties. TPE is well-known for its ability to become fluorescent as an aggregate. Rotation of the phenyl rotors in the monomeric state causes the molecule to relax efficiently through the nonradiative vibrational pathway. However, as stacking of the dyes minimizes rotation of the phenyl rings, increased planarity of the aromatic molecule is achieved and results in increased relaxation from a radiative pathway upon aggregation. Beyond its known AIE property, TPE has also been investigated as chemical adducts to induce AIE in fluorophores that typically become quenched upon aggregation.[50−54] Zhao et al. synthesized surfactant stabilized organic dye nanoparticles by forming fluorescent aggregates in tetraphenylethene-modified perylene bisimide molecules.[53] Stabilization using DSPE-PEG_{2000} and DSPE-PEG-folate during the reprecipitation method resulted in nanoparticles that are ~57 nm in diameter. The dyes when aggregated displayed a 267-fold increase in fluorescence quantum yield when compared to the individually dispersed dyes in the favorable THF solvent. These nanoparticles emit in the NIR and thus are suitable for in vivo imaging applications. In a second example, Qin and colleagues took a molecule, known to be quenched upon aggregation (TPA-DCM), and conjugated two TPE molecules onto the dye, one on each side of the structure.[50] Stable aggregates were formed by sonication of the dye with bovine serum albumin and inducing protein cross-linking with glutaraldehyde. These aggregates protected by the BSA corona display no cell toxicity over 48 h when treated at concentrations up to 800 nM. Furthermore, the aggregates were approximately 3 times more stable than comparable irradiation of fluorescein isothiocyanate in MCF-7 cells. Given their enhanced photostability and enhanced fluorescence, dye aggregates formed from tetraphenylethene conjugation have been investigated with promising results for long-term cell tracking[55] and intravital imaging.[52]

4.1.1.2. DNA-Based Nanostructures. Beyond dye aggregates, which display increased fluorescence in the aggregated state, there are other nanoparticle systems that leverage efficient energy transfer of absorbed light energy for enhanced fluorescence imaging as well as tunable wavelength applications. There are several reports of using DNA as fluorescence tags in cellular environments. The Armitage group developed nanoscale multichromophore assemblies using DNA as a scaffold.[56−58] These macromolecular fluorescent assemblies, known as "DNA nanotags", utilize energy transfer between closely spaced dyes to concentrate light energy and direct them toward one of several acceptor fluorophores in the structure. For their DNA insertion studies, Benvin et al. utilized YO-PRO-1 and YOYO-1, DNA intercalating dyes with high DNA binding affinity (YO-PRO-1 $\approx 10^6$ M^{-1}; YOYO-1 $\approx 10^9$ M^{-1}) and a large extinction coefficient ($\varepsilon_{YO\text{-}PRO\text{-}1} = 5.2 \times 10^4$ M^{-1} ; $\varepsilon_{YOYO\text{-}1} = 9.89 \times 10^4$ M^{-1}).[56] They determined in their three-way junction (3WJ) DNA oligomer nanostructure that a maximum of 15 YO-PRO-1 dyes could be intercalated, which results in an overall extinction coefficient of 780 000 M^{-1}. Insertion of a FRET acceptor dye (Cy3) into the DNA structure via dye displacement or by covalent modification of the DNA resulted in a multichromophore assembly that was able to funnel light from a series of acceptors to a few donors through a FRET mechanism. This intermolecular interaction between the dyes allows more light to be absorbed and also enables wavelength shifting of the fluorescence emission. Last, labeling the 3WJ DNA with streptavidin allowed them to use these nanotags to image $CD3^+$ mouse T-cells after prebinding with a biotinylated anti-CD3 antibody. As a follow-up to this study, Özhalıcı-Ünal and Armitage showed that the same procedure could be used to modify three-dimensional tetrahedron (TH) DNA nanostructures to accomplish the same task (Figure 5).[57] Comparing the photostability of the two nanostructures (10 min irradiation; visible light), TH showed a 5% fluorescence decrease versus a 30% decrease in the linear nanostructure. In addition, TH was more resistant to DNase 1 degradation (0%), than either the linear (~40%) or the 3WJ structures (~90%).

DOI: 10.1021/acs.chemrev.5b00140
Chem. Rev. XXXX, XXX, XXX−XXX

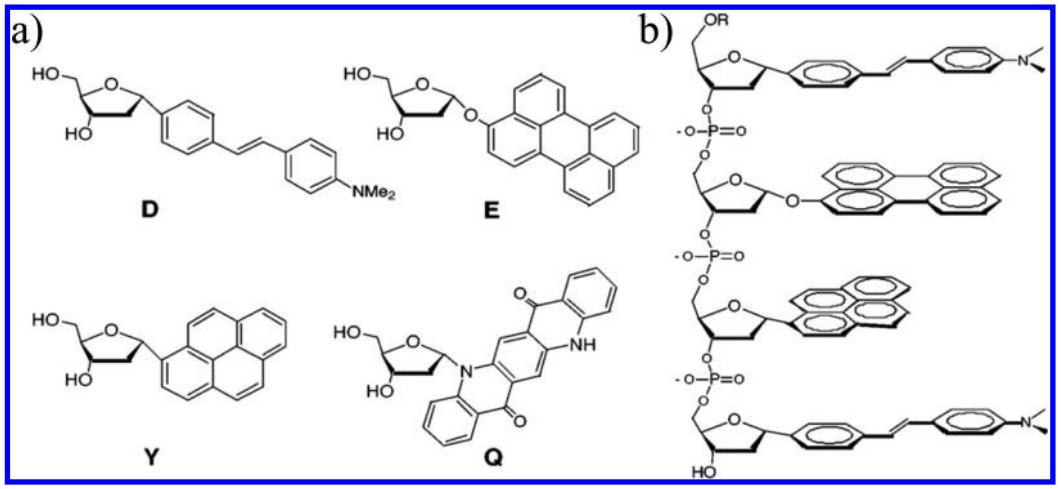

Figure 6. (a) Structure of "fluoroside" molecules examined in the study. (b) Example of tetramer of fluoroside with sequence: 5′DEYD. Reproduced with permission from ref 60. Copyright 2002 American Chemical Society.

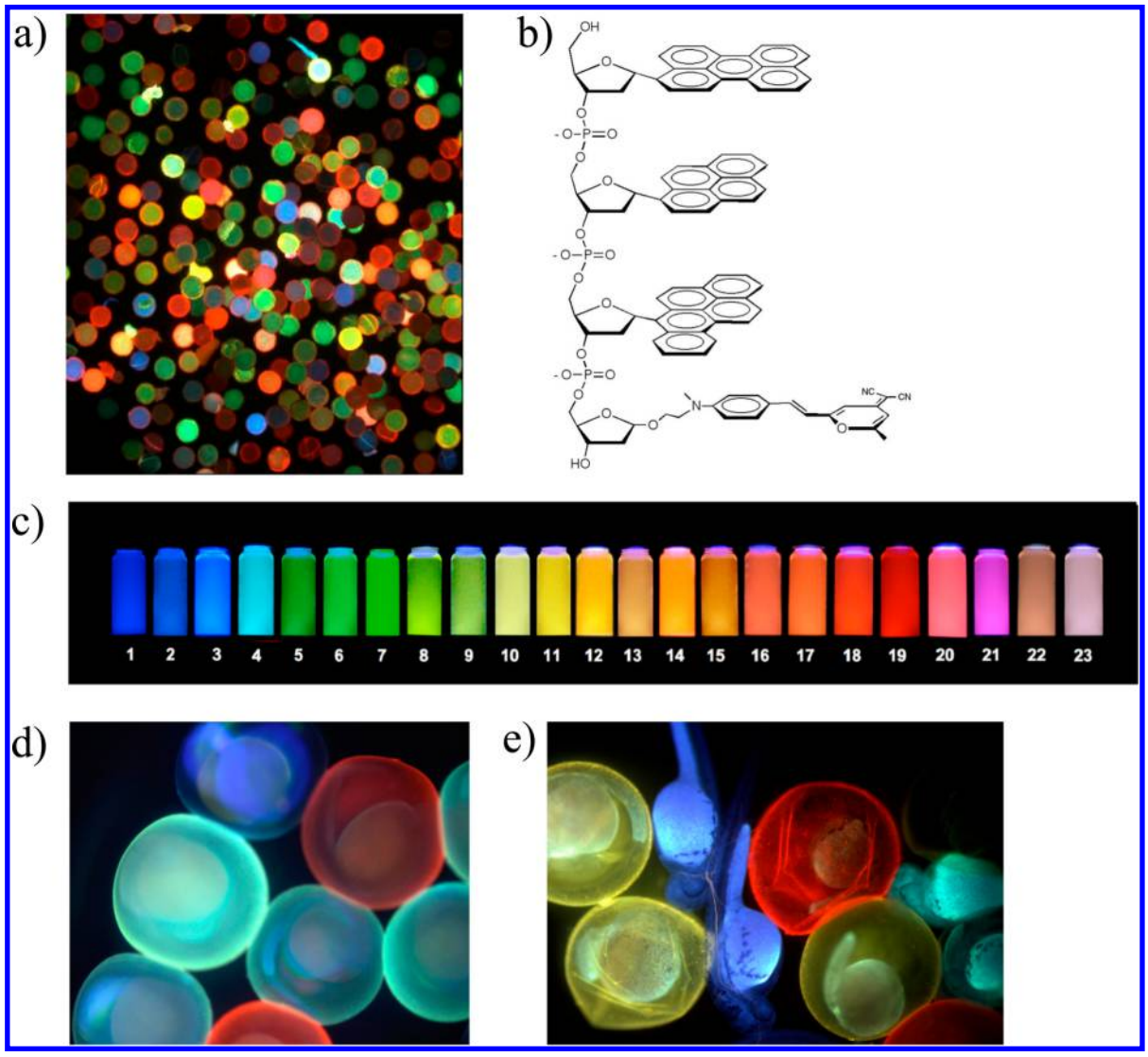

Figure 7. Multicolor set of polyfluoroside labels from a single excitation wavelength. (a) Image from 4096-member tetramer library of oligodeoxyfluorosides on polystyrene beads upon 340−380 nm excitation. (b) Typical structure of tetramer sequence. (c) Combined photograph from 23 selected oligodeoxyfluorosides, which cover the visible spectrum. Samples are dissolved in phosphate buffered saline (excitation = 354 nm). (d) Use of oligodeoxyfluorosides to simultaneously visualize four live zebrafish embryos at 24 h postfertilization and (e) 48 h postfertilization. Reproduced with permission from ref 62. Copyright 2009 American Chemical Society.

DOI: 10.1021/acs.chemrev.5b00140
Chem. Rev. XXXX, XXX, XXX−XXX

Fluorescent DNA-based tags can also be prepared through modification of the nucleotide bases instead of through intercalation.[59] Kool and co-workers built composite DNA fluorophores using custom synthesized "fluorosides".[60−62] These molecules are comprised of deoxyribonucleotide bases with the nitrogenous base replaced by planar aromatic fluorophores (Figure 6a). The overall goal was to design fluorescent DNA dyes (fluorotags) of varying colors that could be excited with a single wavelength of light. In early studies, Gao et al. created a test library of tetramers from these synthetic nucleotides using solid-phase synthesis techniques (Figure 6b).[60] From their initial 256-compound library, they were able to identify three tetrafluors that could be excited from the same light source, but emitted at three separate wavelengths. In some cases, an apparent Stokes shift in excess of 200 nm was observed. Although the authors did not discuss in detail the exact mechanism for the Stokes shift, they attribute the varying fluorescence spectra to varying degrees of interchromophore interactions, which give rise to FRET, excimer, exciplex, and charge-transfer processes.[60] In a follow-up study, Teo et al. expanded the library to 4096 tetramers generated from the permutations of 8 unique fluorosides[62] (Figure 7a−c). They also added spacer monomers to increase water solubility and decrease interchain aggregation. From these studies, they were able to isolate 23 unique fluorotags, which spanned the entire visible fluorescence emission spectrum (350−700 nm). They also tested these fluorotags with success in various biological models including mammalian cells and zebrafish embryos (Figure 7d).[62] DNA fluorotags were also shown to be excellent FRET donors.[63] Conjugating a FRET acceptor (Cy5) at the end of the DNA oligomer resulted in efficient energy transfer from the two dyes with transfer efficiencies reaction over 70% in the 5′-EYYSS-Cy5−3′ sequence.[63] Further demonstrating the applicability of their DNA platform, Wang et al. showed high-speed, multicolored tracking of various single and multicellular organisms.[64] Excitation with a single light source enabled rapid video-rate imaging of Hela cells, zebrafish (*Danio rerio*) embryos, as well as motion-tracking of invertebrate shrimp (*Artemia salina*) and paramecia (*Paramecium caudatum*).

4.1.1.3. Virus-Based Nanoparticles. Nanoparticles based on plant and bacteria-based virus have been investigated for bioimaging applications.[65−68] The protein capsid structure found on viruses is formed from the self-assembly of protein monomers. By introducing unique amino acid sequences at noncritical locations of the protein, it is possible to make modifications on both the internal and the external structures of the virus. Miller et al. utilized the plant-based tobacco mosaic virus (TMV) as a protein scaffold to which organic dyes were conjugated.[69,70] While the focus of the work was on the virus-based light harvesting, the results from this research can nevertheless inform research in viral nanoparticles for biomedical applications. Modifications to TMV were made through a single serine to cysteine modification (S123C) on the capsid protein of the wild-type virus.[69] Chemical modification was conducted on the virus after isolation from *Escherichia coli* by conjugating organic dyes to the protein via thiol-reactive chemistry at the cysteine moiety. Fluorescent donors and acceptor dyes were selected on the basis of their photophysical properties, as well as their spectral overlap. For initial FRET studies, Oregon Green and Alexa Fluor 594 were used. Assembly of the virus resulted in a cylindrical structure where an estimated 700 dyes were conjugated per 100 nm length of the rod.[70] The estimate of dye separation distance was 1.8 nm along the circumference and 2.3 nm along the length of the rod. On the basis of these estimates, the dyes were within the Förster radius for energy transfer. The FRET efficiency was only determined to be 47% for the optimal ratio of acceptor:donor (33:1 mol ratio). Remarkably, an antennae effect was observed in the system. Excitation of the donor dye led to an enhancement of acceptor fluorescence by a factor of 8.2, when compared to exciting the acceptor alone. The results from these studies have interesting implications for their medical photonics applications. The application of these viruses that display a significant antennae effect and efficient energy transfer can in principle be used as fluorescence probes for increased fluorescence through an enhanced optical absorption cross-section. Applications of this virus-based antennae technology might also be useful in the context of other treatment or imaging modalities such as PDT. In fact, this technique of modifying TMV with organic dyes has been applied to porphyrin photosensitizers for light-harvesting applications,[71] but it is conceivable that this system can be adapted for biological phototheranostic use.

Viruses have been used for intravital imaging of prostate cancer.[66] Cowpea mosaic virus (CPMV) was externally labeled with AlexaFluor-647 by a lysine coupling reaction between its terminal amine and *N*-hydroxysuccinimide (NHS)-activated ester on the dye. The targeting bombesin peptide and stabilizing polymers were added a viral coat using click chemistry. Bombesin is a peptide ligand that binds to gastrin-releasing peptide (GRP) receptors, which is overexpressed in PC-3 prostate cancer cells.[72] Cell studies and intravital imaging showed that the virus coated with the targeting ligand displayed uptake within PC-3 prostate cancer cells. Inhibition studies with unlabeled bombesin peptide (10-fold molar excess) resulted in blocking of nanoparticle uptake by cells. Furthermore, intravital imaging results showed that the virus targeted with the peptide displayed a significant increase in fluorescence signal within the tumor as compared to the untargeted control.[66] A second investigation into CPMV as a fluorescence agent for biological imaging suggests that surface dye labeling density can affect the observed fluorescence intensity as well as the cell−virus interactions.[73] CPMV nanoparticles were modified with Cy5 dyes at various ratios to elucidate the optimal amount of dye for loading. They found that 27 dyes per CPMV particle yielded maximal fluorescence, after which quenching occurs. This result is possibly due to the decrease in separation between dyes, which results in the formation of quenched dimers.[73]

Encapsulation of fluorescent molecules through noncovalent interactions is also another strategy for preparing viral nanoparticles for fluorescence imaging. Jung et al. devised a strategy to encapsulate the NIR optical imaging dye, indocyanine green (ICG), within the core of the reconstituted *brome mosaic virus* (BMV). BMV is a plant-derived ribonucleic acid (RNA) virus, which has an icosahedral capsid comprised of 180 identical subunits.[74] The internal face of each subunit is positively charged due to the presence of arginine residues. These amino acids can interact with negatively charged residues of the viral RNA. Jung et al. purified the capsid protein from genetic material and used its charge characteristic to bind negatively charged ICG prior to virus assembly. This enabled encapsulation of ICG upon capsid self-assembly. ICG encapsulated in this way exhibited greater solution stability at physiological temperatures when compared to the free dye. Fluorescence imaging with the gene-free BMV nanoparticles

DOI: 10.1021/acs.chemrev.5b00140
Chem. Rev. XXXX, XXX, XXX−XXX

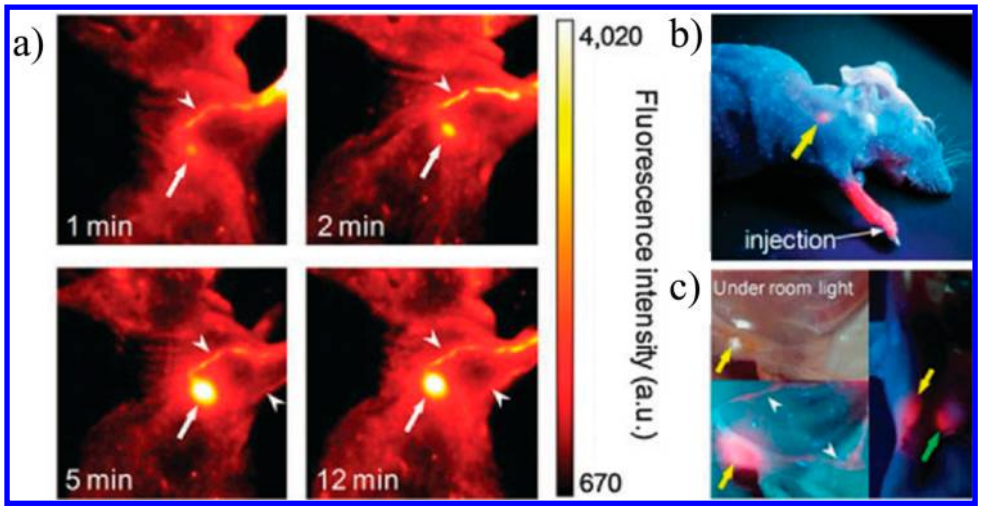

Figure 8. Sentinel lymph node imaging of injected conjugated polymer nanoparticle. (a) NIR whole-body fluorescence images of mouse over 12 min upon injection of NIR polymer dots (10 mL of 1.7 mg mL) into the right front paw. (b,c) True color fluorescence image of mouse after injection with agent to demonstrate visibility of probe under ambient lighting conditions. Yellow and green arrows illustrate the axillary and lateral thoracic lymph nodes, respectively. White arrows denote lymphatic vessels. Reproduced with permission from ref 86. Copyright 2010 Royal Society of Chemistry.

was done by incubating these particles with human bronchial epithelial cells. Uptake and imaging was successfully undertaken. The authors could not make conclusions on the exact mechanism for uptake but speculated that it was due to nonspecific endocytosis or an interaction with cell surface proteins.[75]

4.1.1.4. Conjugated Polymer Nanoparticles. Conjugated polymers (also known as conductive and semiconducting polymers) are organic macromolecules that possess extended π-conjugation along the backbone of their polymer chain. The conjugation enables excited electrons to be delocalized across multiple repeating units and confers these materials with semiconductor-like properties. Furthermore, due to the proximity of chromophores along the chain and through space, conjugated polymers can undergo efficient energy transfer to chromophores on the chain as well as to other organic absorbers nearby. Nanoparticles based on these polymers can be synthesized by direct polymerization in a heterophase systems or by postpolymerization processing through reprecipitation or emulsion evaporation.[76] In terms of biological applications, conjugated polymer nanoparticles possess properties that make them amenable to cell and whole body fluorescence imaging. The strong absorption and fluorescence is accounted for by the large number of chromophores in each nanoparticle, while the interchromophore interactions lead to the formation of intra- and interchain excitons. These excitons give rise to shifts in the absorption and fluorescence spectra as well changes to the fluorescence efficiency from the polymer.[77] Light absorption cross-sections are in the range of 10^{-13} cm^2, while fluorescence quantum yield can exceed 40%.[78] Recent advances in aqueous solution processing and surface modification of these nanoparticles raise the prospect of enhancing their biocompatibility and building in receptor specificity for targeted imaging applications.

The fluorescence properties of conjugated polymer nanoparticles stabilized in water were initially characterized by McNeill and colleagues.[78−84] They were also one of the first groups to investigate their applications for biological imaging. Early work led to the optimization of the reprecipitation technique for synthesizing conjugated polymer nanoparticles.[82] Nanoformulation of polyfluorene (PF), [(9,9-dioctyl-2,7-divinylene-fluorenylene)-*alt-co*-(2-methoxy-5-(2-ethylhexyloxy)-1,4-phenylene)] PFPV, and MEH-PPV polymers led to a decrease in fluorescence in water versus THF, corresponding to a 4-, 7-, and 25-fold reduction in quantum yield, respectively. Despite this reduction, polymers could still be used as cell imaging labels and were successfully imaged in macrophages.[78] Further cell studies revealed that internalized cells were localized in punctate structures adjacent to the nucleus, suggesting they were trapped within vesicles.[85]

Another interesting property of conjugated polymers is the possibility of tuning their optical properties through the addition of fluorescent energy acceptors. Wu et al. discovered it was possible to dope poly(9,9-dihexylfluorenyl-2,7-diyl) (PF) polymers with energy-accepting conjugated polymers to extend the wavelength of emission from PF conjugated polymer nanoparticles.[81] PF conjugated polymers were doped with poly[(9,9-dioctyl-2,7-divinylenefluorenylene)-*alt-co*-(2-methoxy-5-(2-ethylhexyloxy)-1,4-phenylene)] (PFPV), poly[(9,9-dioctylfluorenyl-2,7-diyl)-*co*-(1,4-benzo-(2,1,3)-thiadiazole)] (PFBT), or poly[2-methoxy-5-(2-ethylhexyloxy)-1,4-phenylenevinylene] MEH-PPV polymers at doping percentages from 0% to 10%. They discovered that by increasing the dopant concentration, it was possible to increase fluorescence emission from the nanoparticle at the cost of increased host PF polymer quenching. The enhancement in fluorescence emission reached a plateau at 6%, beyond which no increase in fluorescence emission was observed. The energy transfer process was attributed to a Förster mechanism, although the possibility of Dexter energy transfer was not ruled out. Using this energy transfer strategy, Wu et al. were able to extend the Stokes shift in PV nanoparticles by ca. 30 nm (PFPV), ca. 60 nm (PFBT), and ca. 100 nm (MEH-PPV).[81] One potential application of these results is multiplexed fluorescence imaging of multiple biomarkers in parallel. However, given the broadness of the emission band, successful execution would require another strategy to narrow the emission spectrum in each nanoparticle.

Conjugated polymer nanoparticles have been applied as fluorescent in vivo imaging probes. Because of their small size,

DOI: 10.1021/acs.chemrev.5b00140
Chem. Rev. XXXX, XXX, XXX−XXX

biocompatibility, and bright fluorescence emission, conjugated polymer nanoparticles are excellent tools for studying processes that require sensitive detection. Kim and colleagues demonstrated the application of NIR-emitting cyano-substituted derivatives of poly(*p*-phenylenevinylene) (CN-PPVs) polymers for sentinel lymph node mapping upon administering the nanoparticle in the forepaw of a mouse model[86] (Figure 8). Nanoparticles were decorated with carboxyl groups on the surface of the nanoparticle by co-condensation of the fluorescent polymer with poly(styrene-*co*-maleic anhydride). Anhydride moieties hydrolyze to yield carboxyl groups when exposed to an aqueous environment. These functional groups were then reacted with the 36 amino acid peptide, chlorotoxin, through EDC bioconjugation chemistry to generate the targeted nanoparticles. The chlorotoxin peptide has a strong binding affinity for neuroectodermal tumors[87] and was used to localize the nanoparticle to the brain tumor. Fluorescence imaging in either healthy mice or mice induced with medulloblastoma showed enhanced localization of the targeted nanoparticle in the cerebellum[88] of the tumor-bearing animal versus the control.

4.2. Molecular Interactions in Fluorescence Sensing

Exploiting molecular interactions that take advantage of singlet state radiative relaxation is useful for designing environmental sensing and stimuli responsive organic nanoparticles. While the system for how this is accomplished varies depending on the material platform, the analyte, or the environmental condition detected, the mechanism for how the sensing is translated into a measurable signal is well-defined. For the singlet state relaxation pathway, proximity and orientation of the chromophores in the nanoparticle can be combined with an appropriate mechanism to sense a multitude of stimuli. Short-range through-space interactions are governed by excimer formation, J-aggregation, and photoinduced charge transfer interactions, while longer-range interactions can occur through a FRET mechanism.

The detection of environmental parameters such as tissue temperature and pH has been demonstrated using interacting dyes embedded within organic nanoparticles. These parameters can be used in monitoring treatment progress (i.e., measuring tissue temperature during thermal therapy) or as a way to detect diseases, which shift the pH equilibrium in the body (i.e., cancer).

4.2.1. Nanoparticles for Fluorescence Sensing Applications. *4.2.1.1. Temperature Sensing.* Fluorescent temperature sensing nanoparticles have been developed using stimuli-responsive polymers that exhibit a lower critical solution temperature (LCST). Pietsch et al. developed a thermoresponsive polymer capable of fluorescently reporting temperature using the formation of excimers.[89,90] Employing pyrene conjugated to poly(methyl methacrylate) (PMMA), the authors demonstrated that an increase in temperature between 11 and 21 °C resulted in a decrease of excimer fluorescence. Increasing the solution temperature above the LCST resulted in the conversion of the nanoparticle from a hydrophilic to a hydrophobic environment. This altered the aggregation state of the pyrene molecules, promoting the separation of the dyes, thus causing a decrease in excimer fluorescence. Increasing the temperature of the polymer above its LCST resulted in the increase in nanoparticle size, which was not accounted for in the study. This could have a confounding effect on the measured fluorescence due to the potential for increased scattering of both the excitation and the emission, which would both result in a decrease in measured fluorescence. Furthermore, given that these nanoparticles are only capable of monitoring temperature over a narrow range that is lower than physiological temperature, they are not expected to be useful in measuring tissue temperature during thermal therapy. However, varying the molecular structure and composition of the polymer is expected to enable tuning the LCST to a higher temperature and thus enable measurements in the physiological range. This has been accomplished in thermoresponsive polymers such as poly(*N*-isopropylacrylamide) (PNIPA).[91] Another limitation of using the LCST property in thermosensitive polymers in fluorescence sensing applications is the fact that the phenomenon that alters the excimer fluorescence also induces turbidity through aggregation of the polymer. This behavior alters the scattering properties in solution and can have a negative impact on quantification of signal change.

4.2.1.2. pH Sensing. Dysregulation of pH is often a sign of disease, as the body or cell cannot maintain homeostatic conditions. Many cancers are characterized by a change in pH due to metabolic effects of rapidly proliferating cells under anaerobic conditions.[92] This change in pH represents an opportunity to design a material that can utilize this property as way to detect and assess disease. Recently, the Gao lab developed tunable pH-sensing polymeric nanoparticles.[93,94] The nanoparticle relies on homo-FRET interactions between the fluorophores conjugated to the polymer backbone (Figure 9a). The fluorophores selected for this study are known for their limited Stokes shift and enable quenching of fluorescence when dye molecules are brought in close proximity through micelle formation. The micellization (and hence pH sensing) process is driven by the delicate balance between the hydrophobic and hydrophilic polymer blocks, which is tuned by the ionization of the tertiary amines.[93,94] Modifying the hydrophobicity of the polymer influences the pH where micelle formation occurs (Figure 9b). These pH-sensing polymeric micelles were used to investigate the acidic and angiogenic microenvironment in various cancer tumor models.[95] Cyclic RGD was used to localize micelles to the tumor through $\alpha_v\beta_3$ integrin targeting. Significantly, this study showed that these micelles were capable of differentiating subtle changes in pH in the blood versus tumor microenvironment.

Frank Würthner's group synthesized water-soluble perylene dye vesicles via molecular self-assembly with pH-sensing capabilities.[96,97] Perylene bisimide (PBI) dyes have been used as organic semiconductors for applications in field effect transistors, light emitting diodes, and photovoltaic cells.[98] These dyes tend to be poorly water-soluble due to the large planar aromatic ring structure. Perylene bisimide dyes were modified with PEG-groups or aliphatic tails on both ends of the molecule to achieve a wedge- or a dumbbell-shaped amphiphilic dye molecule[96] (Figure 10). PBI 1 was found to be soluble in THF and exhibited a fluorescence spectrum that matched that of the monomeric perylene bisimide dye (500−600 nm). As THF was gradually replaced by water, the monomeric emission spectrum was slowly replaced by a broad, structure-less emission band (600−800 nm). This fluorescence was attributed to the formation of excimers. Mixing PBI 1−4 at various ratios resulted in the formation of several supramolecular structures including micelles, tubular aggregates, and vesicles.[96] To demonstrate the potential for using these perylene bisimide supramolecular structures for pH sensing, Zhang et al. combined PBI 1 and PBI 2 at a ratio of 20:1.[97] They then

DOI: 10.1021/acs.chemrev.5b00140
Chem. Rev. XXXX, XXX, XXX−XXX

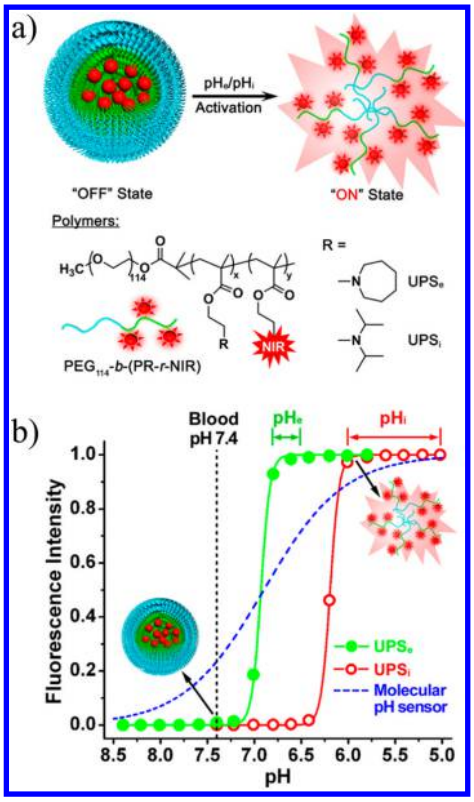

Figure 9. (a) Composition of two types of nanoprobe with pH transitions at 6.9 (UPS$_e$) and 6.2 (UPS$_i$). These nanoprobes activate in response to an increase in tumor acidity. The NIR probe used is Cy5.5 for animal studies. (b) Normalized fluorescence intensity as a function of pH for UPS$_e$ and UPS$_i$ nanoprobes. The blue dashed line simulates the pH response curve for a small molecule pH sensor (pK_a 6.9) calculated from the Henderson−Hasselbalch equation. Note the large difference in pH response in nanoprobes versus small molecule. Reproduced with permission from ref 95. Copyright 2014 Nature Publishing Group.

encapsulated a pH-sensitive bispyrene derivative within the aqueous core of the perylene bisimide nanovesicles. The bispyrene dye formed excimers at low pH but changes to the monomer as the pH of the solution increases. This change can be observed in fluorescence spectra as well as through changes in solution color (Figure 11a−c). The excimer emission spectrum overlaps with the absorption of the perylene bisimide vesicle membrane. Thus, the fluorescence signal arising from the pH sensor is re-encoded to a longer wavelength by the vesicle bilayer (Figure 11d). Energy transfer efficiency from the bispyrene dye and the perylene outer vesicle membrane varies with solution pH, ranging from 10% to 75% (Figure 11e). The spectral overlap J also varies in the same fashion and ranges from 3 to 12 × 10^{15} cm^{-1} M^{-1} nm^4.

Multichromophore DNA-based structures have also been created for fluorescence sensing in living cells. DNA is an attractive platform for the design of fluorescent nanosensors due to their ease of programmability and reproducible synthesis. Using intermolecular interactions between fluorophores as a reporter, Modi et al. synthesized a pH-sensing platform using a three-dimensional DNA motif, known as an I-switch.[99] Sensing was based on the pH sensitivity of cytosine bases placed at key locations along the scaffold (Figure 12a). Protonation of the thiol groups induces a conformational change in the DNA structure to form the i-motif. This change results in FRET interaction between Alexa-488 and Alexa-647 dyes. Using the ratio of fluorescence between these two molecules, it was possible to spatially and temporally track pH within living cells from pH 5.8 to 7 (Figure 12b). Taking this concept one step further, Modi and colleagues used two DNA i-switches with spectrally resolved FRET pairs to image the pH of two subcellular sites. Spatial specificity was achieved by conjugating targeting ligands to the two nanomachines. In this way, they demonstrated the ability to track pH in the early endosome as well as in the trans-Golgi network, two locations in the cell that possess noncytosolic pH.[100]

4.2.1.3. Protease Sensing. The overexpression of certain enzymes can signify the presence of disease. Several cancers are known to overexpress proteases, proteolytic enzymes that are responsible for many regulatory processes within the cell.[101] Given that some proteases are only highly expressed in the cancer tumor, these enzymes represent a good target for the development of imaging agents. The fluorescence quenching/unquenching mechanism is an excellent reporter of enzyme activity. One of the earliest applications of this concept in organic nanoparticles was initiated by Weissleder et al. in the demonstration of tumor-associated lysosomal protease detection using activatable polymeric nanoprobes in a xenografts mouse model.[102] The nanoprobes were synthesized a graft copolymer consisting of poly-L-lysine and methoxypolyethylene glycol with the fluorescence NIR Cy5.5 dye conjugated to the peptide side chains. Cleavage of the polylysine peptide resulted in separation of fluorophores and subsequent unquenching. A 12-fold enhancement in fluorescence was achieved comparing the cleaved and uncleaved probes.

Shi and colleagues designed a peptide-based dye agent, which irreversibly forms fluorescent aggregates upon specific caspase peptide cleavage and proposed a strategy for its use in real-time

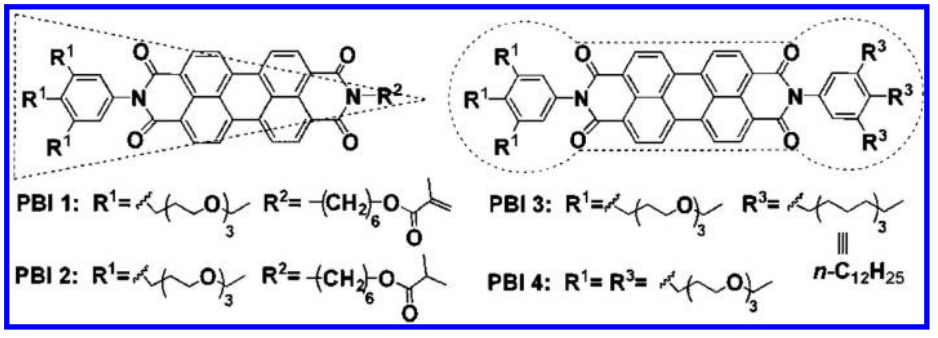

Figure 10. Structures of perylene bisimide derivatives. The dashed lines emphasize the geometry of the molecule. Wedge shape for PBI-1 and PBI-2 and dumbbell for PBI-3 and PBI-4. Reproduced with permission from ref 96. Copyright 2007 American Chemical Society.

DOI: 10.1021/acs.chemrev.5b00140
Chem. Rev. XXXX, XXX, XXX−XXX

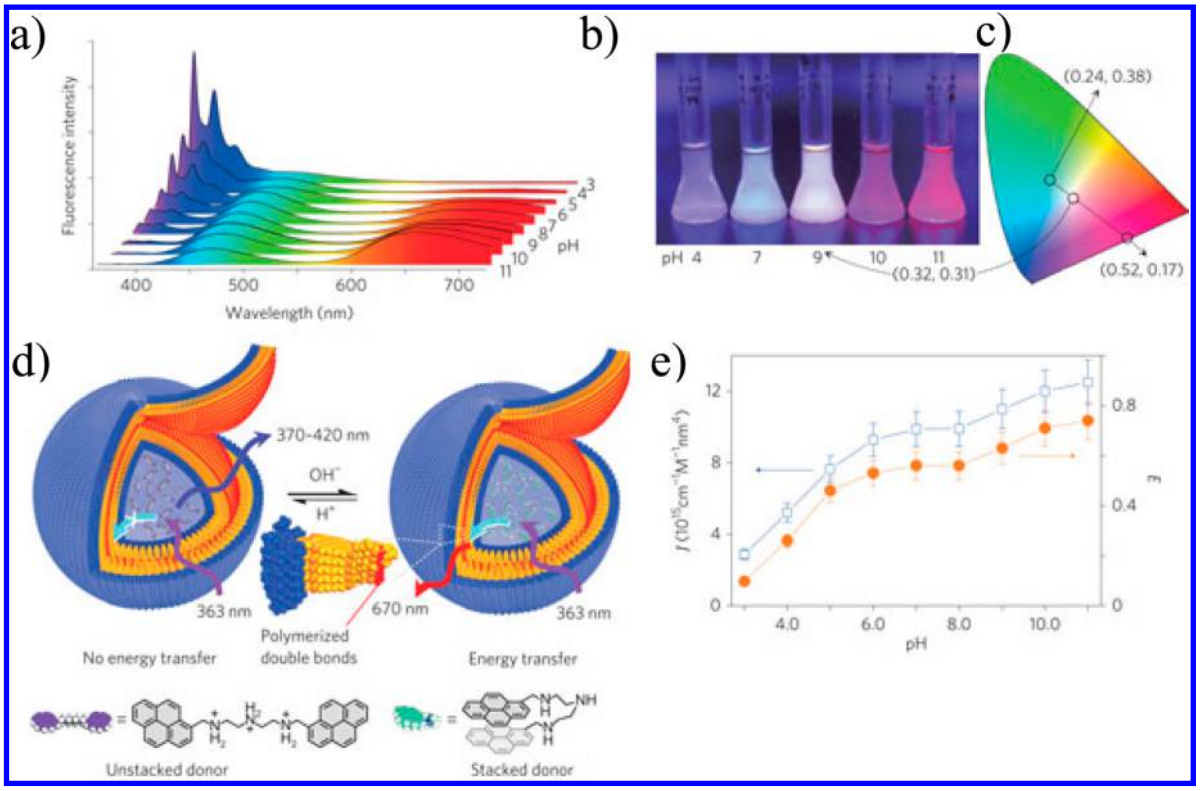

Figure 11. (a) Fluorescence emission spectra of donor-loaded polymerized vesicles at various pH values (3.0−11.0). (b) Photograph of donor-loaded polymerized vesicles in aqueous solution at various pH values under ultraviolet light (366 nm). (c) Color chromaticity diagram. Fluorescence coordinates for the donor excimers (0.24, 0.38), perylene membranes (0.52, 0.17), and white fluorescence coordinate (0.32, 0.31) for the donor-loaded polymerized vesicles at pH 9.0. (d) Schematic illustration of the donor-loaded polymerized vesicles. (e) pH-dependent energy-transfer efficiency (E, orange line) and overlap integral (J, blue line) of donor-loaded polymerized vesicles at pH 3.0−11.0. Each data point represents the average values, and error bars indicate the deviations from average (n = 3). Reproduced with permission from ref 97. Copyright 2009 Nature Publishing Group.

cell apoptosis monitoring.[103] The imaging agent is comprised of a caspase-3/-7 specific sequence (Ac-DEVDK-) with the aggregation-induced emission dye, TPE. TPE is nonfluorescent when solubilized as a monomer, but fluoresces as an aggregate (vide supra). This is due to the enhanced free rotation of the four phenyl rotor structures, which promote dissipation of excitation energy through rotational relaxation.[47] Specific cleavage of the peptide negatively affects the probe's solubility and promotes aggregation of the dye molecules. Aggregation of the dye inhibits rotation of the phenyl rotors and increases fluorescence.

4.2.1.4. H_2O_2 Sensing. Hydrogen peroxide (H_2O_2) is a molecule that is part of the family of reactive oxygen species (ROS) that have important implications in biology. It not only is involved in inflammatory responses, but it is also a byproduct of cellular metabolism and is involved in various cell signal pathways.[104] Because of its functions, the ability to sensitively visualize its presence in vitro and in vivo is important for gaining a greater understanding of cellular processes and also for diagnosis of inflammatory diseases. While H_2O_2 have been detected through the reaction with small molecule reactants, it is challenging to ensure all reactants are present in sufficient quantity at the site of reaction. Thus, organic nanoparticles provide an elegant strategy for H_2O_2 by virtue of the fact that multiple components can be loaded into a single nanoparticle. H_2O_2 sensing was first demonstrated in organic nanoparticles by Lee and co-workers in their design of polymeric peroxalate nanoparticles.[105] Using their nanoparticle platform, they were capable of trapping a three-component chemiluminescent reaction in the nanoparticle scaffold including peroxalate esters, fluorescent dyes, and H_2O_2. In the study, H_2O_2 was reacted with peroxalate to generate a chemically excited molecule, which then decomposes to CO_2 and, in the process, transfers its energy to the fluorescent dye. This dye then emits fluorescence signifying the presence of H_2O_2. The design tested involved perylene, rubrene, and pentacene, which enable the detection of H_2O_2 using three separate colors.

In another example, Lim et al. found that peroxyoxalate CL, a small molecule used for chemiluminescence experiments, can be loaded into Pluronic F-127 stabilized PLGA colloids. Peroxyoxalate CL has been found to be activated by hydrogen peroxide, but not by the hydroxyl radical, superoxide, or nitric oxide, and hence is a useful molecule for H_2O_2 detection.[106] By simultaneous loading of the NIR cyanine dye (Cy5) into the colloid, a nanoparticle system suitable for in vivo NIR imaging of H_2O_2 was achieved. The lower limit of detection for this sensing system was found to be above 10^{-8} M, which is 1 order of magnitude lower than normal in vivo hydrogen peroxide levels.[106] Imaging in vivo using a mouse model showed a 16-fold increase in fluorescence signal when comparing the animal joint treated with lipopolysaccharide (LPS), a molecule used to induce an inflammatory response. The authors followed up this study by showing that the same system would still work when the fluorescent Cy5 dye was replaced with 9,10-distyrylanthracene derivative, an aggregate forming molecule that is fluorescent in the aggregated state.[107]

DOI: 10.1021/acs.chemrev.5b00140
Chem. Rev. XXXX, XXX, XXX−XXX

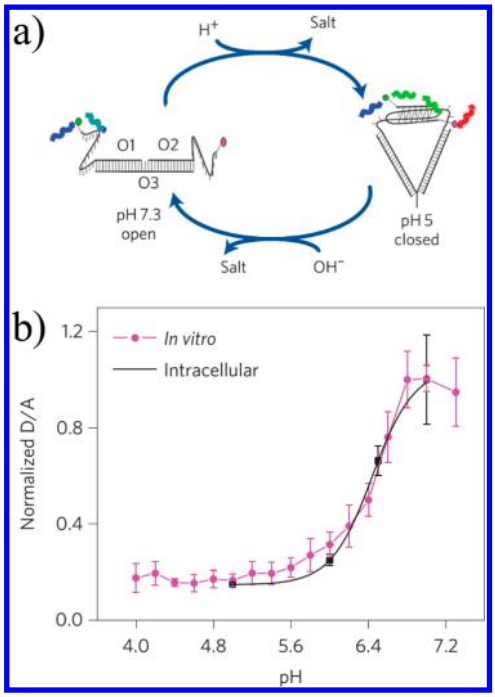

Figure 12. (a) Schematic for the operation of the i-switch DNA nanostructure capable of sensing pH between 5.8 and 7. Closure of the i-motif upon lowering the pH induces FRET between dyes located at both ends of the sequence. Lowering the pH results in separation of cytosine-rich overhangs, which prevents intermolecular interactions between dyes. (b) Ratio of fluorescence between donor and acceptor fluorophores shows the range in which pH can be determined. Reproduced with permission from ref 99. Copyright 2009 Nature Publishing Group.

5. PHOTOTHERANOSTIC TECHNIQUES INVOLVING INTERSYSTEM CROSSING/TRIPLET-STATE RELAXATION

5.1. Molecular Interactions That Modulate Reactive Oxygen Generation

Photodynamic therapy (PDT) is the therapeutic application of the process known as the photodynamic effect. This process involves the excitation of a light absorbing dye to an elevated singlet state, which then converts to the triplet state through intersystem crossing. Once the molecule is in this state, it can generate reactive oxygen species (ROS) through one of two mechanisms. In Type I PDT, the triplet-state photosensitizer interacts with nearby substrates by electron transfer. This activated substrate (i.e., lipids, proteins, nucleic acids) can then transfer energy directly to oxygen to generate free radical production in forms that may include the superoxide anion, hydroxyl radical, or hydrogen peroxide.[108] The second pathway, known as Type II PDT, involves direct transfer of energy from the photosensitizer to molecular oxygen. This interaction leads to the generation of singlet oxygen ($^1O_2$).[109] Singlet oxygen is capable of reacting with cellular components to induce oxidative effects that are toxic to the cell. If sufficient damage is caused within a short amount of time, apoptotic cell death occurs.[108] Intermolecular interactions between photosensitizers can be used to activate or inactivate intersystem crossing. This can occur simply by inducing stable ground-state quenching complexes between photosensitizers by bringing them in close proximity to each other. Aside from dye quenching, the presence of heavy atoms can also have an effect on the conversion of the photosensitizer spin state. Some examples of organic nanoparticle platforms that capitalize on these intermolecular interactions are discussed in the following section.

5.1.1. Energy Transfer in Nanoparticles for Two-Photon PDT. *5.1.1.1. Dendrimers.* Dendrimers have been synthesized for photodynamic therapy. Oar and colleagues synthesized a photosensitizer-linked dendrimer that was efficiently excited by two-photon excitation.[110,111] The dendrimer is comprised of a porphyrin core, branched polymer structure extending from the center, and a surface functionalized with the fluorescent AF-343 donor dye and stabilizing polyethylene glycol (Figure 11). Integration of the absorption spectrum for the synthesized dendrimer allowed for the determination of the donor dye:porphyrin ratio, which was found to be 7.7 AF-343 dyes to 1 porphyrin molecule. Two-photon fluorescence emission spectra of the dendrimer showed that over 99% of the donor emission was quenched, while the photosensitizer emission was found to be high as compared to an acceptor-less control dendrimer. These results indicate that energy transfer occurs efficiently between the two dye systems with an efficiency of 97%.[111] Last, the dendrimer was tested for its ability to sensitize oxygen, by measuring the photoluminescence spectrum of oxygen and by photobleaching of 9,10-anthracenedipropionic acid (ADPA). Results from both experiments provided evidence that singlet oxygen was generated.[111]

5.1.1.2. Conjugated Polymer Nanoparticles. For PDT to occur, the photosensitizer's triplet state energy must be at 0.98 eV or lower.[112] This number is important as it corresponds to the energy gap between triplet ground-state oxygen and singlet oxygen. Most photosensitizers reported to date are based on small molecule organic dyes; however, it is theoretically possible for conjugated polymers to undergo intersystem crossing and sensitize oxygen. Because the triplet state of most conjugated polymers is approximately 0.7 eV lower than its singlet state, energy transfer to oxygen is possible as long as the singlet state transition is 1.68 eV or higher.[113] Evidence for singlet oxygen generation can be observed in the photodegradation of electroluminescent polythiophene thin films, an undesirable process in polymer electronics.[114,115]

One of the first applications of conjugated polymers as photosensitizers in PDT was demonstrated in silica particles coated with positively charged poly(phenylene ethynylene). This polymer coating was found to exert a biocidal effect upon light treatment. The cell kill was attributed to the generation of ROS by the polymer. Singlet oxygen generation by the polymer was confirmed by photoluminescence measurements at 1265 nm and a chemical trap assay. Singlet oxygen quantum yield was determined to be 0.13 when measured in deuterated methanol and 0.069 when measured in water.[116] Additional studies have shown that reactive oxygen generation is not limited to the poly(phenylene ethynylene) polymers. Shen et al. were interested to see whether it was possible to increase the singlet oxygen quantum yield through covalent modifications to the polymer backbone.[117] They investigated poly(fluorene-2,7-ylenevinylene-*co*-phenylene) polymers with varying substitutions to the phenylene backbone. The phenyl group was modified with either electron-withdrawing cyano substitutions (PFVCN) or electron-donating methoxy substitutions (PFVMO). The singlet oxygen quantum yield was measured in each of the three samples. They discovered that while the unmodified control had a singlet oxygen quantum yield of

DOI: 10.1021/acs.chemrev.5b00140
Chem. Rev. XXXX, XXX, XXX−XXX

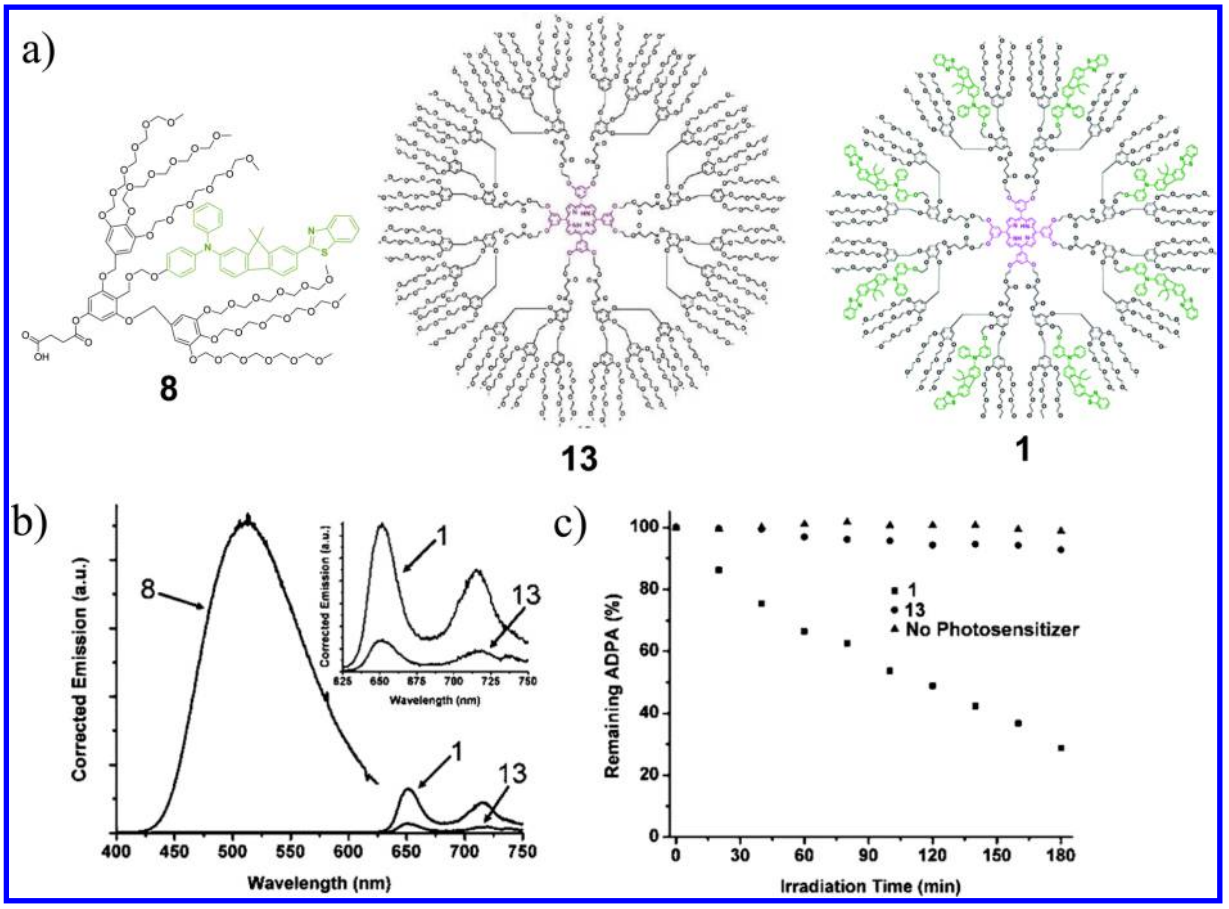

Figure 13. (a) Chemical structures of dendrimers used in study. (b) Two-photon-induced emission spectra for molecules 1, 8, and 13 upon excitation of AF-343. (c) Photobleaching of the chemical trap 9,10-anthracenedipropionic acid upon two-photon excitation at 780 nm. Reproduced with permission from ref 110. Copyright 2005 American Chemical Society.

0.056, modifications that add electron-donating groups (PFVMO) exhibited a decrease in singlet oxygen generation (0.043).[117] Displaying an opposite trend, samples containing electron-withdrawing groups (PFVCN) led to an increase in singlet oxygen quantum yield (0.069).[117] These studies demonstrate that conjugated polymers display intrinsic ROS generating capabilities.

While the singlet oxygen quantum yields reported or conjugated polymer nanoparticles seem unremarkable, especially when compared to more traditional small molecule photosensitizers, there are two advantages that conjugated polymer nanoparticles possess when considering their applications in photodynamic therapy. First, conjugated polymer nanoparticles possess large two-photon absorption coefficients when compared to small molecule dyes. The prospect of achieving two-photon PDT is tantalizing because two-photon illumination can provide much greater spatial control at depth than single photon illumination.[118] The second advantage is the fact that conjugated polymer nanoparticles are porous in nature and can undergo efficient energy transfer. Thus, by doping in a photosensitizer into the polymer matrix, it is possible to enhance the PDT efficacy of the doped molecule. In this approach, the conjugated polymer becomes a light harvesting antennae, serving the purpose of maximizing the probability of photosensitizer excitation. This concept of using conjugated polymer nanoparticles as two-photon light harvesting antennae for PDT has been pursued by several groups.[119−121]

5.1.2. Intermolecular Heavy Atom Effect in PDT. Typically, the presence of heavy atoms (e.g., iodine, chlorine, bromine, etc.) and metals (e.g., zinc, platinum, palladium, etc.) conjugated to a fluorophore or a photosensitizer can enhance its conversion to the triplet state through intersystem crossing. The presence of the heavy atom near the dye increases the efficiency of spin−orbit coupling and is known as the intramolecular heavy atom effect.[14] Intermolecular heavy atom effect can also occur.[122] As the name suggests, this form of the heavy atom effect is mediated by the collision of molecules. Using this process, Lim and colleagues demonstrated a strategy to enhance the singlet oxygen generation efficiency in photosensitizer-conjugated polymeric nanoparticles.[123,124] Their initial experiments focused on whether diatrizoic acid (3,5-bis(acetamido)-2,4,6-triiodobenzoic acid) when coloaded with chlorin e_6 in a polymeric micelle will result in an enhancement of singlet oxygen generation.[123] They found that incorporation of the heavily iodinated sample led to an enhancement of the singlet oxygen quantum yield (Φ_Δ). To enhance the stability of the loaded components, Lim et al. conjugated both the diatrizoic acid as well as the photosensitizer onto the backbone of a glycol chitosan (GC) polymer.[124] This modification minimized leakage of the dye from the polymer as well as ensured close interaction between the photosensitizer and iodinated molecule (Figure 12). Formulation of the nanoparticle resulted in an enhancement of its singlet oxygen generation efficiency when comparing the iodinated nanoparticle (Φ_Δ = 0.59) with the noniodinated

DOI: 10.1021/acs.chemrev.5b00140
Chem. Rev. XXXX, XXX, XXX−XXX

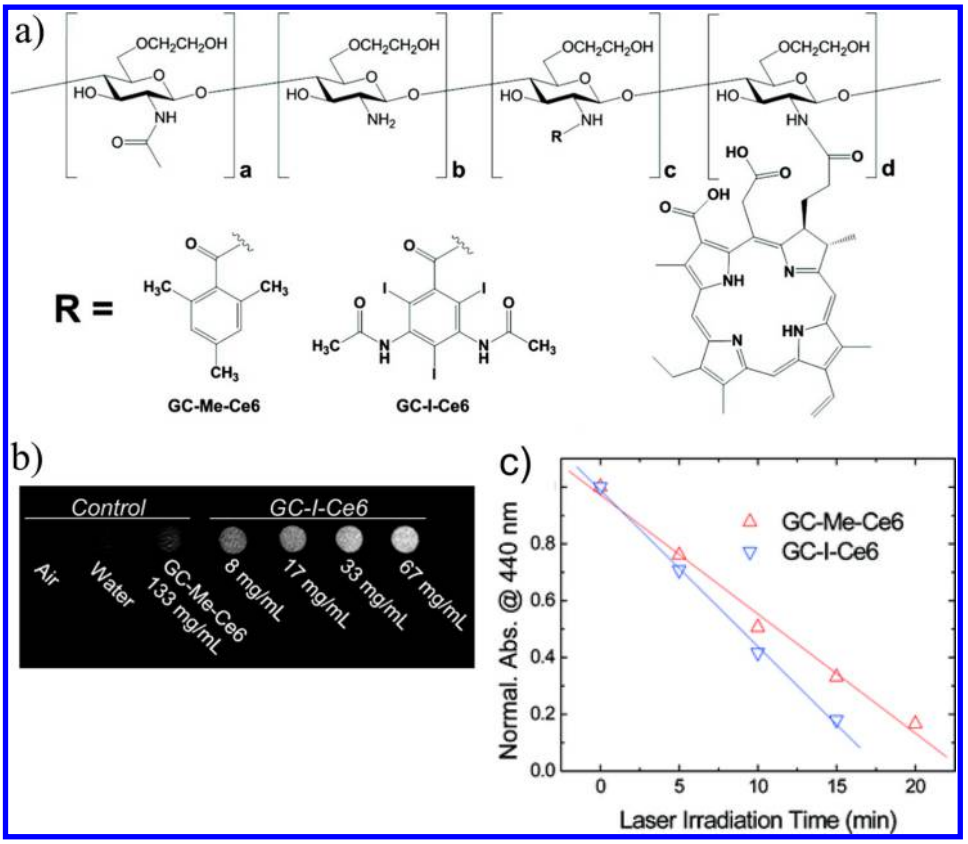

Figure 14. (a) Chemical structure of chlorin e_6-conjugated glycol chitosan polymer nanoparticle modified with diatrizoic acid. (b) Microcomputed tomography image showing the increased contrast generated with concentration (c) Photochemical bleaching of *p*-nitroso-*N*,*N*′-dimethylaniline in the presence of histidine upon irradiation at 671 nm. Reproduced with permission from ref 124. Copyright 2012 American Chemical Society.

control (Φ_Δ = 0.45). One of the most interesting aspects of this technology is the possibility of combining the enhanced singlet oxygen generation with the potential for tracking particle biodistribution using X-ray computed tomography, thus enabling an additional set of data that could be used to inform treatment planning using these nanoparticles.

5.1.3. Nanoparticles for Activatable PDT. The ability to activate a photosensitizer in response to a specific stimuli adds another level of selectivity that is already achieved by PDT's localized nature. This strategy of adding an activation mechanism to photosensitizers reduces the risk for off-target activation and skin photosensitivity, an issue with early photosensitizers. Intermolecular interactions between organic dyes housed within a nanoparticle system allow this technique to be fully realized. The mechanism(s) that maintains the "off" state in the photosensitizer is implemented through either a static quenching or a FRET quenching.

5.1.3.1. Polymeric Nanoparticles. One of the first nanoparticles to exploit this property was in the study of water-soluble copolymers based on *N*-(2-hydroxypropyl)-methacrylamide with meso-chlorin e_6 photosensitizers conjugated through a degradable peptide sequence (GFLG).[125] Self-assembly of the polymer resulted in aggregation-induced quenching as evidenced by a shift in absorption. This effect was promptly reversed after peptide cleavage. Comparing the PDT effect of the cleavable peptide nanoparticle with a noncleavable control in Neuro 2A neuroblastoma bearing mice showed a ~3-fold reduction in tumor volume in the cleavable peptide group after 4 days.

Lee et al. developed conjugated protoporphyrin IX (PPIX) loaded GC nanoparticles by conjugating the photosensitizer to the GC polymer through carbodiimide coupling chemistry. Nanoparticles formed were approximately 280 nm in diameter with 42 molecules of PPIX conjugated per polymer chain. When assembled, these nanoparticles were found to be fluorescently quenched and exhibited a decrease in the amount of reactive oxygen generated.[126] This was attributed to self-quenching through reversible molecular interactions between PPIX molecules. Reversal of self-quenching was observed when sodium dodecyl sulfate (SDS) was added or during long incubation periods within cells. Presumably, the harsh environment found within cellular endosomes facilitated the unquenching process, although the exact mechanism is unknown.

Using a more robust activation mechanism, Oh et al. developed GC-pyropheophorbide *a* nanoparticles linked through a disulfide bond instead of an amide linkage[127] (Figure 13). This modification enabled the release of the photosensitizer in the presence of the reducing environment found within cellular endosomes and lysosomes.[128] Nanoparticles prepared with the thiol linkage were found to exhibit a greater therapeutic potency when irradiated with light than the control nanoparticle with the nonreducible linkage. In a similar application, Yoon et al. demonstrated that the activatable PDT strategy can be recapitulated with PEGylated-hyaluronic acid (HA) polymers.[129] In this example, activation of the nanoparticle was mediated by the activity of the hyaluronidase enzyme, which is known to be upregulated in many cancer cell types. HA polymers were conjugated with 5β-cholanic acid to

DOI: 10.1021/acs.chemrev.5b00140
Chem. Rev. XXXX, XXX, XXX−XXX

increase hydrophobicity of the polymer, while the fluorescence quencher BHQ3 was conjugated to HA. Chlorin e_6 was loaded into the polymer using a cosolvent procedure.[130]

5.1.3.2. Porphyrin−Lipid Nanostructures. Porphysomes are porphyrin−lipid nanovesicles, which are formed through self-assembly.[131,132] The tightly packed pyropheophorbide *a*-lipid (pyro-lipid) dyes embedded within the vesicle bilayer result in an exceptionally large molecular absorption coefficient ($\sim 10^9$ M^{-1}) as well as efficient excited-state quenching (>99% quenching) (Figure 14). In the intact state, the photosensitizers are quenched and hence will generate only a small amount reactive oxygen upon excitation. However, degradation of the porphysome structure leads to an increase in photosensitizer activity due to photophysical unquenching. When degradation occurs within a cellular compartment of a tumor, this can be used advantageously for PDT. Recently, Jin et al. investigated the use of folate-conjugated porphysomes for targeted PDT.[133] Uptake by KB cells expressing the folate receptor led to a rapid unquenching of porphysomes after receptor-mediated endocytosis. Treatment with 671 nm light resulted in a significant reduction in cell viability as compared to the untargeted control porphysomes. In vivo PDT on tumor xenografts injected with folate porphysomes (i.v.) led to a negative change in tumor volume at 7 d post light treatment. This is in contrast to all other treatment groups (vehicle, laser alone, folate-porphysome alone, and untargeted porphysome with laser activation), which on average grew to a size that was ∼4-fold larger than the tumor at day 0.

It is clear from the previous experiments that the structural state of the porphysome will have an impact on its therapeutic activity. To investigate the time course of porphysome structural degradation, self-sensing FRET porphysomes were developed.[25] The system is comprised of pyro-lipid that acts as a donor, while bacteriopheophorbide *a*-lipid was used as the acceptor. When the particle is intact energy transfer occurs and a signal from the acceptor is observed; as the particle degrades, FRET is replaced by emission from the donor itself as it becomes unquenched. Tracking the ratio of the FRET signal with the donor signal allowed for an estimate that intact nanovesicles persist in the tumor at 24 and 48 h after initial injection of FRET porphysomes.

Porphysome structures exhibit a long half-life. Blood clearance half-life was determined by radiolabeling porphyrin−lipid with copper-64 (Cu^{64}) and determining blood radioactivity at various time points after injection.[134,135] Measurement of serum half-life by scintillation counting indicates that porphysomes possess a blood clearance half-life of 1.23 h (first phase) and 11.1 h (second phase).[134] No acute toxicity has been reported for porphysomes in preliminary studies. Mice treated with 1000 mg kg^{-1} showed no behavioral changes nor weight loss. Furthermore, liver function tests, red blood cell count, and white blood cell count were all found to be within their normal range[131] despite the fact that the liver and spleen are involved in the porphysome clearance pathway.[136]

Aside from porphysomes, quenched porphyrin structures have also been observed in porphyrin nanodiscs. These nanoparticles are porphyrin−lipid micelles, circumscribed by a stabilizing layer of amphipathic α-helical proteins.[137] These smaller nanodiscs also behave with the same structure-dependent activation properties observed in porphysomes. The proteins found on the surface of these nanodiscs enable their interaction and uptake by the scavenger-receptor type B class I (SR-BI). These receptors are responsible for reverse cholesterol transport and can be found in the liver, macrophages, and in some cancer cell lines.[138] Nanodiscs were incubated with a cell line that was transfected with the SR-BI receptor. Uptake of the nanodiscs was observed as evidenced by the increase in fluorescence after incubation. Furthermore, the PDT activity of these nanoparticles was tested by incubation with the SR-BI-expressing cell line and subsequent light irradiation (660 nm; 1.7 mW cm^{-2}). A significant difference in cell death was observed when compared to an identical cell line, which did not express the receptor. Continuing the investigation on using amphiphilic peptides to stabilize small porphyrin−lipid nanostructures, Cui and colleagues created porphylipoprotein (PLP) for multimodal therapeutic applications.[139] These nanoparticles are structurally analogous to endogenous lipoproteins but can be used for drug delivery, noninvasive PET monitoring, low background fluorescence imaging, and structure-dependent photosensitizing capabilities. Structurally, these nanoparticles are formulated with 30 mol % porphyrin−lipid that enables efficient quenching of fluorescence when intact (>95% quenched). Furthermore, singlet oxygen generation was suppressed by 9-fold when comparing the intact particle with the detergent disrupted sample. Injection of the agent intravenously into a KB-bearing mouse model and subsequent PDT (671 nm, 100 mW/cm^2, 75 J/cm^2) resulted in tumor cell damage based on H&E histological analysis. Analysis of the heart, lung, liver, kidney, and spleen tissue slices with H&E showed no signs of damage when compared to the treatment control group.

5.2. Oxygen Sensing through Phosphorescence Quenching

Emission from the triplet state occurs via phosphorescence. An important theranostic application of the phosphorescence phenomenon is in the biological detection of oxygen. Because oxygen exists in a triplet ground state, it can easily interact with an excited fluorophore with triplet multiplicity and undergo phosphorescence quenching. This emission quenching provides information on oxygen concentration around the emitting fluorophore. Oxygen sensing fluorophores are capable of transitioning from the singlet to the triplet spin state due to highly efficient spin−orbit coupling, which increases probably for intersystem crossing. Metalloporphyrins are excellent oxygen sensors because they possess a high probability of intersystem crossing through the intramolecular heavy atom phenomenon.[14] However, the application of metalloporphyrins for oxygen sensing is challenged due to unwanted aggregation in aqueous environments and the propensity for the dyes to partition heterogeneously in tissues.[140] These problems can negatively impact the dye's photophysical properties and utility for quantitative oxygen sensing. The first problem has been addressed through chemical modifications, which improve aqueous solubility.[141,142] The latter issue has recently been tackled by controlling the environment around the dye through nanoparticle encapsulation.[143−145] Beyond shielding the oxygen probe from the biological environment, the multicomponent nature of nanoparticles also provides a platform for the incorporation of light harvesting and two-photon absorption functionalities, both of which can improve their use for in vivo oxygen measurements.

5.2.1. Nanoparticles for Two-Photon Oxygen Sensing.

5.2.1.1. Dendrimers. Porphyrin-based dendrimers with two-photon absorption have been synthesized by the Vinogradov group as a way to determine oxygen saturation in aqueous

DOI: 10.1021/acs.chemrev.5b00140
Chem. Rev. XXXX, XXX, XXX−XXX

solutions.[146,147] Pt and Pd tetraaryleporphyrins (PtP or PdP) were inserted into the core of generation 2 poly(arylglycine) dendrimers using a combination of divergent/convergent dendrimer chemistry. Four coumarin 343 dyes were conjugated to the dendrimer such that two-photon excitation resulted in energy transfer to the core porphyrin molecules. Porphyrins coordinated with Pt of Pd exhibit efficient spin−orbit coupling, which promotes the conversion of the dye from the singlet to the triplet state. Excitation of coumarin results in energy transfer to the porphyrin, followed by intersystem crossing to the triplet state. Coumarin dyes were selected due to their high fluorescence quantum yield (ϕ_{FL} = 0.8−1.0).[146] The efficiency of the energy transfer process was determined to be 98% and can be attributed to the large overlap between the coumarin emission spectra and the porphyrin's Soret absorption band as well as the close distance between the dye molecules (r = 13.6 Å determined through molecular modeling simulations).

PdP emits phosphorescence in the triplet state at ∼680 nm. While sufficient for cell imaging, it is preferable to utilize phosphors that emit further in the NIR spectrum for in vivo applications. To that end, Lebedev et al. synthesized tetraaryltetrabenzoporphyrin (PdTBP) dendrimers and tetraaryltetranaphthoporphyrin (PdTNP) dendrimers, which emit phosphorescence at 816 and 961 nm, respectively.[140] PdTBP dendrimers were tested in vivo using intravital imaging of a mouse brain. Relative oxygen concentration was determined by measuring fluorescence from the metalloporphyrin upon excitation of coumarin. Using these new oxygen sensors, Lebedev and co-workers were able to differentiate brain arteries and veins from fluorescence images. Improving on this technique, Sakadzic and others were able to obtain high-resolution oxygen saturation maps within the fine cortical microvasculature of the mouse by imaging their dendrimeric oxygen probes using two-photon excitation.[148]

5.2.1.2. Conjugated Polymer Nanoparticles. Conjugated polymer nanoparticles possess large two-photon cross sections (as high as 10^5 GM) and hence show promise for two-photon imaging.[79] They have also been shown to transfer absorbed energy efficiently from the polymer to doped small molecule imaging agents and photosensitizers.[119−121] A natural extension of this research is to investigate whether doping a phosphorescent metalloporphyrin into the polymer matrix will enable two-photon O_2 detection. Wu and colleagues demonstrated that loading PtOEP into the conjugated polymer nanoparticle resulted in efficient energy transfer (∼89%) from the polymer to the porphyrin.[149] This efficient transfer was confirmed by fluorescence lifetime measurements, which resulted in a faster decay rate in the porphyrin-doped sample (τ_D^{-1} = 56 ns^{-1}) than the undoped sample (τ_D^{-1} = 9 ns^{-1}). Last, the capability of this nanoparticle to detect oxygen in macrophage cells was tested with incubation medium with O_2- and N_2-saturated solutions. The presence of oxygen in the solution resulted in quenching of the porphyrin, while no reduction was observed in the N_2-bubbled control. One potential disadvantage of this setup is the potential for the oxygen sensor to leach out of the particle. One method to overcome this is to covalently conjugate the sensor dye to the polymer chain. Dmitriev et al. synthesized conjugated polymer nanoparticles by copolymerizing fluorene molecules with the Pt-porphyrin, platinum(II)meso-bis(pentafluorophenyl)bis(4-bromophenyl)porphyrin.[150] The polymer was stabilized in aqueous solution through the effect of charged quarternary ammonium and propionic acid moieties. The conjugated polymer nanoparticles varied in size between 35 and 112 nm. Comparing the emission intensity versus excitation power showed an almost quadratic dependence on excitation power. This indicates that absorption occurred through a two-photon mechanism for the polyfluorene structure. Energy transfer between polyfluorene and the Pt-porphyrin occurred with a fluorescence quantum yield of the porphyrin emission found to vary between 0.025−0.043. Interestingly, when the polymer was completely dispersed in a favorable solvent (e.g., THF), intense fluorescence originating from the conjugated polymer was observed. Fluorescence from the Pt-porphyrin only occurred when the construct was dissolved in water. This indicated that close packing of the polymer chain was required for the nanoparticle to undergo long-range energy transfer.

5.3. Triplet−Triplet Annihilation Upconversion Fluorescence

Upconversion fluorescence is an anti-Stokes process, where the excitation photon is at a lower energy than the emitted fluorescence photon. Upconversion fluorescence has an interesting role to play in medical photonics, especially in bioimaging applications. Contrasting this technique with traditional fluorescence, upconversion fluorescence allows for imaging with reduced background signal.[151] This is due to the elimination of autofluorescence, because endogenous fluorophores do not emit through an anti-Stokes mechanism. In addition, depending on the specific dye used for imaging, the excitation wavelength is generally in the NIR. This enables deeper light penetration when compared to fluorophores that absorb and emit in the visible spectrum.

Much of the work conducted on upconversion fluorescence in recent years has been conducted on inorganic systems. Platforms such as inorganic lanthanide-doped upconversion nanoparticles (UCNPs) have been developed and applied with some success in the imaging of cells[152] and animals.[153] Upconversion fluorescence also occurs in organic materials through intermolecular dye interactions. In contrast to the mechanism that is applied in UCNPs, upconversion fluorescence in organic dyes relies on the triplet−triplet annihilation mechanism (vide supra). As opposed to techniques such as two-photon fluorescence imaging, which also utilizes organic dyes, TTA can induce fluorescence even at very low irradiance. This is different when compared to two-photon fluorescence where fluorescence emission intensity scales quadratically with the excitation power.

Several issues arise for current application of TTA for fluorescence applications. The first factor is that the presence of dissolved oxygen in most biological liquids will have a negative impact on the fluorescence intensity because oxygen can quench the triplet state of the acceptor dye. However, there are ways to bypass this problem, such as the addition of an oxygen diffusion-limiting layer. Dendrimers have been utilized to limit the diffusion of oxygen.[146] Lastly, light emission in upconverting fluorescence is typically in the visible range. This may limit the application of this technique to superficial tissue imaging.

5.3.1. Nanoparticles for TTA Upconversion Fluorescence. *5.3.1.1. Polymeric Nanoparticles.* TTA has been investigated as a mechanism to generate contrast agents with fluorescence upconversion.[154−157] Upconverting fluorescence organic nanoparticles were made by embedding Pt(II)-octaethylprophyrin (PtOEP; sensitizer) and diphenylanthracene (DPA; donor) into polystyrene-based nanoparticles.[154] The intended application of this work was for solar light

DOI: 10.1021/acs.chemrev.5b00140
Chem. Rev. XXXX, XXX, XXX−XXX

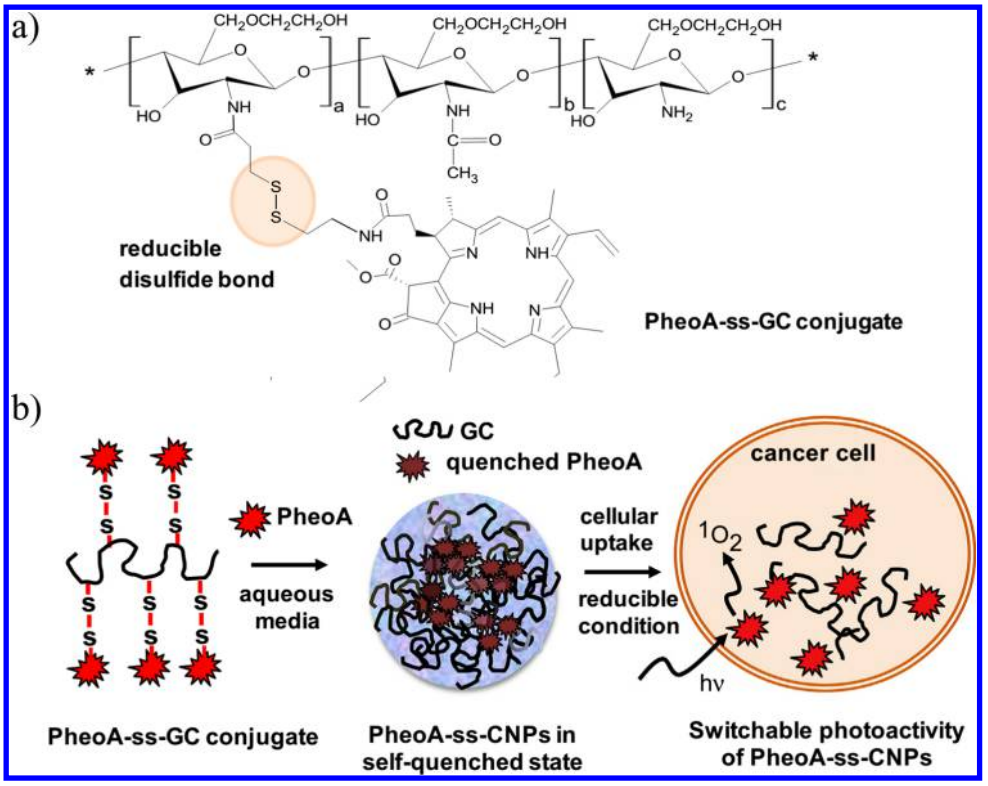

Figure 15. (a) Chemical structure of glycol chitosan nanoparticles with reducible thiol linkages conjugated to pheophorbide A (PheoA-ss-GC). (b) Illustration of self-assembly and degradation pathway for PheoA-ss-GC. Reproduced with permission from ref 127. Copyright 2007 Elsevier.

harvesting applications, but a similar technique can be applied to synthesize biocompatible nanoparticles for biomedical applications.

Wohnhaas et al. developed upconverting TTA nanoparticles for in vitro cell imaging in mesenchymal stem cells and HeLa cells.[157] The goal was to prepare nontoxic nanoparticles for fluorescent cell culture techniques. Nanoparticles were prepared from poly(methyl methacrylate) (PMMA) polymers using an ultrasonication procedure. The sensitizer and acceptor dye pair utilized were palladium(II)meso-tetraaryltetranaphthoporphyrin (PdTNP) and 3,9(10)-bis(4-*tert*-butylphenylethynyl)perylene, respectively. The nanoparticles possessed a hydrodynamic size of 225 nm, and excitation with 633 nm light resulted in emission at 550 nm. However, the authors noted that the fluorescence in air-equilibrated solutions had a 5-fold decrease in emission intensity, indicating that the PMMA polymer barrier was insufficient in preventing the diffusion of oxygen into the nanoparticle. Despite this negative result, incubation with cells showed clear fluorescence emission from the internalized nanoparticles. Furthermore, limited cellular toxicity (>80% survival) was observed when cells were incubated with up to 5 mg mL^{-1} of the nanoparticles. Upconversion fluorescence imaging using TTA nanoparticles provides another method to generate signal amplification and contrast in an in vitro environment. However, extension of this technology to in vivo applications is challenging given the visible spectrum in which the fluorescence emission occurs. Endogenous absorbers, scatterers, and fluorophores have a more substantial influence on measured fluorescence in this part of the visible spectrum; thus the application of these nanoparticles in vivo will likely be limited to superficial applications. One strategy to improve upon these nanoparticles is to use fluorophores that emit in the NIR.

5.3.1.2. Nanoemulsions. Liu and co-workers constructed upconverting TTA nanocapsules for in vivo upconverting fluorescence imaging.[155] They constructed the nanoemulsion by dissolving the sensitizer and acceptor within the hydrophobic oil droplet that has been stabilized by BSA-dextran. For the sensitizer molecule, metalloporphyrin derivatives were used, while DPA, BODIPY-green, and BODIPY-yellow were used for the acceptor dyes. Visible fluorescence was observed after intradermal injection of the nanocapsules and irradiation with low energy NIR light (635 nm; 12.5 mW cm^{-2}) (Figure 15). Boosting the energy (11, 86, and 200 mW cm^{-2}) used in excitation resulted in an enhancement of the signal-to-noise ratio (SNR = 12, 27, and 50) due to the power dependence of TTA fluorescence.

6. PHOTOTHERANOSTIC TECHNIQUES INVOLVING VIBRATIONAL RELAXATION

6.1. Photothermal Therapy (PTT)

PTT seeks to use a high-intensity coherent light source to induce thermal damage in diseased tissue, especially in cancer. The type and extent of damage caused are dependent on the treatment temperature as well as the time spent at a given temperature. For high temperature thermal therapy, tissue temperatures are elevated above 55 °C with the goal of inducing tissue ablation.[158] At this temperature range, proteins in tissue undergo rapid coagulation, which causes cell lethality.[158] At lower temperatures, such as in the range of clinical hyperthermia (~42 °C), the therapeutic goals are to induce direct cell death through protein denaturation,[159] as well as to cause indirect therapeutic effects such as increased infiltration of host immune cells,[160] inhibition of radiation repair machinery,[161] and improved tumor oxygenation.[162]

DOI: 10.1021/acs.chemrev.5b00140
Chem. Rev. XXXX, XXX, XXX−XXX

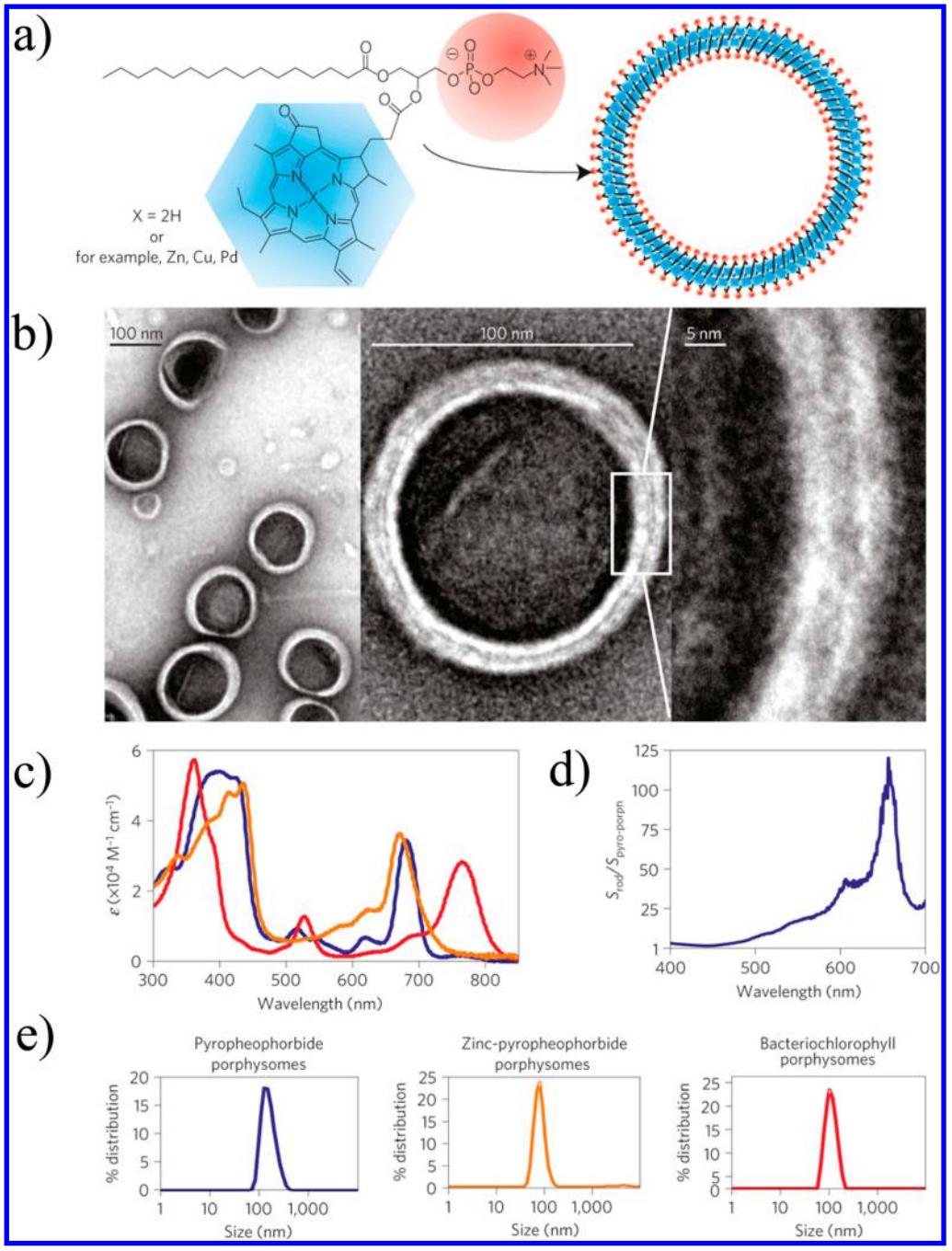

Figure 16. (a) Chemical structure of pyropheophorbide *a*–lipid and schematic illustration of formed porphysome nanovesicle. (b) Transmission electron micrographs of uranyl acetate-stained porphysomes (5% PEG–lipid, 95% pyropheophorbide–lipid). (c) Absorbance of the porphyrin–lipid subunits incorporated in porphysomes formed from pyropheophorbide *a*-lipid (blue), zinc-pyropheophorbide *a*-lipid (orange), and bacteriopheophorbide a-lipid (red) in PBS. (d) Resonance light scattering spectra ratio between gold nanorods and porphysomes adjusted to the same optical density at 680 nm. (e) Dynamic light scattering size measurement of porphysomes. Reproduced with permission from ref 131. Copyright 2011 Nature Publishing Group.

These indirect effects cause continued cytotoxic effects even after treatment and can increase the susceptibility of the tumor to other therapeutic modalities such as radiotherapy or chemotherapy.[163]

Lasers have been used to ablate tissues using endogenous absorber as the primary heat generation mechanism.[164,165] In this application, the laser source (980 nm) causes heating by exciting water in tissues.[166] This lack of specificity can result in heating of normal tissues, leading to potential complications. To improve upon this treatment strategy, light absorbing molecules and nanoparticles were pursued as strategies in which to selectively enhance thermal damage. These agents can reduce the amount of time required for treatment and can provide tumor specificity through ligand targeting and nanoparticle size-dependent enhanced permeability and retention.[167] There have been several studies published on the use of indocyanine green as a photothermal agent in laser tissue welding[168] as well as thermal ablation in melanoma,[169] gastrointestinal neoplasia,[170] and breast tumors.[171] However, there are several disadvantages in using these dyes, which

DOI: 10.1021/acs.chemrev.5b00140
Chem. Rev. XXXX, XXX, XXX–XXX

necessitates the application of nanoparticles. First, the absorption cross section of a single organic dye is small when compared to an assembly of chromophores within a nanoparticle. Second, the photobleaching of organic dyes during prolonged light exposure is a factor. Organic nanoparticles address this problem by possessing many chromophores within each particle, while the formation of quenched states through intermolecular dye interactions can reduce the rate of photobleaching. Presently there are many nanoparticles that can induce the photothermal effect. Examples of organic nanoparticles that can efficiently convert light to heat energy will be covered in the follow section.

6.1.1. Nanoparticles for PTT. *6.1.1.1. Conjugated Polymer Nanoparticles.* Not all conjugated polymer nanoparticles are fluorescent. Some absorb strongly in the visible spectrum but do not emit detectable fluorescence. These properties make these conjugated polymer nanoparticles suited for photothermal therapy (PTT). Conjugated polymers are excellent candidates for photothermal therapy due to the large absorption coefficients afforded by the density of absorbing chromophores. Studies involving the application of these polymers in PTT have mainly focused on the NIR-absorbing materials including polyaniline (PAni),[172−174] polypyrrole (PPy),[175−177] melanin,[178] and poly(3,4-ethylenedioxythiophene):poly(4-styrenesulfonate) (PEDOT:PSS).[179]

PAni nanoparticles are electroconductive polymers that display pH-dependent changes in absorption. Synthesized by the oxidative polymerization of aniline, PAni exists in either the emeraldine base (EB) or the emeraldine salt (ES) form upon nanoprecipitation. Doping the EB form through protonation results in a change in the materials band structure, which has the effect of inducing a red-shift in the absorption band. Yang et al. prepared PAni nanoparticles in the EB form under physiological conditions.[173] Incubation of the PAni nanoparticles with A431 cancer cells resulted in a ∼200 nm red-shift in the absorption of the PAni nanoparticle as it changed from the EB to the ES form. PAni nanoparticles in the EB or ES forms were tested for their photothermal conversion capabilities. Irradiation of 0.5 mg mL^{-1} of the EB or ES form using an 808 nm light source resulted in a 2.6-fold increase in ES solution over the EB form. The success of PAni nanoparticles as a photothermal agent was also demonstrated in two other studies, which showed a large temperature increase in response to laser heating.[172,174] Despite the similar capabilities to convert light into heat, it is interesting to note that these nanoparticles were of different sizes and possessed different surface stabilization. This indicates that photothermal heating of PAni is not highly dependent on particle size nor the type of stabilizers on its surface.

Polypyrrole (PPy) nanoparticles are another class of conjugated polymers that exhibit high molar extinctions in the NIR and excellent photothermal conversion efficiencies.[175−177,180] Chen et al. reported the synthesis of a strongly absorbing PPy nanoparticle with an extinction coefficient of 2.38×10^{10} M^{-1} cm^{-1} at 808 nm, while conversion efficiency was 44.7%.[177] Using these nanoparticles, they were able to induce tumor cell kill by injecting PPy at a dose of 10 mg kg^{-1} and irradiating the area with 808 nm light (1 W cm^{-2}; 5 min). This treatment achieved arrest of tumor growth as well as improved survivability when compared to animals receiving the control treatments.[177]

In the organic photovoltaics field, there has been work on strategies to modulate the light absorption spectrum of conjugated polymers through the adjustment of the polymers band gap. Tuning the band gap can be achieved by doping in a second chromophore into the polymer such that a donor and acceptor pair of chromophores are formed.[181] This strategy has been applied to develop conjugated polymers for PTT applications.[182]

Recent work by Liu and colleagues demonstrated that natural conjugated biopolymers derived from the body can also applied in PTT.[178] Melanin is a natural biopolymer that is present in humans and other animals. It absorbs broadly across the visible and NIR spectrum. In the body, melanin in melanosomes serves the purpose of blocking UV light and dissipating the energy from UV light. This is accomplished by quenching and dissipating the heat through a non-ROS generating pathway,[183] such as vibrational relaxation. Animals were injected intratumorally with the melanin nanoparticles and treated with 808 nm light at a fluence rate of 2 W cm^{-2} for 5 min. This thermal dose was sufficient to halt the growth of tumor for 10 days when compared to the controls. To show they have the capability of accumulating in tumors, melanin nanoparticles were labeled with the MRI contrast agent Gd-DTPA and administered intravenously. After 48 h postinjection, 5.7% ID g^{-1} was measured within the tumor through MRI imaging. To determine whether this agent displayed any toxicity, animals were intravenously injected with increasing amounts of the nanoparticle. They found that the measured LD_{50} (lethal dose at 50%) was 483.95 mg kg^{-1}, which was approximately 500-fold higher than the dose required to generate the photothermal effect with these nanoparticles. A long-term toxicity experiment was conducted where body weight, behavioral changes, and histological abnormalities were measured. Rodents treated with Dpa-nanoparticles did not exhibit weight loss and changes in grooming pattern. Furthermore, histological analysis on the liver revealed no sign of injury.

Cheng et al. developed PEDOT:PSS conjugated polymer nanoparticles for in vivo PTT[179] (Figure 16). Using a layer-by-layer assembly approach, they demonstrated the possibility of generating PEDOT:PSS nanoparticles with stealth-like capabilities. PEDOT:PSS was covered with a positive layer of poly(allylamine hydrochloride), which was followed by a negative layer of poly(acrylic acid). A branched polyethylene glycol (PEG) polymer was conjugated to the surface of the overall nanoparticle through amide chemistry (Figure 18a). The final nanoparticle had an average diameter of 100−200 nm (Figure 18b,c). The absorption spectrum for the samples showed broad absorption in the NIR spectrum with maximum absorption ∼800 nm (Figure 18d). This PEDOT:PSS nanoparticle was tested in vivo. Tumor-bearing BALB/C mice were injected with 10 mg kg^{-1} of nanoparticle, and the circulatory half-life was determined, followed by biodistribution. These conjugated polymer nanoparticles were found to possess a half-life of 0.3 ± 0.24 h (first phase) and 21.4 ± 3.1 h (second phase). Furthermore, the tumor accumulation was found to be 28.02% ID g^{-1}. These pharmacokinetic data indicate that PEG-coated PEDOT:PSS nanoparticles remain in the circulatory system for an extended period of time and can accumulate at high concentrations in the tumor. Irradiation of sample with an 808 nm laser resulted in a significant increase in temperature when compared to water (Figure 18e). Conducting PTT on the tumor at 48 h post injection showed a significant rise in tissue temperature to ∼51 °C after 5 min of treatment. This led to a

DOI: 10.1021/acs.chemrev.5b00140
Chem. Rev. XXXX, XXX, XXX−XXX

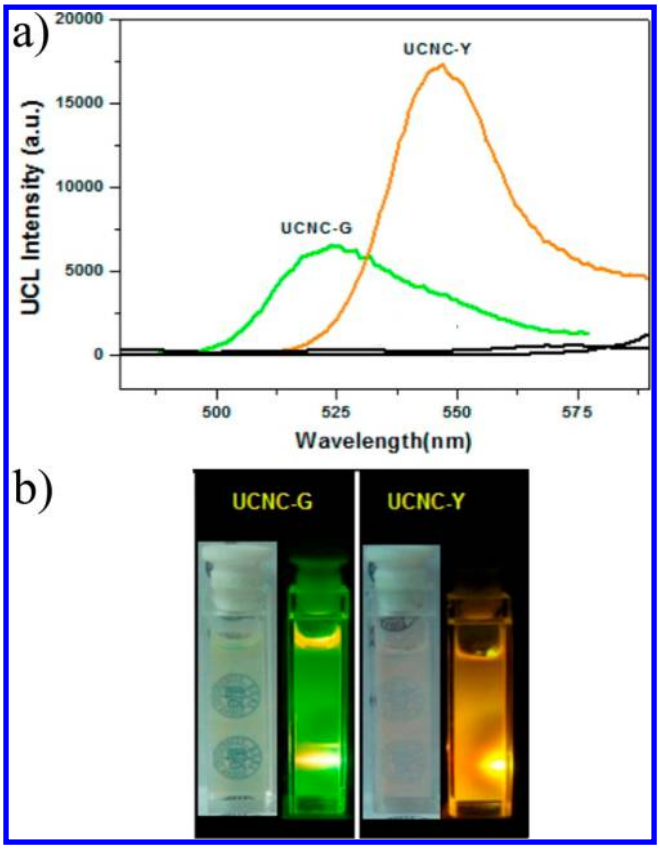

Figure 17. (a) Upconversion fluorescence emission spectra of BSA-dextran upconverting nanoparticles doped with BODIPY-green (UCNC-G) or BODIPY-yellow (UCNC-Y) in water under 635 nm excitation. Concentrations of both sensitizer (PtTPBP) and annihilator (BDP-G/BDP-Y) are fixed in all samples at 5.0×10^{-7} and 5.0×10^{-5} mol L^{-1}, respectively. (b) Photos showing bright visible fluorescence emission from each sample upon excitation with 635 nm light. Reproduced with permission from ref 155. Copyright 2013 American Chemical Society.

decrease in tumor regrowth and increased survival in animals receiving both the PEDOT:PSS nanoparticle and laser treatment when compared to the other control groups. This strategy for stabilizing polymers and functionalizing the particle with a sterically stabilized PEG layer may be useful in the synthesis of other stealth-like polymeric nanoparticle formulations.

Conjugated polymer nanoparticles possess large absorption coefficients due to the high density of chromophores found within its polymer structure and may have use in photoacoustic imaging. However, many conjugated polymers developed for photonic applications absorb in the visible spectrum. Because background absorption and scattering contributes significantly to the measured signal in the visible spectrum, it is important to utilize agents that absorb in the NIR, where the endogenous absorption and scattering is minimized. Polypyrrole (PPy), poly(phenylfluorene thiadiazolo-quinoxaline) (PFTTQ), polyaniline (PAni), poly(fluorenyldivinylene benzothiadiazole) (PFVBT), and dopamine-melanin represent examples of highly absorbing materials in which their peak absorption occurs in the near-infrared region. These polymeric materials are excellent candidates for photoacoustic imaging. Polypyrrole nanoparticles were recently investigated as photoacoustic contrast agent.[184] Absorbance was strongest between 800 and 900 nm ($\sim 2 \times 10^{10}$ M^{-1} cm^{-1}), which lies directly within the first optical window where absorption by blood and water is minimized.[185] To test the limits of detectability, polypyrrole nanoparticles embedded in a gel phantom were placed beneath varying thicknesses of chicken breast muscle tissue. Photoacoustic signal originating from the nanoparticle diluted to 100−200 μg mL^{-1} was still detectable even at a depth of 4.3 cm below muscle tissue.[184] These nanoparticles were also tested in a mouse model. Kunming mice were shaved and injected with 200 μg mL^{-1} of the polypyrrole nanoparticles. A photoacoustic transducer was placed over the brain, and scans were collected over a period of 1 h. A strong photoacoustic signal originating from the vasculature was observed after 1 h postinjection and shows the possibility of using these agents for imaging within biological tissue.

6.1.1.2. Porphyrin−Lipid Nanostructures. The quenched property of porphysomes enables their application in theranostic techniques that utilize vibrational relaxation to generate signal contrast or photothermal heating. The photothermal transduction capabilities in porphysomes were tested in vivo.[186] KB tumor-bearing nude mice were intravenously injected with porphysomes (42 mg kg^{-1}), and after 24 h, the tumor was irradiated with 671 nm light (1.9 W cm^{-2}) for 60 s. This led to a 30 °C increase in tumor temperature, with follow-up studies showing no tumor regrowth over the duration of the study. The ability for these nanoparticles to generate heat during irradiation is advantageous in treating hypoxic cancer tumors when compared to other light-based techniques such as PDT. In this case, the reduction of oxygen in tumor tissue limits the effectiveness of photodynamic therapy. Jin et al. showed in a direct comparison of PDT and PTT treatment parameters in a hypoxia model of cancer that PTT resulted in complete irradication of the tumor without recurrence, and a survival rate of 100% over the study period (50 d). This is in contrast to the hypoxic PDT treatment group, which had no survivors at 20 d post-treatment. These results show that the problem of hypoxia can be addressed using photothermal therapy in conjunction with porphysomes.[187]

While porphysomes are photostable in the intact state, the disrupted particle is susceptible to photodegradation. MacDonald and colleagues showed that this photoinstability can be overcome by chelating manganese into the porphyrin core, which effectively eliminates the ability for the porphyrin−lipid to generate ROS.[188] Consequently, this also imparts magnetic susceptibility to porphysomes, enabling its application for MRI imaging.

6.1.1.3. Dendrimers. Dendrimer structures have also been tested as carriers of quenched porphyrin dyes in PTT. Recently, a telodendrimer-based porphyrin micelle was constructed and investigated for its multimodal properties.[189] These nanoparticles display structure-dependent excited-state quenching. A test of its heating ability showed that at a power of 1.25 W cm^{-2} and injected dose of 25 mg kg^{-1}, the nanoporphyrin particle was capable of generating temperatures that exceeded the threshold for thermal ablation. Chelation of the gadolinium through the metal chelator DTPA enabled the visualization of the particle by magnetic resonance imaging, while PET imaging was accomplished by prelabeling the nanoporphyrin with Cu^{64}.

6.2. Photoacoustic Imaging

Photoacoustic imaging is an emerging imaging technique that combines the advantages of optical imaging and ultrasound. On the basis of the photoacoustic effect,[190] this method relies on absorption of pulsed light in an endogenous or an exogenously

DOI: 10.1021/acs.chemrev.5b00140
Chem. Rev. XXXX, XXX, XXX−XXX

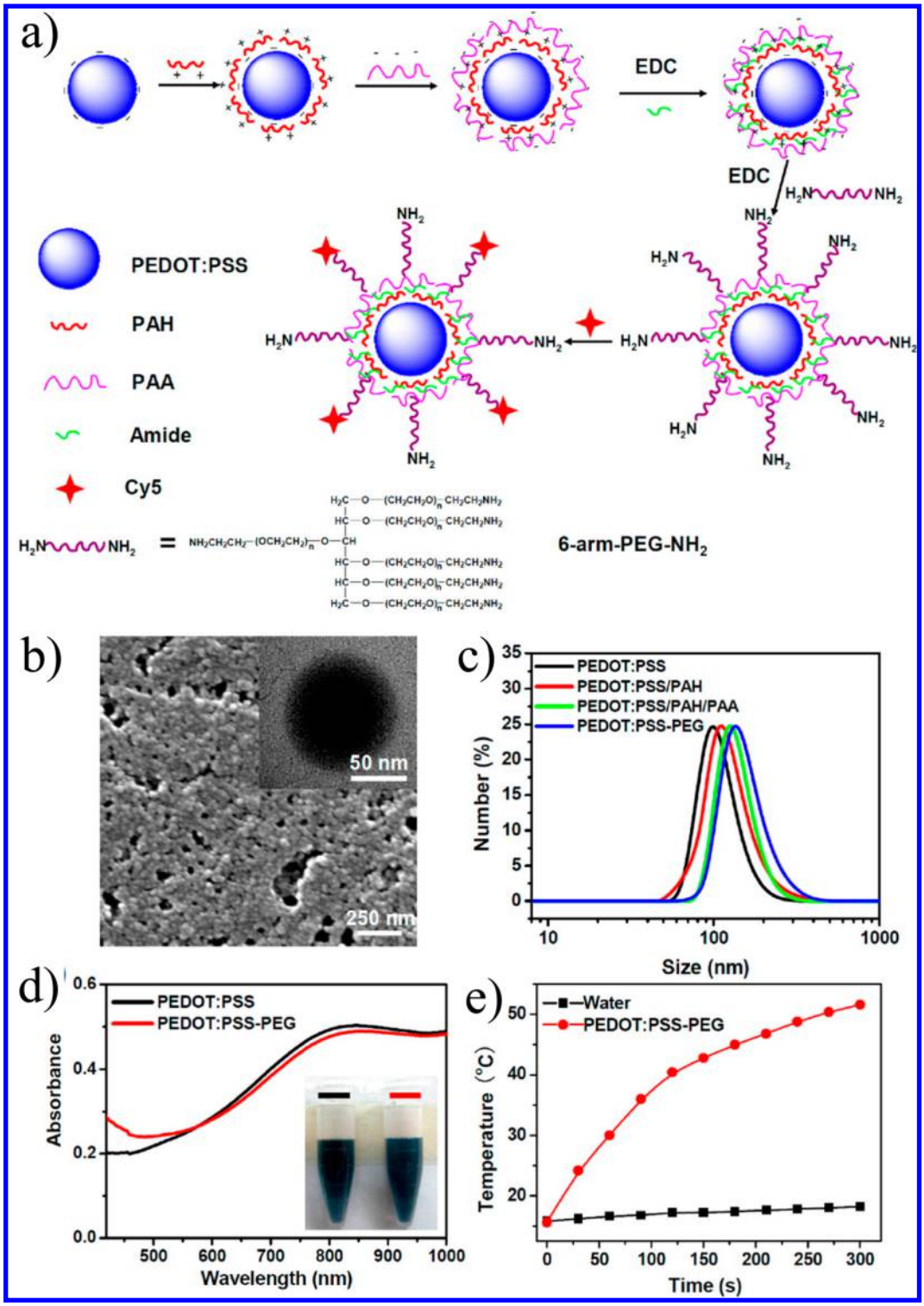

Figure 18. Synthesis of PEDOT:PSS–PEG. (a) Schematic illustrating synthesis. (b) Scanning electron microscopy image of nanoparticle on a silicon substrate. Inset: Transmission electron micrograph of nanoparticle. (c) Dynamic light scattering measurements during each coating step of synthesis. (d) Absorption spectra of PEDOT:PSS and PEDOT:PSS–PEG at a concentration of 0.02 mg mL^{-1} in water. Inset: Photo of PEDOT:PSS (left) and PEDOT:PSS–PEG (right) solutions at a concentration of 0.1 mg mL^{-1} in water. (e) Heating curves for PEDOT:PSS–PEG (0.1 mg mL^{-1}) under irradiation by 808 nm laser (1W cm^{-2}). Reproduced with permission from ref 179. Copyright 2012 American Chemical Society.

administered chromophore. Heat generated in surrounding tissues by the vibrational relaxation of chromophores generates pressure waves that can then be detected using an ultrasound transducer. Photoacoustic imaging is capable of imaging at depths that exceed the depth limit for other optical techniques.[191] However, aside from blood vessels and some rare examples in cancer (e.g. melanoma), biological tissues are intrinsically low contrast. To enhance its utility in the imaging and detection of disease, it is important to develop imaging agents with large absorption coefficients, which absorb in the near-infrared window.

DOI: 10.1021/acs.chemrev.5b00140
Chem. Rev. XXXX, XXX, XXX–XXX

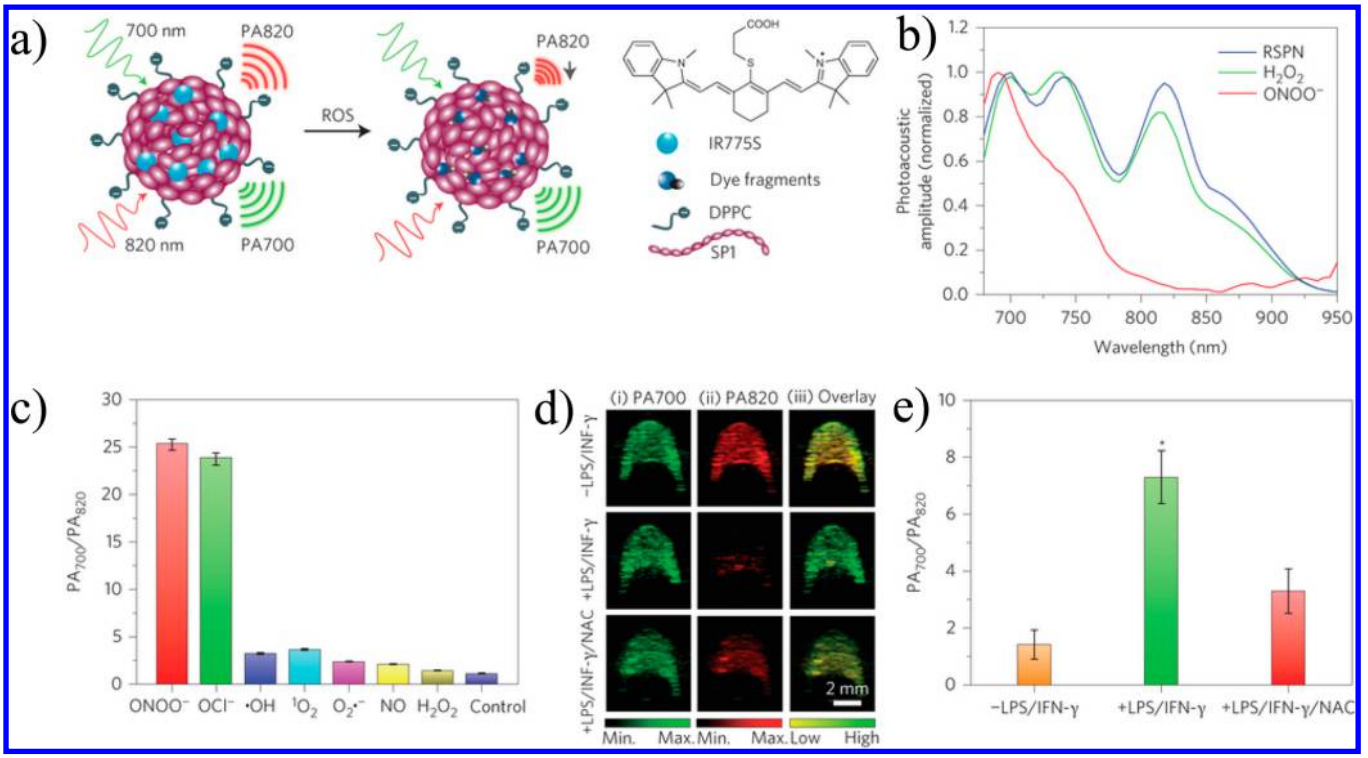

Figure 19. (a) Proposed ROS sensing mechanism for SPN. (b) Photoacoustic spectra of RSPN in the absence and presence of ROS. (c) Ratio of photoacoustic signal at 700 nm to that at 820 nm (PA_{700}/PA_{820}) after incubation with indicated ROS (5 μM). (d) Photoacoustic images of macrophage RAW 264.7 cell pellets without (top) or with (middle) stimulation with LPS/INF-γ, and with *N*-acetylcysteine, a free-radical scavenger protection (bottom). (e) Quantification of the absorption ratio (PA_{700}/PA_{820}) for cell pellets pictured in (d). Error bars represent standard deviations (n = 4). Reproduced with permission from ref 192. Copyright 2014 Nature Publishing Group.

6.2.1. Nanoparticles for Photoacoustic Imaging. *6.2.1.1. Conjugated Polymer Nanoparticles.* In addition to contrast enhancement, the utility of conjugated polymer nanoparticles as activatable photoacoustic probe for sensing of reactive oxygen species (ROS) was recently investigated by Pu et al.[192] ROS is a chemical mediator involved in a host of pathological conditions ranging from cancer to cardiovascular disease.[193] The authors were interested in investigating whether conjugated polymers along with photoacoustic imaging could be used to track the ROS generation process in vivo. NIR-absorbing conjugated polymers were first selected and tested for stability toward ROS (Figure 17). One candidate (termed SPN1) that exhibited good stability toward ROS was selected for further studies. This polymer was then formed into nanoparticles via the reprecipitation technique. The particle was doped with the ROS-sensitive cyanine dye IR775S and further stabilized using dipalmitoylphosphatidylcholine. The cyanine dye was found to be chemically bleached upon the addition of $ONOO^-$ and ClO^-, but was stable toward $^{\bullet}NO$, $^{\bullet}OH$, $O_2^{\bullet-}$, $^1O_2$, and H_2O_2. By monitoring the photoacoustic signal ratio at 700 and 820 nm, they were able detect ROS generation by murine RAW267.7 macrophages after stimulation with an inflammatory agent (LPS/INF-γ). Using this technique, they were also able to detect the ROS in vivo after injecting the SPN1 intramuscularly into a mouse model of tissue inflammation (Figure 19).

6.2.1.2. Surfactant-Based Nanoparticles. Aggregation in dyes within surfactant membranes can result in fluorescence quenching, which is useful for photoacoustic imaging. Zhang et al. demonstrated that squaraine dyes form ordered H-aggregates when embedded in lipid vesicles.[194] The extent of H-aggregation could be controlled by the ratio of squaraine dye to phospholipid in the formulation. Because H-aggregates are nonfluorescent, they can be used as efficient photoacoustic contrast agents. Intravenous injection of the squaraine-loaded liposomes resulted in a visible photoacoustic signal visualized in the tumor. Yet another example is the application of perylene diimide dyes assembled in $mPEG_{5000}$-DSPE micelles as photoacoustic-imaging contrast agents.[175] Particles formed were approximately 60 nm in size and absorbed light maximally at 700 nm. These particles were used in the imaging of orthotopic mouse of brain cancer. Visualization of the brain after 2 d post injection of the particles showed signal contrast within the brain at a depth of 4.0 mm.[175] A wavelength scan of the area with signal contrast indicated that the detected signal was likely arising from accumulation of the perylene diimide nanoparticles.

Zhang et al. developed a novel dye-loaded polymeric micelle to visualize the intestinal tract using dual modality positron emission tomography and photoacoustic imaging.[195] In their study, the authors explored strategies in which to solubilize a series of dyes of varying hydrophobicity. The overall goal was to develop a multimodal nanobased imaging agent capable of positron emission tomography (PET) imaging and photoacoustic imaging. Of the series they examined, the phthalocyanine-type dyes, phthalocyanine (Pc), benzophthalocyanine (BPc), zinc benzophthalocyanine (ZnBPc), benzonaphthalocyanine (BNPc), and 5,9,14,18,23,27,32,36-octabutoxy-2,3-naphthalocyanine (ONc) dyes, were the most promising but were also difficult to solubilize. Pluronic F-127 (F127) was used as the polymeric surfactant to stabilize both the Pc and the Nc in aqueous solution. These solubilized dye aggregates were

DOI: 10.1021/acs.chemrev.5b00140
Chem. Rev. XXXX, XXX, XXX−XXX

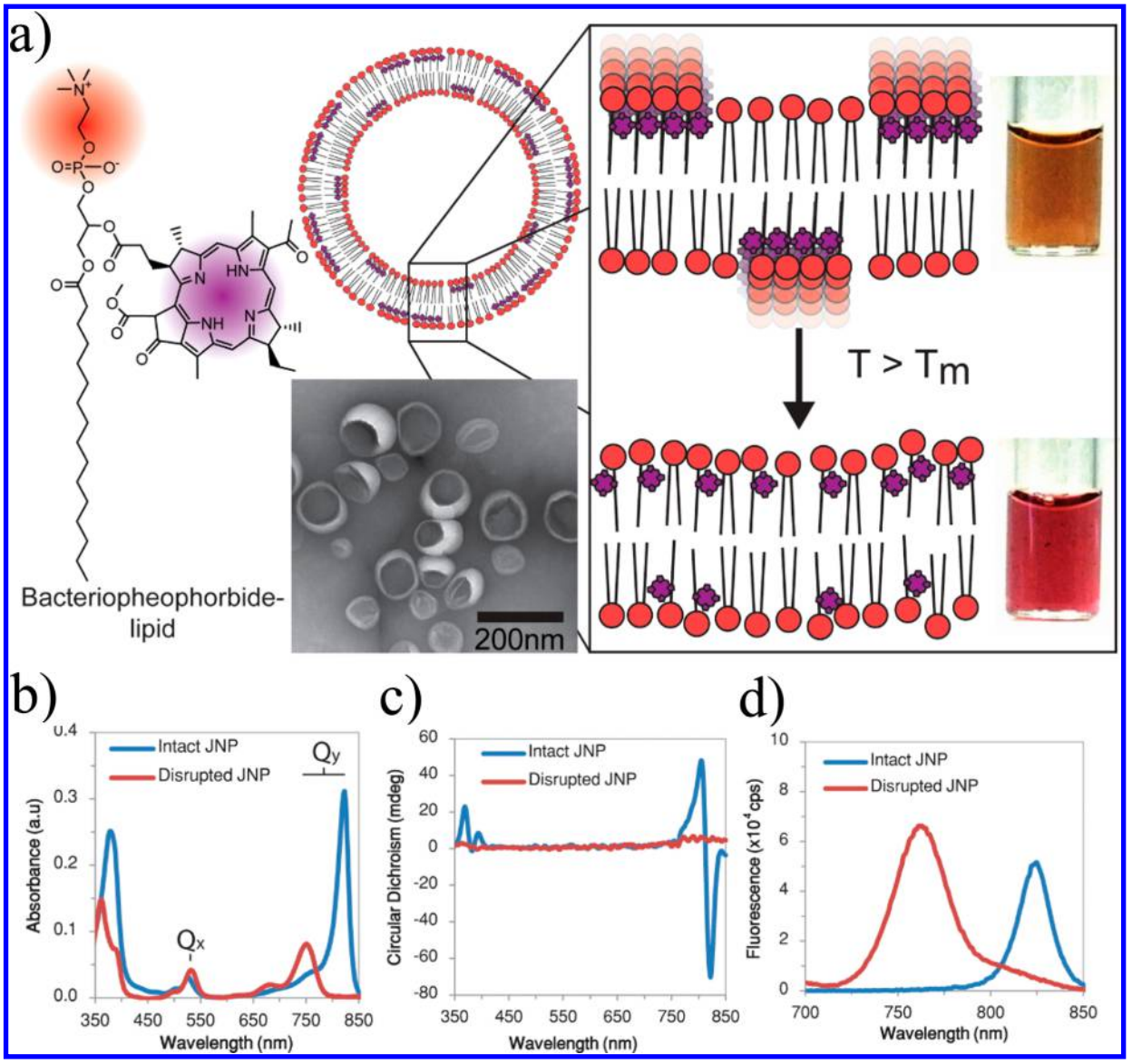

Figure 20. (a) Schematic of the J-aggregating nanoparticle (JNP). Insets: (left) Transmission electron micrograph of JNP; (right) illustration of disaggregation upon change in lipid phase behavior. Photograph of JNP sample below and above phase transition temperature. (b) Absorption spectra of JNP in the intact (blue) and detergent disrupted (red) state. (c) Circular dichroism spectra of JNPP in the intact (blue) and detergent disrupted (red) state. (d) Fluorescence spectra of JNP in the intact (blue) and detergent disrupted (red) state. Reproduced with permission from ref 196. Copyright 2014 American Chemical Society.

referred to as "nanonaps". Once purified of free F127, nanonaps were sized by dynamic light scattering (DLS) and were found to form spheres of approximately 20 nm. Photoacoustic imaging of the most NIR shifted dye, ONc, was conducted in the intestine of 6-week old BALB/c mice. Using the ONc nanonaps, the authors successfully imaged the gut after oral gavage. The excellent signal contrast can be attributed to the imaging wavelength at ca. 875 nm where background photoacoustic signal is minimal. It can also be attributed to the strong optical absorption of the molecules as well as the formation of nonfluorescent aggregates, both factors of which will influence the intensity of the measured signal.

6.2.1.3. Porphyrin–Lipid Nanostructures. Photoacoustic imaging with porphysomes has also been demonstrated using sentinel lymph node imaging.[131] However, the photoacoustic signal generated from tissue at 680 nm overlaps with other endogenous absorbers. This increases the background signal and is an unwanted effect. To address this concern, porphysomes were prepared with bacteriopheophorbide *a* lipid (Bchl-lipid). In working with Bchl-lipid, it was discovered that bacteriopheophorbide *a* conjugated to a phospholipid (Bchl-lipid) will exhibit J-aggregation when inserted into a liposomal membrane[196] (Figure 20a). The dye when solubilized in methanol typically exhibits maximal absorption at 750 nm. Upon aggregation within a lipid membrane, the dye undergoes a red-shift to 824 nm along with band narrowing and increased light absorption (Figure 20b). It also displays absorption of circularly polarized light and a small Stokes shift (1–2 nm) (Figure 20c,d). The absorption band can be clearly distinguished when imaged using photoacoustic imaging. The narrow and enhanced absorption bands are both useful properties to possess for photoacoustic imaging-based contrast agents. Another discovery made was the aggregation in the membrane is dictated by the phase behavior of the liposomal

DOI: 10.1021/acs.chemrev.5b00140
Chem. Rev. XXXX, XXX, XXX–XXX

membrane. Increasing the temperature in the membrane beyond the phase transition temperature of the host phospholipid resulted in a reversal in the shifted absorption band. By monitoring the absorption band using photoacoustic imaging, it was possible to detect a temperature threshold change both in tissue mimicking gel phantoms and in solid tumors. Taken together, the results indicate that these J-aggregating nanoparticles may find suitable use as temperature threshold sensors when used in conjunction with photoacoustic imaging.

Porphyrins can also be incorporated in micrometer-sized particles such as giant unilamellar vesicles[197] and microbubbles.[198−200] Recently, it was discovered that ordered J-aggregates could be formed in the lipid shell of perfluorocarbon microbubbles through ordered aggregation of Bchl-lipid.[200] These porphyrin-containing gas-filled microbubbles were capable of generating strong contrast for ultrasound and photoacoustic imaging. Interestingly, application of low-frequency ultrasound to burst the bubbles resulted in the formation of nanoparticles from the microbubbles. Electron microscopy and nanoparticle tracking analysis showed that nanoparticles (5−500 nm) were formed after ultrasound bursting. While the ultrasound contrast was eliminated through this process, the remaining nanoparticles retained a strong photoacoustic signal at the wavelength that corresponded to the absorption maximum of the J-aggregate peak. In situ bursting of these porphyrin microbubbles resulted in a micro-to-nano conversion, which enabled retention of the nanoparticles as visualized through photoacoustic imaging. The ability to localize nanoparticles to the treatment site may allow for the delivery of therapeutics in a targeted manner.

7. CONCLUSIONS AND OUTLOOK

Medical photonics in recent decades has been spurred on by improvements in light generation and delivery technologies. Parallel advancements in chemical probes have undoubtedly increased the relevance of photonic devices in biomedical applications. Early work on the chemical probes involved modification of small molecule chromophores through organic synthesis. The general goal was to improve the photophysical and physicochemical properties of the individual molecule through bond-breaking and -forming reactions. In recent years, there has been growing interest in building mesoscale molecular assemblies, architectures where the spatial location of individual molecules dictates the properties of the system. In the context of probe development for biomedical photonic applications, molecular interactions between chromophores are hugely important. They can potentiate a photophysical process, nullify it, or change it altogether. Knowledge of what these processes are, and how they can be controlled through molecular self-assembly, will allow for the development of improved probes with greater functionalities for phototheranostic applications.

AUTHOR INFORMATION

Corresponding Author

*E-mail: gang.zheng@uhnres.utoronto.ca.

Notes

The authors declare no competing financial interest.

Biographies

Kenneth K. Ng received his B.Sc. in 2008 in Biology and Pharmacology from McMaster University. He subsequently completed his Ph.D. under the supervision of Prof. Gang Zheng in 2014 at the Institute of Biomaterials and Biomedical Engineering at the University of Toronto. For his thesis, he studied the properties of porphyrin−lipid supramolecular assemblies and their photonic applications in medicine. He is interested in nanoscale structures formed by self-assembly and investigating biologically inspired systems at the intersection of biology, chemistry, and photonics.

Dr. Gang Zheng is a Professor of Medical Biophysics, Biomedical Engineering and Pharmaceutical Sciences at the University of Toronto. He is also a Senior Scientist, the Joey and Toby Tanenbaum/Brazilian Ball Chair in Prostate Cancer Research at the Princess Margaret Cancer Center, and the Scientific Lead for Nanotechnology and Radiochemistry at the Techna Institute, UHN. He obtained his Ph.D. from SUNY Buffalo and postdoctoral training from Roswell Park Cancer Institute, and joined the faculty of the University of Pennsylvania in 2001 before moving to Canada in 2006. His research has been focused on nanomedicine, molecular imaging, and photodynamic therapy. He is an Associate Editor for *Bioconjugate Chemistry*.

ACKNOWLEDGMENTS

We acknowledge funding support from the Natural Sciences and Engineering Research Council of Canada, the Canadian Institutes for Health Research, the Ontario Institute for Cancer Research, Prostate Cancer Canada, the Canadian Foundation of Innovation, the Terry Fox New Frontiers Program Project Grant, the U.S. Army Ovarian Cancer Research Program, the Joey and Toby Tanenbaum/Brazilian Ball Chair in Prostate Cancer Research, and the Princess Margaret Cancer Foundation.

DOI: 10.1021/acs.chemrev.5b00140
Chem. Rev. XXXX, XXX, XXX−XXX

ABBREVIATIONS

3WJ	three-way junction
AIE	aggregation-induced emission
BPc	benzophthalocyanine
Bchl-lipid	bacteriopheophorbide *a*-lipid
BNPc	benzonaphthalocyanine
BSA	bovine serum albumin
CPMV	cowpea mosaic virus
DET	dexter energy transfer
DLS	dynamic light scattering
DNA	DNA
DPA	diphenylanthracene
DTT	dithiothreitol
EB	emeraldine base
ES	emeraldine salt
fluorotags	fluorescent DNA tags
FRET	Förster resonance energy transfer
GC	glycol chitosan
GRP	gastrin-releasing peptide
GS	ground state
HA	hyaluronic acid
ISC	intersystem crossing
LH2	light harvesting complex 2
LCST	lower critical solution temperature
LPS	lipopolysaccharide
MEH-PPV	poly[2-methoxy-5-(2-ethylhexyloxy)-1,4-phenylenevinylene]
NIR	near-infrared
ONc	5,9,14,18,23,27,32,36-octabutoxy-2,3-naphthalocyanine
PAni	polyaniline
PAV	poly(arylenevinylene)
PBI	perylene bisimide
Pc	phthalocyanine
PdP	Pd tetraaryleporphyrins
PDT	photodynamic therapy
PEDOT	polythiophene
PEDOT:PSS	poly(3,4-ethylenedioxythiophene):poly(4-styrenesulfonate)
PEG_{5000}-DSPE	methoxy(polyethylene glycol)-1,2-dioctadecanoyl-*sn*-glycero-3-phosphocholine
PET	positron emission tomography
PF	poly(9,9-dihexylfluorenyl-2,7-diyl)
PFBT	poly[(9,9-dioctylfluorenyl-2,7-diyl)-*co*-(1,4-benzo-(2,1′,3)-thiadiazole)]
PFPV	poly[(9,9-dioctyl-2,7-divinylenefluorenylene)-*alt*-*co*-(2-methoxy-5-(2-ethylhexyloxy)-1,4-phenylene)]
PFTTQ	poly(phenylfluorene thiadiazolo-quinoxaline)
PFVBT	poly(fluorenyldivinylene benzothiadiazole)
PFVCN	cyano-substituted poly(fluorene-2,7-ylenevinylene-*co*-phenylene)
PLP	porphylipoprotein
PMMA	poly(methyl methacrylate)
PP	polyphenylene
PPE	poly(phenylenethynylene)
PPy	polypyrrole
PtOEP	Pt(II)octaethylprophyrin
PtP	Pt(II)tetraaryleporphyrins
Pyro-lipid	pyropheophorbide *a*-lipid
PTT	photothermal therapy
RET	resonance energy transfer
RNA	ribonucleic acid
ROS	reactive oxygen species
TH	tetrahedron DNA nanostructure
THF	tetrahydrofuran
TMV	tobacco mosaic virus
TPE	tetraphenylethene
TTA	triplet triplet annihilation
TTET	triplet triplet energy transfer
UCNP-G	upconverting nanoparticle with BODIPY-green dye
UCNP-Y	upconverting nanoparticle with BODIPY-yellow dye
ZnBPc	zinc benzophthalocyanine

REFERENCES

(1) Monti, A.; de Groot, H. J. M.; Buda, F. In-silico design of a donor−antenna−acceptor supramolecular complex for photoinduced charge separation. *J. Phys. Chem. C* **2014**, *118*, 15600−15609.

(2) Charaf-Eddin, A.; Planchat, A.; Mennucci, B.; Adamo, C.; Jacquemin, D. Choosing a functional for computing absorption and fluorescence band shapes with TD-DFT. *J. Chem. Theory Comput.* **2013**, *9*, 2749−2760.

(3) Xiao, D.; Martini, L. A.; Snoeberger, R. C.; Crabtree, R. H.; Batista, V. S. Inverse design and synthesis of acac-coumarin anchors for robust tio2 sensitization. *J. Am. Chem. Soc.* **2011**, *133*, 9014−9022.

(4) Hong, G.; Diao, S.; Antaris, A. L.; Dai, H. Carbon nanomaterials for biological imaging and nanomedicinal therapy. *Chem. Rev.* **2015**, DOI: 10.1021/acs.chemrev.5b00008.

(5) Bartelmess, J.; Quinn, S. J.; Giordani, S. Carbon nanomaterials: Multi-functional agents for biomedical fluorescence and raman imaging. *Chem. Soc. Rev.* **2015**, *44*, 4672.

(6) Jaque, D.; Martinez Maestro, L.; del Rosal, B.; Haro-Gonzalez, P.; Benayas, A.; Plaza, J. L.; Martin Rodriguez, E.; Garcia Sole, J. Nanoparticles for photothermal therapies. *Nanoscale* **2014**, *6*, 9494−9530.

(7) Lucky, S. S.; Soo, K. C.; Zhang, Y. Nanoparticles in photodynamic therapy. *Chem. Rev.* **2015**, *115*, 1990−2042.

(8) Lim, E.-K.; Kim, T.; Paik, S.; Haam, S.; Huh, Y.-M.; Lee, K. Nanomaterials for theranostics: Recent advances and future challenges. *Chem. Rev.* **2015**, *115*, 327−394.

(9) Fan, X.; Zheng, W.; Singh, D. J. Light scattering and surface plasmons on small spherical particles. *Light: Sci. Appl.* **2014**, *3*, e179.

(10) Frackowiak, D. The jablonski diagram. *J. Photochem. Photobiol., B* **1988**, *2*, 399−401.

(11) Wang, L. V.; Hu, S. Photoacoustic tomography: In vivo imaging from organelles to organs. *Science* **2012**, *335*, 1458−1462.

(12) Emelianov, S. Y.; Li, P.-C.; O'Donnell, M. Photoacoustics for molecular imaging and therapy. *Phys. Today* **2009**, *62*, 34.

(13) Huang, X.; El-Sayed, I. H.; Qian, W.; El-Sayed, M. A. Cancer cell imaging and photothermal therapy in the near-infrared region by using gold nanorods. *J. Am. Chem. Soc.* **2006**, *128*, 2115−2120.

(14) Solov'ev, K. N.; Borisevich, E. A. Intramolecular heavy-atom effect in the photophysics of organic molecules. *Phys.-Usp.* **2005**, *48*, 231.

(15) Clegg, R. M. In *Reviews in Fluorescence*; Geddes, C., Lakowicz, J., Eds.; Springer: New York, 2006; Vol. *2006*.

(16) Clegg, R. M.; Sener, M. *Govindjee Proc.*; SPIE: 2010; Vol. *7561*, p 75610C.

(17) Muñoz-Losa, A.; Curutchet, C.; Krueger, B. P.; Hartsell, L. R.; Mennucci, B. Fretting about fret: Failure of the ideal dipole approximation. *Biophys. J.* **2009**, *96*, 4779−4788.

(18) Scholes, G. D. Long-range resonance energy transfer in molecular systems. *Annu. Rev. Phys. Chem.* **2003**, *54*, 57−87.

(19) Cabanillas-Gonzalez, J.; Fox, A. M.; Hill, J.; Bradley, D. D. C. Model for energy transfer in polymer/dye blends based on point−surface dipole interaction. *Chem. Mater.* **2004**, *16*, 4705−4710.

DOI: 10.1021/acs.chemrev.5b00140
Chem. Rev. XXXX, XXX, XXX−XXX

(20) Scholes, G. D.; Jordanides, X. J.; Fleming, G. R. Adapting the förster theory of energy transfer for modeling dynamics in aggregated molecular assemblies. *J. Phys. Chem. B* **2001**, *105*, 1640−1651.
(21) Hevekerl, H.; Spielmann, T.; Chmyrov, A.; Widengren, J. Förster resonance energy transfer beyond 10 nm: Exploiting the triplet state kinetics of organic fluorophores. *J. Phys. Chem. B* **2011**, *115*, 13360−13370.
(22) Snapp, E. L.; Hegde, R. S.; Bonifacino, Juan S. Rational design and evaluation of fret experiments to measure protein proximities in cells. *Current protocols in cell biology/editorial board* **2006**, 1 DOI: 10.1002/0471143030.cb1709s32.
(23) Chen, J.; Lovell, J. F.; Lo, P. C.; Stefflova, K.; Niedre, M.; Wilson, B. C.; Zheng, G. A tumor mrna-triggered photodynamic molecular beacon based on oligonucleotide hairpin control of singlet oxygen production. *Photochem. Photobiol. Sci.* **2008**, *7*, 775−781.
(24) Tsourkas, A.; Behlke, M. A.; Bao, G. Hybridization of 2′-o-methyl and 2′-deoxy molecular beacons to rna and DNA targets. *Nucleic Acids Res.* **2003**, *31*, 5168−5174.
(25) Ng, K. K.; Takada, M.; Jin, C. C. S.; Zheng, G. Self-sensing porphysomes for fluorescence-guided photothermal therapy. *Bioconjugate Chem.* **2015**, *26*, 345−351.
(26) Lu, J.; Owen, S. C.; Shoichet, M. S. Stability of self-assembled polymeric micelles in serum. *Macromolecules* **2011**, *44*, 6002−6008.
(27) Lakowicz, J. R. In *Principles of Fluorescence Spectroscopy*; Lakowicz, J. R., Ed.; Springer: New York, 2006.
(28) Zhao, J.; Ji, S.; Guo, H. Triplet-triplet annihilation based upconversion: From triplet sensitizers and triplet acceptors to upconversion quantum yields. *RSC Adv.* **2011**, *1*, 937−950.
(29) Liu, Q.; Feng, W.; Yang, T.; Yi, T.; Li, F. Upconversion luminescence imaging of cells and small animals. *Nat. Protoc.* **2013**, *8*, 2033−2044.
(30) Cheng, Y. Y.; Khoury, T.; Clady, R. G. C. R.; Tayebjee, M. J. Y.; Ekins-Daukes, N. J.; Crossley, M. J.; Schmidt, T. W. On the efficiency limit of triplet-triplet annihilation for photochemical upconversion. *Phys. Chem. Chem. Phys.* **2010**, *12*, 66−71.
(31) Birks, J. B.; Christophorou, L. G. Excimer fluorescence spectra of pyrene derivatives. *Spectrochim. Acta* **1963**, *19*, 401−410.
(32) Birks, J. B.; Kazzaz, A. A. *Proc. R. Soc. London, Ser. A* **1968**, *304*, 291.
(33) Jelley, E. E. Molecular, nematic and crystal states of i: I-diethyl-ψ-cyanine chloride. *Nature* **1937**, *139*, 2.
(34) Jelley, E. E. Spectral absorption and fluorescence of dyes in the molecular state. *Nature* **1936**, *138*, 2.
(35) Scheibe, G. Variability of the absorption spectra of some sensitizing dyes and its cause. *Angew. Chem., Int. Ed.* **1936**, *49*, 563.
(36) Würthner, F.; Kaiser, T. E.; Saha-Möller, C. R. J-aggregates: From serendipitous discovery to supramolecular engineering of functional dye materials. *Angew. Chem., Int. Ed.* **2011**, *50*, 3376−3410.
(37) Spano, F. C.; Kuklinski, J. R.; Mukamel, S. Temperature-dependent superradiant decay of excitons in small aggregates. *Phys. Rev. Lett.* **1990**, *65*, 211−214.
(38) Kasha, M.; Rawls, H. R.; Ashraf El-Bayoumi, M. The exciton model in molecular spectroscopy. *Pure Appl. Chem.* **1965**, *11*, 371−392.
(39) Spano, F. C. The spectral signatures of frenkel polarons in h- and j-aggregates. *Acc. Chem. Res.* **2010**, *43*, 429−439.
(40) Pan, D.; Cai, X.; Kim, B.; Stacy, A. J.; Wang, L. V.; Lanza, G. M. Rapid synthesis of near infrared polymeric micelles for real-time sentinel lymph node imaging. *Adv. Healthcare Mater.* **2012**, *1*, 582−589.
(41) Akers, W. J.; Kim, C.; Berezin, M.; Guo, K.; Fuhrhop, R.; Lanza, G. M.; Fischer, G. M.; Daltrozzo, E.; Zumbusch, A.; Cai, X.; et al. Noninvasive photoacoustic and fluorescence sentinel lymph node identification using dye-loaded perfluorocarbon nanoparticles. *ACS Nano* **2011**, *5*, 173−182.
(42) Anayama, T.; Jin, C. S.; Mcveigh, P.; Nakajima, T.; Ng, K.; Lovell, J. F.; Hirohashi, K.; Wada, H.; Wilson, B.; Yasufuku, K.; et al. *J. Thorac. Oncol.* **2013**, S771−S771.
(43) Wu, Y. C.; Kulbatski, I.; Medeiros, P. J.; Maeda, A.; Bu, J.; Xu, L.; Chen, Y.; DaCosta, R. S. Autofluorescence imaging device for real-time detection and tracking of pathogenic bacteria in a mouse skin wound model: Preclinical feasibility studies. *J. Biomed. Opt.* **2014**, *19*, 085002−085002.
(44) Liu, Y.; Bauer, A. Q.; Akers, W. J.; Sudlow, G.; Liang, K.; Shen, D.; Berezin, M. Y.; Culver, J. P.; Achilefu, S. Hands-free, wireless goggles for near-infrared fluorescence and real-time image-guided surgery. *Surgery* **2011**, *149*, 689−698.
(45) Luo, J.; Xie, Z.; Lam, J. W. Y.; Cheng, L.; Chen, H.; Qiu, C.; Kwok, H. S.; Zhan, X.; Liu, Y.; Zhu, D.; et al. Aggregation-induced emission of 1-methyl-1,2,3,4,5-pentaphenylsilole. *Chem. Commun.* **2001**, 1740−1741.
(46) An, B.-K.; Kwon, S.-K.; Jung, S.-D.; Park, S. Y. Enhanced emission and its switching in fluorescent organic nanoparticles. *J. Am. Chem. Soc.* **2002**, *124*, 14410−14415.
(47) Mei, J.; Hong, Y.; Lam, J. W. Y.; Qin, A.; Tang, Y.; Tang, B. Z. Aggregation-induced emission: The whole is more brilliant than the parts. *Adv. Mater.* **2014**, *26*, 5429−5479.
(48) Yu, Y.; Feng, C.; Hong, Y.; Liu, J.; Chen, S.; Ng, K. M.; Luo, K. Q.; Tang, B. Z. Cytophilic fluorescent bioprobes for long-term cell tracking. *Adv. Mater.* **2011**, *23*, 3298−3302.
(49) Lim, C.-K.; Kim, S.; Kwon, I. C.; Ahn, C.-H.; Park, S. Y. Dye-condensed biopolymeric hybrids: Chromophoric aggregation and self-assembly toward fluorescent bionanoparticles for near infrared bioimaging. *Chem. Mater.* **2009**, *21*, 5819−5825.
(50) Qin, W.; Ding, D.; Liu, J.; Yuan, W. Z.; Hu, Y.; Liu, B.; Tang, B. Z. Biocompatible nanoparticles with aggregation-induced emission characteristics as far-red/near-infrared fluorescent bioprobes for in vitro and in vivo imaging applications. *Adv. Funct. Mater.* **2012**, *22*, 771−779.
(51) Geng, J.; Li, K.; Qin, W.; Ma, L.; Gurzadyan, G. G.; Tang, B. Z.; Liu, B. Eccentric loading of fluorogen with aggregation-induced emission in plga matrix increases nanoparticle fluorescence quantum yield for targeted cellular imaging. *Small* **2013**, *9*, 2012−2019.
(52) Ding, D.; Goh, C. C.; Feng, G.; Zhao, Z.; Liu, J.; Liu, R.; Tomczak, N.; Geng, J.; Tang, B. Z.; Ng, L. G.; et al. Ultrabright organic dots with aggregation-induced emission characteristics for real-time two-photon intravital vasculature imaging. *Adv. Mater.* **2013**, *25*, 6083−6088.
(53) Zhao, Q.; Li, K.; Chen, S.; Qin, A.; Ding, D.; Zhang, S.; Liu, Y.; Liu, B.; Sun, J. Z.; Tang, B. Z. Aggregation-induced red-NIR emission organic nanoparticles as effective and photostable fluorescent probes for bioimaging. *J. Mater. Chem.* **2012**, *22*, 15128−15135.
(54) Zhang, X.; Zhang, X.; Wang, S.; Liu, M.; Tao, L.; Wei, Y. Surfactant modification of aggregation-induced emission material as biocompatible nanoparticles: Facile preparation and cell imaging. *Nanoscale* **2013**, *5*, 147−150.
(55) Li, K.; Qin, W.; Ding, D.; Tomczak, N.; Geng, J.; Liu, R.; Liu, J.; Zhang, X.; Liu, H.; Liu, B. Photostable fluorescent organic dots with aggregation-induced emission (aie dots) for noninvasive long-term cell tracing. *Sci. Rep.* **2013**, *3*, 1 DOI: 10.1038/srep01150.
(56) Benvin, A. L.; Creeger, Y.; Fisher, G. W.; Ballou, B.; Waggoner, A. S.; Armitage, B. A. Fluorescent DNA nanotags: Supramolecular fluorescent labels based on intercalating dye arrays assembled on nanostructured DNA templates. *J. Am. Chem. Soc.* **2007**, *129*, 2025−2034.
(57) Özhalıcı-Ünal, H.; Armitage, B. A. Fluorescent DNA nanotags based on a self-assembled DNA tetrahedron. *ACS Nano* **2009**, *3*, 425−433.
(58) Stadler, A. L.; Delos Santos, J. O.; Stensrud, E. S.; Dembska, A.; Silva, G. L.; Liu, S.; Shank, N. I.; Kunttas-Tatli, E.; Sobers, C. J.; Gramlich, P. M. E.; et al. Fluorescent DNA nanotags featuring covalently attached intercalating dyes: Synthesis, antibody conjugation, and intracellular imaging. *Bioconjugate Chem.* **2011**, *22*, 1491−1502.
(59) Teo, Y. N.; Kool, E. T. DNA-multichromophore systems. *Chem. Rev.* **2012**, *112*, 4221−4245.

DOI: 10.1021/acs.chemrev.5b00140
Chem. Rev. XXXX, XXX, XXX−XXX

(60) Gao, J.; Strässler, C.; Tahmassebi, D.; Kool, E. T. Libraries of composite polyfluors built from fluorescent deoxyribosides. *J. Am. Chem. Soc.* **2002**, *124*, 11590−11591.
(61) Cuppoletti, A.; Cho, Y.; Park, J.-S.; Strässler, C.; Kool, E. T. Oligomeric fluorescent labels for DNA. *Bioconjugate Chem.* **2005**, *16*, 528−534.
(62) Teo, Y. N.; Wilson, J. N.; Kool, E. T. Polyfluorophores on a DNA backbone: A multicolor set of labels excited at one wavelength. *J. Am. Chem. Soc.* **2009**, *131*, 3923−3933.
(63) Teo, Y. N.; Kool, E. T. Polyfluorophore excimers and exciplexes as fret donors in DNA. *Bioconjugate Chem.* **2009**, *20*, 2371−2380.
(64) Wang, S.; Guo, J.; Ono, T.; Kool, E. T. DNA polyfluorophores for real-time multicolor tracking of dynamic biological systems. *Angew. Chem., Int. Ed.* **2012**, *51*, 7176−7180.
(65) Lewis, J. D.; Destito, G.; Zijlstra, A.; Gonzalez, M. J.; Quigley, J. P.; Manchester, M.; Stuhlmann, H. Viral nanoparticles as tools for intravital vascular imaging. *Nat. Med.* **2006**, *12*, 354−360.
(66) Steinmetz, N. F.; Ablack, A. L.; Hickey, J. L.; Ablack, J.; Manocha, B.; Mymryk, J. S.; Luyt, L. G.; Lewis, J. D. Intravital imaging of human prostate cancer using viral nanoparticles targeted to gastrin-releasing peptide receptors. *Small* **2011**, *7*, 1664−1672.
(67) Chariou, P. L.; Lee, K. L.; Wen, A. M.; Gulati, N. M.; Stewart, P. L.; Steinmetz, N. F. Detection and imaging of aggressive cancer cells using an epidermal growth factor receptor (egfr)-targeted filamentous plant virus-based nanoparticle. *Bioconjugate Chem.* **2015**, *26*, 262−269.
(68) Ghosh, D.; Lee, Y.; Thomas, S.; Kohli, A. G.; Yun, D. S.; Belcher, A. M.; Kelly, K. A. M13-templated magnetic nanoparticles for targeted in vivo imaging of prostate cancer. *Nat. Nanotechnol.* **2012**, *7*, 677−682.
(69) Miller, R. A.; Stephanopoulos, N.; McFarland, J. M.; Rosko, A. S.; Geissler, P. L.; Francis, M. B. Impact of assembly state on the defect tolerance of tmv-based light harvesting arrays. *J. Am. Chem. Soc.* **2010**, *132*, 6068−6074.
(70) Miller, R. A.; Presley, A. D.; Francis, M. B. Self-assembling light-harvesting systems from synthetically modified tobacco mosaic virus coat proteins. *J. Am. Chem. Soc.* **2007**, *129*, 3104−3109.
(71) Endo, M.; Fujitsuka, M.; Majima, T. Porphyrin light-harvesting arrays constructed in the recombinant tobacco mosaic virus scaffold. *Chem. - Eur. J.* **2007**, *13*, 8660−8666.
(72) Reile, H.; Armatis, P. E.; Schally, A. V. Characterization of high-affinity receptors for bombesin/gastrin releasing peptide on the human prostate cancer cell lines pc-3 and du-145: Internalization of receptor bound 125i-(tyr4) bombesin by tumor cells. *Prostate* **1994**, *25*, 29−38.
(73) Wen, A. M.; Infusino, M.; De Luca, A.; Kernan, D. L.; Czapar, A. E.; Strangi, G.; Steinmetz, N. F. Interface of physics and biology: Engineering virus-based nanoparticles for biophotonics. *Bioconjugate Chem.* **2015**, *26*, 51−62.
(74) de Wispelaere, M.; Chaturvedi, S.; Wilkens, S.; Rao, A. L. N. Packaging and structural phenotype of brome mosaic virus capsid protein with altered n-terminal β-hexamer structure. *Virology* **2011**, *419*, 17−23.
(75) Jung, B.; Rao, A. L. N.; Anvari, B. Optical nano-constructs composed of genome-depleted brome mosaic virus doped with a near infrared chromophore for potential biomedical applications. *ACS Nano* **2011**, *5*, 1243−1252.
(76) Pecher, J.; Mecking, S. Nanoparticles of conjugated polymers. *Chem. Rev.* **2010**, *110*, 6260−6279.
(77) Schwartz, B. J. Conjugated polymers as molecular materials: How chain conformation and film morphology influence energy transfer and interchain interactions. *Annu. Rev. Phys. Chem.* **2003**, *54*, 141−172.
(78) Wu, C.; Bull, B.; Szymanski, C.; Christensen, K.; McNeill, J. Multicolor conjugated polymer dots for biological fluorescence imaging. *ACS Nano* **2008**, *2*, 2415−2423.
(79) Wu, C.; Szymanski, C.; Cain, Z.; McNeill, J. Conjugated polymer dots for multiphoton fluorescence imaging. *J. Am. Chem. Soc.* **2007**, *129*, 12904−12905.
(80) Wu, C.; Zheng, Y.; Szymanski, C.; McNeill, J. Energy transfer in a nanoscale multichromophoric system: Fluorescent dye-doped conjugated polymer nanoparticles. *J. Phys. Chem. C* **2008**, *112*, 1772−1781.
(81) Wu, C.; Peng, H.; Jiang, Y.; McNeill, J. Energy transfer mediated fluorescence from blended conjugated polymer nanoparticles. *J. Phys. Chem. B* **2006**, *110*, 14148−14154.
(82) Wu, C.; Szymanski, C.; McNeill, J. Preparation and encapsulation of highly fluorescent conjugated polymer nanoparticles. *Langmuir* **2006**, *22*, 2956−2960.
(83) Szymanski, C.; Wu, C.; Hooper, J.; Salazar, M. A.; Perdomo, A.; Dukes, A.; McNeill, J. Single molecule nanoparticles of the conjugated polymer meh−ppv, preparation and characterization by near-field scanning optical microscopy. *J. Phys. Chem. B* **2005**, *109*, 8543−8546.
(84) Wu, C.; McNeill, J. Swelling-controlled polymer phase and fluorescence properties of polyfluorene nanoparticles. *Langmuir* **2008**, *24*, 5855−5861.
(85) Howes, P.; Green, M.; Levitt, J.; Suhling, K.; Hughes, M. Phospholipid encapsulated semiconducting polymer nanoparticles: Their use in cell imaging and protein attachment. *J. Am. Chem. Soc.* **2010**, *132*, 3989−3996.
(86) Kim, S.; Lim, C.-K.; Na, J.; Lee, Y.-D.; Kim, K.; Choi, K.; Leary, J. F.; Kwon, I. C. Conjugated polymer nanoparticles for biomedical in vivo imaging. *Chem. Commun.* **2010**, *46*, 1617−1619.
(87) Veiseh, M.; Gabikian, P.; Bahrami, S.-B.; Veiseh, O.; Zhang, M.; Hackman, R. C.; Ravanpay, A. C.; Stroud, M. R.; Kusuma, Y.; Hansen, S. J.; et al. Tumor paint: A chlorotoxin:Cy5.5 bioconjugate for intraoperative visualization of cancer foci. *Cancer Res.* **2007**, *67*, 6882−6888.
(88) Wu, C.; Hansen, S. J.; Hou, Q.; Yu, J.; Zeigler, M.; Jin, Y.; Burnham, D. R.; McNeill, J. D.; Olson, J. M.; Chiu, D. T. Design of highly emissive polymer dot bioconjugates for in vivo tumor targeting. *Angew. Chem., Int. Ed.* **2011**, *50*, 3430−3434.
(89) Pietsch, C.; Vollrath, A.; Hoogenboom, R.; Schubert, U. S. A fluorescent thermometer based on a pyrene-labeled thermoresponsive polymer. *Sensors* **2010**, *10*, 7979−7990.
(90) Pietsch, C.; Hoogenboom, R.; Schubert, U. S. Pmma based soluble polymeric temperature sensors based on ucst transition and solvatochromic dyes. *Polym. Chem.* **2010**, *1*, 1005−1008.
(91) Hoogenboom, R.; Thijs, H. M. L.; Jochems, M. J. H. C.; van Lankvelt, B. M.; Fijten, M. W. M.; Schubert, U. S. Tuning the lcst of poly(2-oxazoline)s by varying composition and molecular weight: Alternatives to poly(n-isopropylacrylamide)? *Chem. Commun.* **2008**, 5758−5760.
(92) Hanahan, D.; Weinberg; Robert, A. Hallmarks of cancer: The next generation. *Cell* **2011**, *144*, 646−674.
(93) Ma, X.; Wang, Y.; Zhao, T.; Li, Y.; Su, L.-C.; Wang, Z.; Huang, G.; Sumer, B. D.; Gao, J. Ultra-ph-sensitive nanoprobe library with broad pH tunability and fluorescence emissions. *J. Am. Chem. Soc.* **2014**, *136*, 11085−11092.
(94) Zhou, K.; Liu, H.; Zhang, S.; Huang, X.; Wang, Y.; Huang, G.; Sumer, B. D.; Gao, J. Multicolored ph-tunable and activatable fluorescence nanoplatform responsive to physiologic pH stimuli. *J. Am. Chem. Soc.* **2012**, *134*, 7803−7811.
(95) Wang, Y.; Zhou, K.; Huang, G.; Hensley, C.; Huang, X.; Ma, X.; Zhao, T.; Sumer, B. D.; DeBerardinis, R. J.; Gao, J. A nanoparticle-based strategy for the imaging of a broad range of tumours by nonlinear amplification of microenvironment signals. *Nat. Mater.* **2013**, *13*, 204−212.
(96) Zhang, X.; Chen, Z.; Würthner, F. Morphology control of fluorescent nanoaggregates by co-self-assembly of wedge- and dumbbell-shaped amphiphilic perylene bisimides. *J. Am. Chem. Soc.* **2007**, *129*, 4886−4887.
(97) Zhang, X.; Rehm, S.; Safont-Sempere, M. M.; Würthner, F. Vesicular perylene dye nanocapsules as supramolecular fluorescent pH sensor systems. *Nat. Chem.* **2009**, *1*, 623−629.
(98) Schmidt-Mende, L.; Fechtenkötter, A.; Müllen, K.; Moons, E.; Friend, R. H.; MacKenzie, J. D. Self-organized discotic liquid crystals for high-efficiency organic photovoltaics. *Science* **2001**, *293*, 1119−1122.

DOI: 10.1021/acs.chemrev.5b00140
Chem. Rev. XXXX, XXX, XXX−XXX

(99) Modi, S.; Swetha, M. G.; Goswami, D.; Gupta, G. D.; Mayor, S.; Krishnan, Y. A DNA nanomachine that maps spatial and temporal pH changes inside living cells. *Nat. Nanotechnol.* **2009**, *4*, 325−330.
(100) Modi, S.; Nizak, C.; Surana, S.; Halder, S.; Krishnan, Y. Two DNA nanomachines map pH changes along intersecting endocytic pathways inside the same cell. *Nat. Nanotechnol.* **2013**, *8*, 459−467.
(101) Choi, K. Y.; Swierczewska, M.; Lee, S.; Chen, X. Protease-activated drug development. *Theranostics* **2012**, *2*, 156−178.
(102) Weissleder, R.; Tung, C.-H.; Mahmood, U.; Bogdanov, A. In vivo imaging of tumors with protease-activated near-infrared fluorescent probes. *Nat. Biotechnol.* **1999**, *17*, 375−378.
(103) Shi, H.; Kwok, R. T. K.; Liu, J.; Xing, B.; Tang, B. Z.; Liu, B. Real-time monitoring of cell apoptosis and drug screening using fluorescent light-up probe with aggregation-induced emission characteristics. *J. Am. Chem. Soc.* **2012**, *134*, 17972−17981.
(104) Rhee, S. G.; Kang, S. W.; Jeong, W.; Chang, T.-S.; Yang, K.-S.; Woo, H. A. Intracellular messenger function of hydrogen peroxide and its regulation by peroxiredoxins. *Curr. Opin. Cell Biol.* **2005**, *17*, 183−189.
(105) Lee, D.; Khaja, S.; Velasquez-Castano, J. C.; Dasari, M.; Sun, C.; Petros, J.; Taylor, W. R.; Murthy, N. In vivo imaging of hydrogen peroxide with chemiluminescent nanoparticles. *Nat. Mater.* **2007**, *6*, 765−769.
(106) Lim, C.-K.; Lee, Y.-D.; Na, J.; Oh, J. M.; Her, S.; Kim, K.; Choi, K.; Kim, S.; Kwon, I. C. Chemiluminescence-generating nanoreactor formulation for near-infrared imaging of hydrogen peroxide and glucose level in vivo. *Adv. Funct. Mater.* **2010**, *20*, 2644−2648.
(107) Lee, Y.-D.; Lim, C.-K.; Singh, A.; Koh, J.; Kim, J.; Kwon, I. C.; Kim, S. Dye/peroxalate aggregated nanoparticles with enhanced and tunable chemiluminescence for biomedical imaging of hydrogen peroxide. *ACS Nano* **2012**, *6*, 6759−6766.
(108) Robertson, C. A.; Evans, D. H.; Abrahamse, H. Photodynamic therapy (pdt): A short review on cellular mechanisms and cancer research applications for pdt. *J. Photochem. Photobiol., B* **2009**, *96*, 1−8.
(109) Dolmans, D. E. J. G. J.; Fukumura, D.; Jain, R. K. Photodynamic therapy for cancer. *Nat. Rev. Cancer* **2003**, *3*, 380−387.
(110) Oar, M. A.; Serin, J. M.; Dichtel, W. R.; Fréchet, J. M. J.; Ohulchanskyy, T. Y.; Prasad, P. N. Photosensitization of singlet oxygen via two-photon-excited fluorescence resonance energy transfer in a water-soluble dendrimer. *Chem. Mater.* **2005**, *17*, 2267−2275.
(111) Oar, M. A.; Dichtel, W. R.; Serin, J. M.; Fréchet, J. M. J.; Rogers, J. E.; Slagle, J. E.; Fleitz, P. A.; Tan, L.-S.; Ohulchanskyy, T. Y.; Prasad, P. N. Light-harvesting chromophores with metalated porphyrin cores for tuned photosensitization of singlet oxygen via two-photon excited fret. *Chem. Mater.* **2006**, *18*, 3682−3692.
(112) Ochsner, M. Photophysical and photobiological processes in the photodynamic therapy of tumours. *J. Photochem. Photobiol., B* **1997**, *39*, 1−18.
(113) Salleo, A.; Chabinyc, M. In *Organic Electronics: Materials, Manufacturing, and Applications*; Klauk, H., Ed.; Wiley-VCH Verlag GmbH & Co.: Weinheim, Germany, 2006.
(114) Scurlock, R. D.; Wang, B.; Ogilby, P. R.; Sheats, J. R.; Clough, R. L. Singlet oxygen as a reactive intermediate in the photodegradation of an electroluminescent polymer. *J. Am. Chem. Soc.* **1995**, *117*, 10194−10202.
(115) Abdou, M. S. A.; Holdcroft, S. Solid-state photochemistry of π-conjugated poly(3-alkylthiophenes). *Can. J. Chem.* **1995**, *73*, 1893−1901.
(116) Chemburu, S.; Corbitt, T. S.; Ista, L. K.; Ji, E.; Fulghum, J.; Lopez, G. P.; Ogawa, K.; Schanze, K. S.; G. Whitten, D. Light-induced biocidal action of conjugated polyelectrolytes supported on colloids. *Langmuir* **2008**, *24*, 11053−11062.
(117) Shen, X.; Li, L.; Min Chan, A. C.; Gao, N.; Yao, S. Q.; Xu, Q.-H. Water-soluble conjugated polymers for simultaneous two-photon cell imaging and two-photon photodynamic therapy. *Adv. Opt. Mater.* **2013**, *1*, 92−99.
(118) Collins, H. A.; Khurana, M.; Moriyama, E. H.; Mariampillai, A.; Dahlstedt, E.; Balaz, M.; Kuimova, M. K.; Drobizhev, M.; Yang, V. X. D.; Phillips, D.; et al. Blood-vessel closure using photosensitizers engineered for two-photon excitation. *Nat. Photonics* **2008**, *2*, 420−424.
(119) Shen, X.; Li, L.; Wu, H.; Yao, S. Q.; Xu, Q. H. Photosensitizer-doped conjugated polymer nanoparticles for simultaneous two-photon imaging and two-photon photodynamic therapy in living cells. *Nanoscale* **2011**, *3*, 5140−5146.
(120) Grimland, J. L.; Wu, C.; Ramoutar, R. R.; Brumaghim, J. L.; McNeill, J. Photosensitizer-doped conjugated polymer nanoparticles with high cross-sections for one- and two-photon excitation. *Nanoscale* **2011**, *3*, 1451−1455.
(121) Shen, X.; He, F.; Wu, J.; Xu, G. Q.; Yao, S. Q.; Xu, Q. H. Enhanced two-photon singlet oxygen generation by photosensitizer-doped conjugated polymer nanoparticles. *Langmuir* **2011**, *27*, 1739−1744.
(122) Kasha, M. Collisional perturbation of spin-orbital coupling and the mechanism of fluorescence quenching. A visual demonstration of the perturbation. *J. Chem. Phys.* **1952**, *20*, 71−74.
(123) Lim, C. K.; Shin, J.; Lee, Y. D.; Kim, J.; Park, H.; Kwon, I. C.; Kim, S. Heavy-atomic construction of photosensitizer nanoparticles for enhanced photodynamic therapy of cancer. *Small* **2011**, *7*, 112−118.
(124) Lim, C. K.; Shin, J.; Kwon, I. C.; Jeong, S. Y.; Kim, S. Iodinated photosensitizing chitosan: Self-assembly into tumor-homing nanoparticles with enhanced singlet oxygen generation. *Bioconjugate Chem.* **2012**, *23*, 1022−1028.
(125) Krinick, N. L.; Sun, Y.; Joyner, D.; Spikes, J. D.; Straight, R. C.; Kopeček, J. A polymeric drug delivery system for the simultaneous delivery of drugs activatable by enzymes and/or light. *J. Biomater. Sci., Polym. Ed.* **1994**, *5*, 303−324.
(126) Lee, S. J.; Koo, H.; Lee, D. E.; Min, S.; Lee, S.; Chen, X.; Choi, Y.; Leary, J. F.; Park, K.; Jeong, S. Y.; et al. Tumor-homing photosensitizer-conjugated glycol chitosan nanoparticles for synchronous photodynamic imaging and therapy based on cellular on/off system. *Biomaterials* **2011**, *32*, 4021−4029.
(127) Oh, I. H.; Min, H. S.; Li, L.; Tran, T. H.; Lee, Y. K.; Kwon, I. C.; Choi, K.; Kim, K.; Huh, K. M. Cancer cell-specific photoactivity of pheophorbide a-glycol chitosan nanoparticles for photodynamic therapy in tumor-bearing mice. *Biomaterials* **2013**, *34*, 6454−6463.
(128) Arunachalam, B.; Phan, U. T.; Geuze, H. J.; Cresswell, P. Enzymatic reduction of disulfide bonds in lysosomes: Characterization of a gamma-interferon-inducible lysosomal thiol reductase (gilt). *Proc. Natl. Acad. Sci. U. S. A.* **2000**, *97*, 745−750.
(129) Yoon, H. Y.; Koo, H.; Choi, K. Y.; Lee, S. J.; Kim, K.; Kwon, I. C.; Leary, J. F.; Park, K.; Yuk, S. H.; Park, J. H.; et al. Tumor-targeting hyaluronic acid nanoparticles for photodynamic imaging and therapy. *Biomaterials* **2012**, *33*, 3980−3989.
(130) Aliabadi, H. M.; Elhasi, S.; Mahmud, A.; Gulamhusein, R.; Mahdipoor, P.; Lavasanifar, A. Encapsulation of hydrophobic drugs in polymeric micelles through co-solvent evaporation: The effect of solvent composition on micellar properties and drug loading. *Int. J. Pharm.* **2007**, *329*, 158−165.
(131) Lovell, J. F.; Jin, C. S.; Huynh, E.; Jin, H.; Kim, C.; Rubinstein, J. L.; Chan, W. C.; Cao, W.; Wang, L. V.; Zheng, G. Porphysome nanovesicles generated by porphyrin bilayers for use as multimodal biophotonic contrast agents. *Nat. Mater.* **2011**, *10*, 324−332.
(132) Huynh, E.; Zheng, G. Porphysome nanotechnology: A paradigm shift in lipid-based supramolecular structures. *Nano Today* **2014**, *9*, 212−222.
(133) Jin, C. S.; Cui, L.; Wang, F.; Chen, J.; Zheng, G. Phototherapy: Targeting-triggered porphysome nanostructure disruption for activatable photodynamic therapy (adv. Healthcare mater. 8/2014). *Adv. Healthcare Mater.* **2014**, *3*, 1122.
(134) Liu, T. W.; MacDonald, T. D.; Shi, J.; Wilson, B. C.; Zheng, G. Intrinsically copper-64-labeled organic nanoparticles as radiotracers. *Angew. Chem., Int. Ed.* **2012**, *51*, 13128−13131.
(135) Liu, T. W.; MacDonald, T. D.; Jin, C. S.; Gold, J. M.; Bristow, R. G.; Wilson, B. C.; Zheng, G. Inherently multimodal nanoparticle-driven tracking and real-time delineation of orthotopic prostate tumors and micrometastases. *ACS Nano* **2013**, *7*, 4221−4232.

DOI: 10.1021/acs.chemrev.5b00140
Chem. Rev. XXXX, XXX, XXX−XXX

(136) Lovell, J. F.; Jin, C. S.; Huynh, E.; MacDonald, T. D.; Cao, W.; Zheng, G. Enzymatic regioselection for the synthesis and biodegradation of porphysome nanovesicles. *Angew. Chem., Int. Ed.* **2012**, *51*, 2429−2433.
(137) Liang, X.; Deng, Z.; Jing, L.; Li, X.; Dai, Z.; Li, C.; Huang, M. Prussian blue nanoparticles operate as a contrast agent for enhanced photoacoustic imaging. *Chem. Commun.* **2013**, *49*, 11029−11031.
(138) Huang, H.; Cruz, W.; Chen, J.; Zheng, G. Learning from biology: Synthetic lipoproteins for drug delivery. *Wiley Interdiscip. Rev.: Nanomed. Nanobiotechnol.* **2015**, *7*, n/a−n/a.
(139) Cui, L.; Lin, Q.; Jin, C. S.; Jiang, W.; Huang, H.; Ding, L.; Muhanna, N.; Irish, J. C.; Wang, F.; Chen, J.; et al. A pegylation-free biomimetic porphyrin nanoplatform for personalized cancer theranostics. *ACS Nano* **2015**, *9*, 4484−4495.
(140) Lebedev, A. Y.; Cheprakov, A. V.; Sakadžić, S.; Boas, D. A.; Wilson, D. F.; Vinogradov, S. A. Dendritic phosphorescent probes for oxygen imaging in biological systems. *ACS Appl. Mater. Interfaces* **2009**, *1*, 1292−1304.
(141) Vanderkooi, J. M.; Maniara, G.; Green, T. J.; Wilson, D. F. An optical method for measurement of dioxygen concentration based upon quenching of phosphorescence. *J. Biol. Chem.* **1987**, *262*, 5476−5482.
(142) Wilson, D. F.; Rumsey, W. L.; Green, T. J.; Vanderkooi, J. M. The oxygen dependence of mitochondrial oxidative phosphorylation measured by a new optical method for measuring oxygen concentration. *J. Biol. Chem.* **1988**, *263*, 2712−2718.
(143) Fercher, A.; Borisov, S. M.; Zhdanov, A. V.; Klimant, I.; Papkovsky, D. B. Intracellular o2 sensing probe based on cell-penetrating phosphorescent nanoparticles. *ACS Nano* **2011**, *5*, 5499−5508.
(144) Liu, H.; Yang, H.; Hao, X.; Xu, H.; Lv, Y.; Xiao, D.; Wang, H.; Tian, Z. Development of polymeric nanoprobes with improved lifetime dynamic range and stability for intracellular oxygen sensing. *Small* **2013**, *9*, 2639−2648.
(145) Su, F.; Alam, R.; Mei, Q.; Tian, Y.; Youngbull, C.; Johnson, R. H.; Meldrum, D. R. Nanostructured oxygen sensor - using micelles to incorporate a hydrophobic platinum porphyrin. *PLoS One* **2012**, *7*, e33390.
(146) Finikova, O. S.; Lebedev, A. Y.; Aprelev, A.; Troxler, T.; Gao, F.; Garnacho, C.; Muro, S.; Hochstrasser, R. M.; Vinogradov, S. A. Oxygen microscopy by two-photon-excited phosphorescence. *ChemPhysChem* **2008**, *9*, 1673−1679.
(147) Briñas, R. P.; Troxler, T.; Hochstrasser, R. M.; Vinogradov, S. A. Phosphorescent oxygen sensor with dendritic protection and two-photon absorbing antenna. *J. Am. Chem. Soc.* **2005**, *127*, 11851−11862.
(148) Sakadzic, S.; Roussakis, E.; Yaseen, M. A.; Mandeville, E. T.; Srinivasan, V. J.; Arai, K.; Ruvinskaya, S.; Devor, A.; Lo, E. H.; Vinogradov, S. A.; et al. Two-photon high-resolution measurement of partial pressure of oxygen in cerebral vasculature and tissue. *Nat. Methods* **2010**, *7*, 755−759.
(149) Wu, C.; Bull, B.; Christensen, K.; McNeill, J. Ratiometric single-nanoparticle oxygen sensors for biological imaging. *Angew. Chem., Int. Ed.* **2009**, *48*, 2741−2745.
(150) Dmitriev, R. I.; Borisov, S. M.; Düssmann, H.; Sun, S.; Müller, B. J.; Prehn, J.; Baklaushev, V. P.; Klimant, I.; Papkovsky, D. B. Versatile conjugated polymer nanoparticles for high-resolution O_2 imaging in cells and 3d tissue models. *ACS Nano* **2015**, *9*, 5275−5288.
(151) Lin, M.; Zhao, Y.; Wang, S.; Liu, M.; Duan, Z.; Chen, Y.; Li, F.; Xu, F.; Lu, T. Recent advances in synthesis and surface modification of lanthanide-doped upconversion nanoparticles for biomedical applications. *Biotechnol. Adv.* **2012**, *30*, 1551−1561.
(152) Jin, J.; Gu, Y.-J.; Man, C. W.-Y.; Cheng, J.; Xu, Z.; Zhang, Y.; Wang, H.; Lee, V. H.-Y.; Cheng, S. H.; Wong, W.-T. Polymer-coated nayf4:Yb3+, er3+ upconversion nanoparticles for charge-dependent cellular imaging. *ACS Nano* **2011**, *5*, 7838−7847.
(153) Chatterjee, D. K.; Rufaihah, A. J.; Zhang, Y. Upconversion fluorescence imaging of cells and small animals using lanthanide doped nanocrystals. *Biomaterials* **2008**, *29*, 937−943.
(154) Liu, Q.; Yang, T.; Feng, W.; Li, F. Blue-emissive upconversion nanoparticles for low-power-excited bioimaging in vivo. *J. Am. Chem. Soc.* **2012**, *134*, 5390−5397.
(155) Liu, Q.; Yin, B.; Yang, T.; Yang, Y.; Shen, Z.; Yao, P.; Li, F. A general strategy for biocompatible, high-effective upconversion nanocapsules based on triplet−triplet annihilation. *J. Am. Chem. Soc.* **2013**, *135*, 5029−5037.
(156) Monguzzi, A.; Frigoli, M.; Larpent, C.; Tubino, R.; Meinardi, F. Low-power-photon up-conversion in dual-dye-loaded polymer nanoparticles. *Adv. Funct. Mater.* **2012**, *22*, 139−143.
(157) Wohnhaas, C.; Mailänder, V.; Dröge, M.; Filatov, M. A.; Busko, D.; Avlasevich, Y.; Baluschev, S.; Miteva, T.; Landfester, K.; Turshatov, A. Triplet−triplet annihilation upconversion based nanocapsules for bioimaging under excitation by red and deep-red light. *Macromol. Biosci.* **2013**, *13*, 1422−1430.
(158) Diederich, C. J. Thermal ablation and high-temperature thermal therapy: Overview of technology and clinical implementation. *Int. J. Hyperthermia* **2005**, *21*, 745−753.
(159) Kampinga, H. H. Cell biological effects of hyperthermia alone or combined with radiation or drugs: A short introduction to newcomers in the field. *Int. J. Hyperthermia* **2006**, *22*, 191−196.
(160) Burd, R.; Dziedzic, T. S.; Xu, Y.; Caligiuri, M. A.; Subjeck, J. R.; Repasky, E. A. Tumor cell apoptosis, lymphocyte recruitment and tumor vascular changes are induced by low temperature, long duration (fever-like) whole body hyperthermia. *J. Cell. Physiol.* **1998**, *177*, 137−147.
(161) Raaphorst, G. P.; Azzam, E. I.; Feeley, M. Potentially lethal radiation damage repair and its inhibition by hyperthermia in normal hamster cells, mouse cells, and transformed mouse cells. *Radiat. Res.* **1988**, *113*, 171−182.
(162) Jones, E. L.; Prosnitz, L. R.; Dewhirst, M. W.; Marcom, P. K.; Hardenbergh, P. H.; Marks, L. B.; Brizel, D. M.; Vujaskovic, Z. Thermochemoradiotherapy improves oxygenation in locally advanced breast cancer. *Clin. Cancer Res.* **2004**, *10*, 4287−4293.
(163) Brizel, D. M.; Scully, S. P.; Harrelson, J. M.; Layfield, L. J.; Dodge, R. K.; Charles, H. C.; Samulski, T. V.; Prosnitz, L. R.; Dewhirst, M. W. Radiation therapy and hyperthermia improve the oxygenation of human soft tissue sarcomas. *Cancer Res.* **1996**, *56*, 5347−5350.
(164) Lindner, U.; Lawrentschuk, N.; Weersink, R. A.; Davidson, S. R.; Raz, O.; Hlasny, E.; Langer, D. L.; Gertner, M. R.; Van der Kwast, T.; Haider, M. A. Focal laser ablation for prostate cancer followed by radical prostatectomy: Validation of focal therapy and imaging accuracy. *Eur. Urol.* **2010**, *57*, 1111−1114.
(165) Raz, O.; Haider, M. A.; Davidson, S. R.; Lindner, U.; Hlasny, E.; Weersink, R.; Gertner, M. R.; Kucharczyk, W.; McCluskey, S. A.; Trachtenberg, J. Real-time magnetic resonance imaging−guided focal laser therapy in patients with low-risk prostate cancer. *Eur. Urol.* **2010**, *58*, 173−177.
(166) Ahrar, K.; Gowda, A.; Javadi, S.; Borne, A.; Fox, M.; McNichols, R.; Ahrar, J. U.; Stephens, C.; Stafford, R. J. Preclinical assessment of a 980-nm diode laser ablation system in a large animal tumor model. *J. Vasc. Interv. Radiol* **2010**, *21*, 555−561.
(167) Iyer, A. K.; Khaled, G.; Fang, J.; Maeda, H. Exploiting the enhanced permeability and retention effect for tumor targeting. *Drug Discovery Today* **2006**, *11*, 812−818.
(168) Chuck, R. S.; Oz, M. C.; Delohery, T. M.; Johnson, J. P.; Bass, L. S.; Nowygrod, R.; Treat, M. R. Dye-enhanced laser tissue welding. *Lasers Surg. Med.* **1989**, *9*, 471−477.
(169) Chong, L. P.; Özler, S. A.; De Queiroz, J. M. J.; Liggett, P. E. Indocyanine green-enhanced diode laser treatment of melanoma in a rabbit model. *Retina* **1993**, *13*, 251−259.
(170) Greenwell, T. J.; Wyman, A.; Rogers, K. Chromophore-enhanced 805 nm laser therapy for gastrointestinal neoplasia. *Eur. J. Surg. Oncol.* **2001**, *27*, 368−372.
(171) Chen, W. R.; Adams, R. L.; Heaton, S.; Dickey, D. T.; Bartels, K. E.; Nordquist, R. E. Chromophore-enhanced laser-tumor tissue photothermal interaction using an 808-nm diode laser. *Cancer Lett.* **1995**, *88*, 15−19.

DOI: 10.1021/acs.chemrev.5b00140
Chem. Rev. XXXX, XXX, XXX−XXX

(172) Zhou, J.; Lu, Z.; Zhu, X.; Wang, X.; Liao, Y.; Ma, Z.; Li, F. NIR photothermal therapy using polyaniline nanoparticles. *Biomaterials* **2013**, *34*, 9584−9592.
(173) Yang, J.; Choi, J.; Bang, D.; Kim, E.; Lim, E. K.; Park, H.; Suh, J. S.; Lee, K.; Yoo, K. H.; Kim, E. K.; et al. Convertible organic nanoparticles for near-infrared photothermal ablation of cancer cells. *Angew. Chem., Int. Ed.* **2011**, *50*, 441−444.
(174) Abel, S. B.; Molina, M. A.; Rivarola, C. R.; Kogan, M. J.; Barbero, C. A. Smart polyaniline nanoparticles with thermal and photothermal sensitivity. *Nanotechnology* **2014**, *25*, 495602.
(175) Fan, Q.; Cheng, K.; Yang, Z.; Zhang, R.; Yang, M.; Hu, X.; Ma, X.; Bu, L.; Lu, X.; Xiong, X. Perylene-diimide-based nanoparticles as highly efficient photoacoustic agents for deep brain tumor imaging in living mice. *Adv. Mater.* **2015**, *27*, 843.
(176) Yang, K.; Xu, H.; Cheng, L.; Sun, C.; Wang, J.; Liu, Z. In vitro and in vivo near-infrared photothermal therapy of cancer using polypyrrole organic nanoparticles. *Adv. Mater.* **2012**, *24*, 5586−5592.
(177) Chen, M.; Fang, X.; Tang, S.; Zheng, N. Polypyrrole nanoparticles for high-performance in vivo near-infrared photothermal cancer therapy. *Chem. Commun.* **2012**, *48*, 8934−8936.
(178) Liu, Y.; Ai, K.; Liu, J.; Deng, M.; He, Y.; Lu, L. Dopamine-melanin colloidal nanospheres: An efficient near-infrared photothermal therapeutic agent for in vivo cancer therapy. *Adv. Mater.* **2013**, *25*, 1353−1359.
(179) Cheng, L.; Yang, K.; Chen, Q.; Liu, Z. Organic stealth nanoparticles for highly effective in vivo near-infrared photothermal therapy of cancer. *ACS Nano* **2012**, *6*, 5605−5613.
(180) Chen, X. W.; Ke, M. R.; Li, X. S.; Lan, W. L.; Zhang, M. F.; Huang, J. D. Synthesis, supramolecular behavior, and in vitro photodynamic activities of novel zinc(ii) phthalocyanines ″side-strapped″ with crown ether bridges. *Chem. - Asian J.* **2013**, *8*, 3063−3070.
(181) Tautz, R.; Da Como, E.; Limmer, T.; Feldmann, J.; Egelhaaf, H.-J.; von Hauff, E.; Lemaur, V.; Beljonne, D.; Yilmaz, S.; Dumsch, I.; et al. Structural correlations in the generation of polaron pairs in low-bandgap polymers for photovoltaics. *Nat. Commun.* **2012**, *3*, 970.
(182) MacNeill, C. M.; Coffin, R. C.; Carroll, D. L.; Levi-Polyachenko, N. H. Low band gap donor-acceptor conjugated polymer nanoparticles and their NIR-mediated thermal ablation of cancer cells. *Macromol. Biosci.* **2013**, *13*, 28−34.
(183) Liu, Y.; Simon, J. D. Isolation and biophysical studies of natural eumelanins: Applications of imaging technologies and ultrafast spectroscopy. *Pigm. Cell Res.* **2003**, *16*, 606−618.
(184) Zha, Z.; Deng, Z.; Li, Y.; Li, C.; Wang, J.; Wang, S.; Qu, E.; Dai, Z. Biocompatible polypyrrole nanoparticles as a novel organic photoacoustic contrast agent for deep tissue imaging. *Nanoscale* **2013**, *5*, 4462−4467.
(185) Smith, A. M.; Mancini, M. C.; Nie, S. Bioimaging: Second window for in vivo imaging. *Nat. Nanotechnol.* **2009**, *4*, 710−711.
(186) Jin, C. S.; Lovell, J. F.; Zheng, G. One minute, sub-one-watt photothermal tumor ablation using porphysomes, intrinsic multifunctional nanovesicles. *J. Visualized Exp.* **2013**, e50536.
(187) Jin, C. S.; Lovell, J. F.; Chen, J.; Zheng, G. Ablation of hypoxic tumors with dose-equivalent photothermal, but not photodynamic, therapy using a nanostructured porphyrin assembly. *ACS Nano* **2013**, *7*, 2541−2550.
(188) MacDonald, T. D.; Liu, T. W.; Zheng, G. An mri-sensitive, non-photobleachable porphysome photothermal agent. *Angew. Chem., Int. Ed.* **2014**, *53*, 6956−6959.
(189) Li, Y.; Lin, T. Y.; Luo, Y.; Liu, Q.; Xiao, W.; Guo, W.; Lac, D.; Zhang, H.; Feng, C.; Wachsmann-Hogiu, S.; et al. A smart and versatile theranostic nanomedicine platform based on nanoporphyrin. *Nat. Commun.* **2014**, *5*, 4712.
(190) Bell, A. G. On the production and reproduction of sound by light. *Am. J. Sci.* **1880**, *20* (Series3), 305−324.
(191) Wang, L. *Optics in the Life Sciences*; Monterey, CA, 2011; p OMA1.
(192) Pu, K.; Shuhendler, A. J.; Jokerst, J. V.; Mei, J.; Gambhir, S. S.; Bao, Z.; Rao, J. Semiconducting polymer nanoparticles as photoacoustic molecular imaging probes in living mice. *Nat. Nanotechnol.* **2014**, *9*, 233−239.
(193) Medzhitov, R. Origin and physiological roles of inflammation. *Nature* **2008**, *454*, 428−435.
(194) Zhang, D.; Zhao, Y. X.; Qiao, Z. Y.; Mayerhoffer, U.; Spenst, P.; Li, X. J.; Wurthner, F.; Wang, H. Nano-confined squaraine dye assemblies: New photoacoustic and near-infrared fluorescence dual-modular imaging probes in vivo. *Bioconjugate Chem.* **2014**, *25*, 2021−2029.
(195) Zhang, Y.; Jeon, M.; Rich, L. J.; Hong, H.; Geng, J.; Zhang, Y.; Shi, S.; Barnhart, T. E.; Alexandridis, P.; Huizinga, J. D.; et al. Non-invasive multimodal functional imaging of the intestine with frozen micellar naphthalocyanines. *Nat. Nanotechnol.* **2014**, *9*, 631−638.
(196) Ng, K. K.; Shakiba, M.; Huynh, E.; Weersink, R. A.; Roxin, A.; Wilson, B. C.; Zheng, G. Stimuli-responsive photoacoustic nanoswitch for in vivo sensing applications. *ACS Nano* **2014**, *8*, 8363−8373.
(197) Huynh, E.; Lovell, J. F.; Fobel, R.; Zheng, G. Optically controlled pore formation in self-sealing giant porphyrin vesicles. *Small* **2014**, *10*, 1184−1193.
(198) Huynh, E.; Lovell, J. F.; Helfield, B. L.; Jeon, M.; Kim, C.; Goertz, D. E.; Wilson, B. C.; Zheng, G. Porphyrin shell microbubbles with intrinsic ultrasound and photoacoustic properties. *J. Am. Chem. Soc.* **2012**, *134*, 16464−16467.
(199) Huynh, E.; Jin, C. S.; Wilson, B. C.; Zheng, G. Aggregate enhanced trimodal porphyrin shell microbubbles for ultrasound, photoacoustic, and fluorescence imaging. *Bioconjugate Chem.* **2014**, *25*, 796−801.
(200) Huynh, E.; Leung, B. Y. C.; Helfield, B. L.; Shakiba, M.; Gandier, J.-A.; Jin, C. S.; Master, E. R.; Wilson, B. C.; Goertz, D. E.; Zheng, G. In situ conversion of porphyrin microbubbles to nanoparticles for multimodality imaging. *Nat. Nanotechnol.* **2015**, *10*, 325−332.

DOI: 10.1021/acs.chemrev.5b00140
Chem. Rev. XXXX, XXX, XXX−XXX